IMMOBILIZATION OF PROTEINS ON ZEOLITE AND ZEO-TYPE MATERIALS FOR BIOSENSOR APPLICATIONS BASED ON CONDUCTOMETRIC BIOSENSORS AND ION SENSITIVE FIELD EFFECT TRANSISTORS

A THESIS SUBMITTED TO
THE GRADUATE SCHOOL OF NATURAL AND APPLIED SCIENCES
OF
MIDDLE EAST TECHNICAL UNIVERSITY

BY

ESİN SOY

IN PARTIAL FULFILLMENT OF THE REQUIREMENTS
FOR
THE DEGREE OF MASTER OF SCIENCE
IN
MICRO AND NANOTECHNOLOGY

JUNE 2011

Approval of the thesis:

IMMOBILIZATION OF PROTEINS ON ZEOLITE AND ZEO-TYPE MATERIALS FOR BIOSENSOR APPLICATIONS BASED ON CONDUCTOMETRIC BIOSENSORS AND ION SENSITIVE FIELD EFFECT TRANSISTORS

submitted by **ESİN SOY** in partial fulfillment of the requirements for the degree of **Master of Science in Micro and Nanotechnology Department, Middle East Technical University** by,

Prof. Dr. Canan Özgen
Dean, Graduate School of **Natural and Applied Sciences** _____

Prof. Dr. Mürvet Volkan
Head of Department, **Micro and Nanotechnology** _____

Assist. Prof. Burcu Akata Kurç
Supervisor, **Dept. of Micro and Nanotechnology, METU** _____

Assist. Prof. Can Özen
Co-Supervisor, **Department of Biotechnology, METU** _____

Examining Committee Members:

Prof. Dr. Hayrettin Yücel
Department of Chemical Eng., METU _____

Assist. Prof. Burcu Akata Kurç
Department of Micro and Nanotechnology, METU _____

Assist. Prof. Can Özen
Department of Biotechnology, METU _____

Assoc. Prof. Caner Durucan
Department of Metallurgical and Materials Eng., METU _____

Dr. Kemal Behlülgil
Central Laboratory, METU _____

Date: 13.06.2011

I hereby declare that all information in this document has been obtained and presented in accordance with academic rules and ethical conduct. I also declare that, as required by these rules and conduct, I have fully cited and referenced all material and results that are not original to this work.

Name, Last Name: ESİN SOY

Signature:

ABSTRACT

IMMOBILIZATION OF PROTEINS ON ZEOLITE AND ZEO-TYPE MATERIALS FOR BIOSENSOR APPLICATIONS BASED ON CONDUCTOMETRIC BIOSENSORS AND ION SENSITIVE FIELD EFFECT TRANSISTORS

Soy, Esin

M.Sc., Department of Micro and Nanotechnology

Supervisor : Assist. Prof. Dr. Burcu Akata Kurç

Co-Supervisor: Assist. Prof. Dr. Can Özen

June 2011, 145 Pages

Over the last decade, immobilization of proteins onto inorganic materials is becoming more crucial to extend a deep understanding of interaction between proteins and nanoparticles. With understanding of the real interaction lying under the protein-nanoparticle relations, it is possible to organize the conformation and orientation of surface and framework species of nanoparticles to generate ideal surfaces for potential biotechnological applications. Due to their unique properties such as large clean surface, tunable surface properties, adjustable surface charge, and dispersibility in aqueous solutions, zeolite and zeo-type materials are one of the remarkable classes of inorganic materials that are widely studied in the

literature. These properties make zeolites promising alternative candidates for the immobilization of enzymes and incorporation into biosensing devices.

In the current study, a new approach was developed for direct determination of urea, glucose, and butyrylcholine where zeolites were incorporated to the electrode surfaces of a conductometric biosensor and Ion Sensitive Field Effect Transistors were used to immobilize the enzymes. Biosensor responses, operational stabilities, and storage stabilities of the new approach were compared with results obtained from the standard membrane methods for the same measurements. For this purpose, different surface modification technique, which are simply named as Zeolite Modified Transducers (ZMTs) were compared with Standard Membrane Transducers (SMTs). During the conductometric measurements ZMT electrodes were used, which allowed the direct evaluation of the effect of zeolite morphology on the biosensor responses for the first time. It was seen that silicalite added electrodes lead to increased performances with respect to SMTs. As a result, the zeolite modified urea and glucose biosensors were successfully applied for detecting urea and glucose, which can offer improved possibilities to design biosensors. The results obtained show that zeolites could be used as alternatives for enzyme immobilization in conductometric biosensors development.

Furthermore, the sensitivities of urease and butyrylcholinesterase biosensors, prepared by the incorporation of zeolite Beta crystals with varying acidity on the surface of pH-sensitive field-effect transistors (pH-FETs), have been studied and compared. In order to study exclusively the effect of zeolite acidity, highly crystalline pure zeolite Beta sample with Si/Al ratio of 17 was synthesized and subjected to different heat treatment protocols. In this way, the surface acidic OH groups were controllably altered, as confirmed by Fourier transform infrared

(FTIR) spectroscopy without changing any other zeolitic properties, such as zeolite morphology and Si/Al ratio. Upon incorporation of zeolite Beta, the biosensors sensitivity towards urea and butyrylcholine increased 2 and 3 times, respectively. Operational stability and possibility to use the biosensors for inhibition analysis were also investigated. The combined ion-sensitive field-effect transistor (ISFET) and FTIR data provided evidence that urease and *butyrylcholinesterase* responded to changes in the nature of surface OH groups in zeolite Beta samples. Accordingly, it was found that the Brønsted acidity of zeolite Beta is important for the ultimate ISFET performance.

Additionally, analytical characteristics of urease and butyrylcholinesterase based ISFET sensors were investigated by the incorporation of zeolite (70 nm zeolite beta crystals with varying Si/Al ratio, particle size, and surface charge) and zeo-type materials with varying pore diameter and surface charge for the first time. The results obtained by the zeolite modified ISFET transducers suggested that the Si/Al ratio, particle size and surface charge of the zeolite Beta crystals were strongly influenced the biosensor performances due to the electrostatic interactions between enzyme molecules, substrates, and zeolite surface as well as the nature of the enzymatic reaction.

Keywords: Biosensor, Zeolite, Protein, Conductometry, Ion Sensitive Field Effect Transistor.

ÖZ

KONDÜKTOMETRİK VE İYON SEÇİCİ ALAN ETKİLİ TRANSİSTÖR TİPLİ BİYOSENSÖR UYGULAMALARINDA KULLANILMAK ÜZERE PROTEİNLERİN ZEOLİT VE ZEOLİT BENZERİ MALZEMELER ÜZERİNE İMMOBİLİZASYONU

Soy, Esin
Yüksek Lisans, Mikro ve Nanoteknoloji Bölümü
Tez Yöneticisi : Yrd. Doç. Dr. Burcu Akata Kurç
Ortak Tez Yöneticisi: Yrd. Doç. Dr. Can Özen

Haziran 2011, 145 sayfa

Son yıllarda, protein ve nano malzemeler arasındaki ilişkinin daha iyi anlaşılabilmesi amacıyla, proteinlerin inorganik malzemeler üzerine immobilizasyonu oldukça önem kazanmıştır. Protein-nanomalzeme ilişkisinin daha ayrıntılı anlaşılmasıyla, ileri biyoteknolojik araştırmalarda kullanılmak üzere, istenilen uygulamaya göre fiziksel ve kimyasal değişikliklerin yapılabildiği ideal yüzeylerin üretilmesi mümkündür. Geniş ve temiz yüzeyleri, değiştirilebilir yüzey özellikleri ve sıvıda dağılabilme gibi özellikleri sebebiyle zeolite ve zeolite benzeri malzemeler, literatürde bu amaçla sıkça kullanılan inorganik malzemeler arasındadır. Bu özellikler zeolitleri, proteinlerin bağlanması ve biyosensör cihazlarında kullanılmaları amacıyla alternatif birer malzeme haline getirmektedirler.

Bu çalışmada, kondüktometrik ve iyon seçici alan etkili transistörlerde, zeolit ve benzeri malzemeler ile modifiye edilen biyosensor elektrotlarının üre, glukoz ve bütirilkolin saptamasında kullanılması amaçlanmıştır. Sistemin optimizasyonu, modifiye edilmiş elektrotlara bağlanan enzimlerin aktiviteleri, çalışma ve saklanma stabilitleri ile inhibisyon davranışları araştırılmış ve zeolite ile modifiye edilmemiş biyosensörlerden alınan sonuçlar ile karşılaşıtırılmıştır. Bu çalışmada, değişik bir modifikasyon tekniği olarak Zeolit Membran Elektrotları (ZMT), Standart Membrane Elektrotları (SMT) ile ilk defa olarak karşılaştırılmıştır. Bulduğumuz bilgiler ışığında, silikalit örnekleri ile modifiye edilmiş üre elektrotları ve amonyum ile katyon değişimi yapılmış zeolite Beta parçacıkları ile modifiye edilmiş glukoz elektrotları en düşük saptama limiti ve en yüksek enzimatik aktivite ile en iyi çalışan kondüktometrik elektrotlar olmuşlardır. Ayrıca, bahsi geçen elektrotlar, yüksek çalışma ve saklama stabilitesi de göstererek, kondüktometrik biyosensörlerde zeolitlerin performans arttırıcı etkisinini gözler önüne sermiştir.

Kondüktometrik biyosensörlere ek olarak, urease ve bütirilkolinesteraz içeren iyon seçici alan etkili transistor (ISFET) tipli biyosensörlerin analitik özellikleri de zeolite ve zeolite benzeri malzemeler kullanılarak araştırılmıştır. Bu nedenle, ISFET elektrotları değişik sıcaklık derecelerinde kalsine edilmiş zeolite Beta örnekleriyle modifiye edilmişlerdir. Bu sayede zeolitin yüzey hidroksil grupları ve Brønsted asit bölgelerinde meydana getirilecek değişikliğin biyosensor performansına etkisinin araştırılması amaçlanmıştır. Yalnızca zeolitin yüzey gruplarının etkisini görebilmek amacıyla, Si/Al oranı 17 olan zeolit Beta örnekleri farklı sıcaklıklarda kalsine edilmiştir. Bu şekilde, sadece yüzeydeki hidroksil grupları ve Brønsted asit bölgeleri FTIR karakterizasyonu ile de gösterildiği üzere değiştirilmiş ve diğer özellikler, Si/Al oranı, gözenek hacmi, gözenek boyutu, zeolit tipi vs, üzerinde herhangi bir değişiklik yapılmamıştır. Bu sayede zeolitin

yüzey grupları ve asitliğinin, üre ve bütirilkolin biyosensörleri üzerindeki etkisinin daha iyi anlaşılabilmesi sağlanmaya çalışılmıştır. Kalsine edilmiş zeolit Beta ile modifiye edilmiş biyonsensörlerde 2 ila 3 kata kadar daha yüksek aktivite saptanmıştır. Ayrıca biyosensörlerin stabilitesinin de oldukça yüksek olduğu ve inhibisyon analizlerinde de başarılı bir şekilde kullanılabilecekleri saptanmıştır. ISFET ve FTIR yöntemlerinden ortak olarak elde edilen verilere göre, üre ve bütirilkolin biyosensörleri, zeolit Beta malzemelerindeki asidik grupların değişmesine paralel olarak bir gelişim göstermişlerdir. Biyosensör performansı üzerinde yüzey hidroksil gruplarının tam olarak bir etkisi gözlenememiştir. Bu çalışma, Brønsted asit gruplarının ISFET tip biyosensör performansını etkilediğini gösteren ilk çalışma olmuştur.

Yukarıdaki çalışmalara ek olarak, ISFET elektrotları 70 nm boyutunda ve farklı Si/Al oranı, parçacık boyutu ve yüzey yüküne sahip zeolite Beta kristalleri ve farklı gözenek boyutuna sahip zeolit benzeri malzemeler ile modifiye edilmiş ve nano boyutta zeolitin özelliklerinin biyosensör performansına etkisi araştırılmıştır. Elde edilen verilere göre zeolitin Si/Al oranı, malzemenin elektrostatik ve hidrofobik özelliklerini değiştirerek, substrat molekülleri ile elektrostatik etkileşimini arttırmıştır ve buna ek olarak enzimatik reaksiyonlara proton donor olarak katkıda bulunmuştur. Ayrıca, parçacık boyutu, yüzey alanı, yüzey yükü ve gözenek boyutu da enzimatik aktivite ve biyosensör stabilitesini etkileyen faktörler arasındadır.

Sonuç olarak zeolit ve zeolit benzeri malzemeler kullanılarak modifiye edilmiş elektrotların kullanıldığı kondüktometrik ve ISFET tipli biyosensörler, direkt üre, glukoz ve bütirilkolin tespiti için kullanılmış ve biyosensör performansını arttırıcı etkileri tespit edilmiştir. Elde edilen sonuçlar, yeni nesil biyosensör dizaynı için gelecekteki çalışmalara ışık tutacak niteliktedir.

Anahtar Kelimeler: Biyosensör, Zeolit, Protein, Kondüktometri, İyon Seçici Alan Etkili Transistör.

to my mother...

ACKNOWLEDGEMENTS

First and foremost I offer my sincerest gratitude to my supervisor, Dr. Burcu Akata, who has supported me thoughout my thesis with her patience and knowledge whilst allowing me the room to work in my own way. Her supervision, advice, and guidance from the very early stage of this research as well as giving me extraordinary experiences through out the work. Above all and the most needed, she provided me unflinching encouragement and support in various ways.

Foremost, I would like to express my sincere gratitude to my co-advisor Dr. Can Özen for the continuous support of my master study and research, for his guidance, motivation, enthusiasm, and immense knowledge.

Furthermore, I would like to thank to the rest of my thesis committee; Prof. Dr. Hayrettin Yücel, Dr. Caner Durucan, and Dr. Kemal Behlülgil for their valuable comments.

I would like to thank the members of my research group, Sezin Galioğlu, Berna Ozansoy Kasap, Seçkin Öztürk, Sedat Canlı, and Kaan Kirdeciler for their precious guidance, inspiration and supports. I also thank Gözde Eke, Aysu Küçükturhan, Eda Ayşe Aksoy, Serap Tekin, and Levent Yıldız for their supports in Central Laboratory and Biotechnology Recearch Center. I owe my gratitude to Dr. Juliusz Warzywoda, Prof. Dr. Albert Sacco Jr., and Dr. Mariam N. Ismail for their helps about zeolite synthesis, characterization and FTIR measurements conducted in Center for Advanced Microgravity Materials Processing (CAMMP), Department of Chemical Engineering, Northeastern University, Boston, USA. Special thanks to Prof. Dr. Nicole Jaffrezic Renault, Prof. Dr. Sergei V.

Dzyadevych, Dr. Valentyna N. Arkhypova, and Prof. Dr. Alexey Soldatkin for their helps and advice about biosensor measurements conducted in Laboratory of Analytical Sciences (UCBL), Claude Bernard University Lyon 1, Lyon, France, and Institute of Molecular Biology and Genetics, Laboratory of Biomolecular Electronics (IMBG), Kiev, Ukraine.

I also wish to express my love and gratitude to all my family members, Semih Soy, Leman Aykoç, Ebru Soy, Serenay Bilge, Fuat Zafer Yapici, Vildan Şen Yapici, and Berrin Yapici for their faithful support, love and encouragement during my whole study.

I would like to give my endless gratitude to my mother, Gülsüm Soy, who supported and motivated me with her endless love and understanding during the whole period of my study. She has given me her unequivocal support throughout, as always, for which my mere expression of thanks likewise does not suffice.

Last, but not least, my deepest gratitude goes to Engin Yapici for his sacrifice, personal support and great patience at all times. He always gives me warm encouragement and love in every situation. His support and encouragement was in the end what made this dissertation possible.

I am also appreciative of the financial support that I received for this study through Scientific and Technical Research Council of Turkey (TUBITAK) and European Union project with the project number PIRSES-GA-2008-230802.

TABLE OF CONTENTS

ABSTRACT iv

ÖZ vii

ACKNOWLEDGEMENTS xii

TABLE OF CONTENTS xiv

LIST OF TABLES xix

LIST OF FIGURES xx

LIST OF SYMBOLS xxv

CHAPTERS

1. INTRODUCTION 1

1.1 Zeolite and Zeo-type Materials 1

1.1.1 Structure of Zeolites 1

1.1.1 Acidity of Zeolites 4

1.2 Importance of Protein Monitoring in Biotechnology 7

1.3 Protein Immobilization 8

1.3.1 Protein Immobilization Techniques 9

1.3.2 Immobilization on Support 11

1.4 Principles of Electrochemical Biosensors 12

1.4.1 Conductometric Biosensors 13

1.4.2 ISFET Biosensors 15

2. LITERATURE REVIEW 18

2.1 The Role of Adding Zeolite Materials on Enzymatic Studies 18

2.1.1 Effect of Hydrophobicity 19

2.1.2 Effect of Pore Size 20

2.1.3 Effect of Particle Size 21

2.1.4 Effect of Acidity 22

2.2 Enzyme Immobilization on Zeolite Surfaces 23

2.3 Zeolite and Zeo-type Materials in Biosensor Applications 23

3. EXPERIMENTAL 17

3.1 Synthesis of Zeolite and Zeo-type Materials 25

3.1.1 Zeolite A with Varying Particle Diameter 25

3.1.2 Zeolite Beta with Varying Si/Al Ratio 26

3.1.3 Silicalite and SBA-15 Synthesis 27

3.2 Modification of Zeolite and Zeo-type Materials 28

3.2.1 Functionalization of Zeolite Beta and SBA-15 28

3.2.2 Ion Exchange of Zeolite Beta 30

3.2.3 Heat Treatment of Zeolite Beta 30

3.3 Material Characterization 31

3.3.1 X-Ray Diffraction (XRD) 31
3.3.2 Scanning Electron Microscopy (SEM) 32
3.3.3 Surface and Pore Size Analysis 32
3.3.4 Zeta Potential 33
3.3.5 Fourier Transform Infrared Spectrophotometry (FTIR) 33
3.4 Protein Adsorption 34
3.4.1 UV-VIS Measurement 35
3.5 Biosensor Measurement 35
3.5.1 Conductometric Biosensors 38
3.5.2 ISFET Biosensors 40
4. RESULTS AND DISCUSSION 42
4.1 Protein Immobilization by Physical Adsorption 42
4.1.1 Synthesis of Zeolite and Zeo-type Materials 42
4.1.1.1 Zeolite A with Varying Particle Diameter 42
4.1.1.2 Zeolite Beta with Varying Si/Al Ratio 47
4.1.1.3 Silicalite and SBA-15 51
4.1.2 Modification of Zeolite and Zeo-type Materials 54
4.1.2.1 Surface Functionalization 55
4.1.2.2 Ion Exchange 57
4.1.3 UV-VIS Measurements 58

4.1.3.1 Effect of Particle Diameter 60

4.1.3.2 Effect of Si/Al Ratio 61

4.1.3.3 Effect of Surface Charge 63

4.1.3.4 Effect of pH 63

4.1.3.5 Effect of Extra-Framework Cations 65

4.1.3.6 Effect of Pore Size 66

4.2 Biosensor Measurements 68

4.2.1 Conductometric Urea and Glucose Biosensors 68

4.2.1.1 Effect of Zeolite Loading into Bioselective Membranes 70

4.2.1.2 Effect of Cross-Linking Time 71

4.2.1.3 Effect of Buffer Concentration and pH 72

4.2.1.4 Effect of Zeolite Morphology 74

4.2.2 ISFET Based Urea and Butyrylcholine Biosensors 76

4.2.2.1 Effect of Surface Silanol Groups and Brønsted Acidity of Heat Treated Zeolite Beta on the Analytical Characteristics of ISFET Biosensors 76

4.2.2.1.1 Synthesis and Modification of Zeolites 76

4.2.2.1.1.1 Heta Treatment 77

4.2.2.1.2 Biosensor Measurements 84

4.2.2.1.2.1 Sensitivity 84

4.2.2.1.2.2 Operational Stability and Inhibition 86

4.2.2.2 Effect of Si/Al, Particle Diameter and Surface Charge of Nano Sized Zeolite Beta on the Analytical Characteristics of ISFET Biosensors 91

4.2.2.2.1 Synthesis and Modification of Zeolites 91

4.2.2.2.2 Biosensor Measurements 97

4.2.2.2.2.1 Sensitivity 97

4.2.2.2.2.2 Operational Stability and Inhibition 103

4.2.2.3 Effect of Pore Size and Surface Charge of Silica Particles on the Analytical Caracteristics of ISFET Biosensors 107

4.2.2.3.1 Synthesis and Modification of Zeolite and Zeo-type Materials..... 107

4.2.2.3.2 Biosensor Measurements 108

4.2.2.3.2.1 Sensitivity 108

4.2.2.3.3.2 Operational Stability and Inhibition 110

5. CONCLUSIONS 116

6. RECOMMENDATIONS 119

REFERENCES 121

APPENDICES 129

A. CHARACTERISTICS XRD PEAKS OF ZEOLITE A, BETA, SILICALITE, AND SBA-15 IN THE LITERATURE..... 131

B. TABLE OF AS-SYNTHESIZED MATERIALS 135

C. T-PLOT ANALYSIS OF ZEOLITE AND ZEO-TYPE MATERIALS 136

D. UV-VIS ABSORPTION SPECTRA OF PROTEINS 144

E. MASS BALANCE CALCULATION OF ADSORBED PROTEINS 145

LIST OF TABLES

TABLES

Table 4.1: Summary of textural properties of zeolite A micro crystals 46

Table 4.2: Summary of textural properties of sub-micron zeolite Beta crystals ... 50

Table 4.3: Summary of the textural properties of silica particles 54

Table 4.4: Textural properties of the functionalized and non-functionalized zeolite Beta and SBA-15 particles 56

Table 4.5: Summary of the properties of ion exchanged sub-micron zeolite Beta crystals 57

Table 4.6: Molecular weights and isoelectric points of proteins 58

Table 4.7: Adsorption of proteins onto zeolite A and Beta crystals 59

Table 4.8: Summary of the textural properties of zeolites 55

Table 4.9: Properties of as-synthesized and heat treated zeolite BEA samples ... 80

Table 4.10: Summary of the textural properties of zeolite Beta nano crystals 94

Table 4.11: Textural properties of the functionalized and non-functionalized zeolite Beta nano crystals 95

Table 4.12: Summary of the nano sized zeolite Beta materials used in the ISFET study 96

LIST OF FIGURES

FIGURES

Figure 1.1: Primary building units of zeolites. 2

Figure 1.2: 3D channel structure of zeolite A (A) and zeolite Beta (B) 2

Figure 1.3: Schematic representations of Brønsted acid sites (A) and silanol groups (B) of zeolite. 6

Figure 1.4: Schematic representation of widely used approaches for the immobilization of proteins; physical adsorption (A), entrapment (B), cross linking (C) 10

Figure 1.5: Design of the conductometric transducer (with a reference and a working electrode) and of the experimental set-up for conductometric measurementS..... 14

Figure 1.6: Schematic picture of separated p-channel ISFET, its gate is coming to contact with electrolyte solution..... 14

Figure 3.1: Shematic presentation of reflux system 29

Figure 3.2: Schematic presentation of standard membrane transducer (A) and zeolite modified transducer (B) 38

Figure 4.1: XRD patterns of zeolite A micro crystals with varying particle particle size 43

Figure 4.2: FE-SEM images of zeolite A crystals with varying particle size 44

Figure 4.3: Particle Size Disperser results of Zeolite A (LTA) micro crystals with varying particle size 45

Figure 4.4: XRD patterns of sub micron zeolite Beta crystals with varying Si/Al ratio 48

Figure 4.5: FE-SEM images of sub-micron zeolite Beta crystals with varying Si/Al ratio BEA-30 (A), BEA-50 (B), BEA-60 (C), and BEA-120 (D). 49

Figure 4.6: Particle size distribution results of sub-micron zeolite Beta crystals with varying Si/Al ratio. 50

Figure 4.7: XRD patterns of Silicalite (A) and SBA-15 (B) particles 52

Figure 4.8: FE-SEM images of silica particles using Formula XI (A) and Formula XII (B) 53

Figure 4.9: Zeta potential distribution of functionalized zeolite Beta samples by using two different experimental procedures; non-functionalized zeolite Beta (A), functionalized zeolite Beta by using procedure 1 [B] and procedure 2 [C]. 55

Figure 4.10: Schematic representation of protein adsorption onto zeolite A particles with varying particle diameters. Larger surface area provided by larger zeolite A crystals leads proteins to elongate through the surface and partially unfold, which results in more interaction between proteins and crystal. 60

Figure 4.11: Adsorption of glucose oxidase, hemoglobin, and lysozyme onto zeolite Beta particles under different pH conditions. 64

Figure 4.12: Illustration of adsorption behaviors of proteins according to pore diameters of silica particles 66

Figure 4.13: Adsorption of glucose oxidase, hemoglobin and lysozyme molecules onto silicalite, SBA-15 and functionalized SBA-15 particles. 67

Figure 4.14: The dependence of responses of glucose biosensors on weight percent of ZMTs at pH 7.4. 70

Figure 4.15: The dependence of responses of conductometric biosensors on cross-linking time in glutaraldehyde vapor for ZMTs 71

Figure 4.16: The dependence of responses of conductometric biosensors on concentration (A) and pH (B) of phosphate buffer for ZMTs 73

Figure 4.17: Calibration curves of biosensors based on immobilized urease with silicalite-2 (1), without zeolite (2), zeolite Y (3), and zeolite A (4) modified sensors. 74

Figure 4.18: Calibration curves of biosensors based on immobilized urease with NH_4^+ Beta 25 (2), Silicalite-1 (3), Silicalite-2 (4), H^+ Beta 300 (5), H^+ Beta 150 (6) and SMT (1). 75

Figure 4.19: XRD patterns of the as-synthesized and heat-treated zeolite Beta samples. 78

Figure 4.20: FE-SEM micrographs of as-synthesized zeolite Beta (left) and BEA-1 (zeolite Beta heat-treated at 500 °C with the ramp of 1 °C min^{-1}; right image) (right) crystals. 79

Figure 4.21: Absorbance FTIR spectra in the OH-stretching region of different heat-treated zeolite Beta samples recorded at 100 °C: BEA-1 (heat treated at 500 °C with the ramp of 1 °C/min), BEA-2 (heat treated at 700 °C with the ramp of 10 °C/min), and BEA-3 (heat treated at 700 °C with the ramp of 1 °C/min). 82

Figure 4.22: Calibration curves of biosensors based on immobilized BuChE (A) and urease (B), with/without heat-treated zeolite Beta samples. Measurements were conducted in 5 mM PBS, pH 7.4. 85

Figure 4.23: Operational stability of biosensors with immobilized BuChE (A) and urease (B). Measurements were conducted in 5 mM phosphate buffer, pH 7.4; BuChl and urea concentration was 5 mM. 87

Figure 4.24: Dependence of residual activity of bio-membranes based on BuChE (A) and urease (B) on concentration of glycoalkaloids and mercury ions (Hg^{+2}). Measurements were conducted in 5 mM PBS, pH 7.4. 89

Figure 4.25: XRD patterns of nano sized zeolite Beta crystals with varying Si/Al ratio 92

Figure 4.26: FE-SEM images of nano sized zeolite Beta crystals with varying Si/Al ratio, 50 (A), 75 (B), and 100 (C) 93

Figure 4.27: Calibration curves of biosensors based on immobilized BuChE (A) and urease (B), with/without nano sized zeolite Beta samples with varying Si/Al ratio. Measurements were conducted in 5 mM PBS, pH 7.4. 98

Figure 4.28: Calibration curves of biosensors based on immobilized BuChE (A) and urease (B), with/without nano sized zeolite Beta samples with varying particle diameter. Measurements were conducted in 5 mM PBS, pH 7.4. 101

Figure 4.29: Calibration curves of biosensors based on immobilized BuChE (A) and urease (B), with/without nano sized zeolite Beta samples with varying surface charge. Measurements were conducted in 5 mM PBS, pH 7.4. 103

Figure 4.30: Operational stability of biosensors based on immobilized BuChE (A) and urease (B). Measurements were conducted in 5 mM PBS, pH 7.4, BuChCl and urea concentration was 5 mM. 105

Figure 4.31: Dependence of residual activity of bioselective membranes based BuChE and urease on concentration of glycoalkoloids and mercury ions (Hg^{+2}), respectively. Measurements were conducted in 5 mM PBS, pH 7.4 107

Figure 4.32: Calibration curves of biosensors based on immobilized BuChE (a) and urease (b), with/without silica samples. Measurements were conducted in 5 mM PBS, pH 7.4. 110

Figure 4.33: Operational stability of biosensors based on immobilized BuChE (a) and urease (b). Measurements were conducted in 5 mM PBS, pH 7.4, BuChCl and urea concentration was 5 mM. 112

Figure 4.34: Dependence of residue activity of bioselective membranes based BuChE and urease on concentration of glycoalkoloids and mercury ions (Hg^{+2}), respectively. Measurements were conducted in 5 mM PBS, pH 7.4. 113

LIST OF SYMBOLS

LTA: Zeolite A

BEA: Zeolite Beta

PBS: Phosphate Buffer Saline

BuChE: Butyrylcholinesterase

BuChl: Butyrylcholine

GA: Gluteraldehyde

BSA: Bovine Serum Albumin

Con.A: Concanavalin A

Hem: Hemoglobin

LYS: Lysozyme

GOx: Glucose Oxidase

ISFET: Ion Sensitive Field Effect Transistor

EnFET: Enzyme Field Effect Transistor

ZMT: Zeolite Modified Transducer

STM: Standart Membrane Transducer

CHAPTER 1

INTRODUCTION

1.1 Zeolite and Zeo-type Materials

1.1.1 Structure of Zeolites

Within the last decade, various studies have been assigned to understanding the structural and physico-chemical properties of zeolite and zeo-type materials [1-5]. In general, zeolite and zeo-type materials are known with their three dimensional framework based on the primary tetrahedral building units (TO_4). These building units are composed of tetrahedrally bonded (T) atoms, usually either a silicon or aluminium atom, coordinated to four oxygen atoms (Figure 1.1). It is possible to build periodic channels and cavities throughout the structure by linking these tetrahedras together (Figure 1.2) [6].

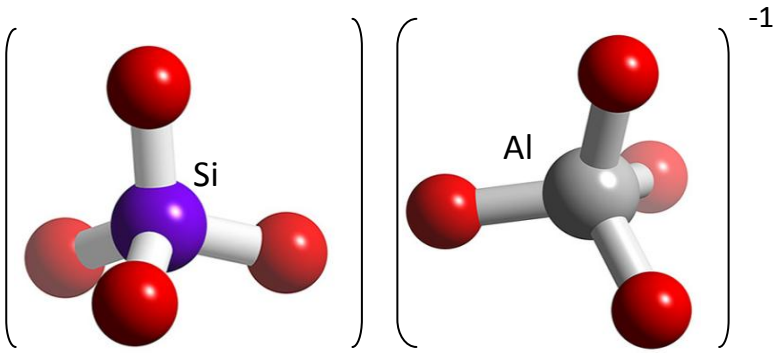

Figure 1.1: Primary building units of zeolites.

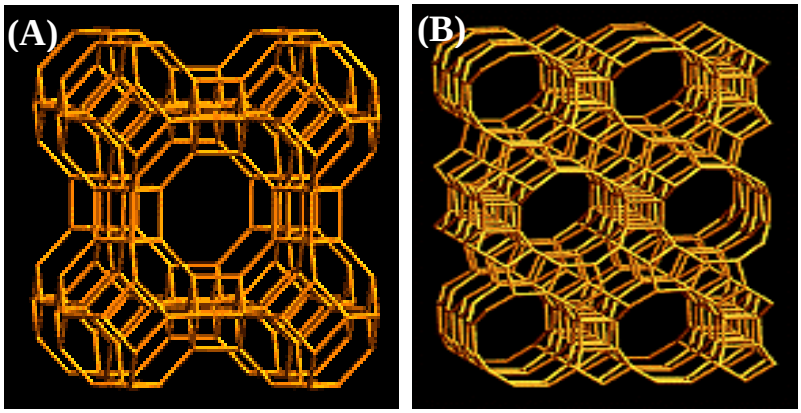

Figure 1.2: 3-D channel structure of zeolite A (A) and zeolite Beta (B).

In the structure, some Si atoms are substituted by Al atoms, resulting in a negatively charged structure that originates from the difference between Al $(AlO_4)^{-1}$ and Si tetrahedras (SiO_4) [7]. The negative sites of the Al atoms are balanced by extraframework cations, usually alkaline and alkaline earth cations,

which typically act as templates and can be exchanged by other cations (i.e., Co, Cal, P, Mg…) thus, providing zeolite with the property of ion exchange.

Zeolites are traditionally synthesized by hydrothermal reaction and can be described by a specific formula;

$$M_n (Al_nSi_{m-n}O_{2m}).xH_2O \quad (1.1)$$

where M is an extraframework cation, resides in channels and cavities, perform as template and responsible for the ion exchange capability of the zeolite material. Furthermore, the ability to tune the pore size and surface area of the zeolite and zeo-type materials is possible by simple adjustment of the type and concentration of the template material or H_2O in the synthesis formula [8-9].

Some of the principal advantages of zeolites are their low cost of extraction, their availability in great volumes, tunable surface properties and their excellent stability in chemical and thermal processes. By changing Si/Al ratio, materials possessing different hydrophobic/hydrophilic characters and acidic characters can be generated. They can also be submitted to diverse treatments (i.e., heat/acid treatment) in order to give those desired physical and chemical properties. These properties make zeolites as desirable materials in petrochemistry, environmental science, agriculture and many other fields [10-15].

1.1.2 Acidity of Zeolites

To date, external silanol groups and Brønsted acidity of zeolite materials have been investigated for their roles in the immobilization of proteins [33-34]. Using five different zeolite types, Sakaguchi et al. [50] suggested that the driving force for the adsorption of proteins on different zeolites can be due to Brønsted acid sites, which disturb the hydrophobic interaction on the zeolite surface. One of the major advantages of zeolite crystals is that their acidic/basic character can be modified by several approaches. Varying Si/Al ratio is the one way to determine the acidic strength and stability of zeolite structure [20-21]. Furthermore, by changing Si/Al ratio, crystals possessing different hydrophobic/hydrophilic characters can be generated. In general, a zeolite with high Si/Al ratio displays more hydrophobic nature and is more resistant to harsh environmental conditions such as acid and heat [22-23]. Besides, the number of charged sites in the framework has a strong influence on the capacity of cation exchange which can be controlled by varying the aluminum content in the framework [24]. On the other hand, increasing aluminum content also decreases the hydrophobicity of the zeolite. Because of this additional effect, a change in the aluminum content is responsible for the varied catalytic performances of zeolites.

Likewise, exchanging extra-framework cations with H^+ is another way to modify the acidity of the zeolites. Ion exchange can be carried out with various cationic species but ion exchange with H^+ cations leads to production of highly acidic surfaces [25]. Most interestingly, zeolites possess acidic active sites in different concentrations and the acidic properties of the zeolites can be tuned by modification of the surface acid sites by simple heat treatment applications. Heat treatment methodology is used frequently to modify the acidity, tune the porosity,

and improve the stability of zeolites [26]. The extent of acidic and other modifications induced into the zeolite depends on the harshness of the treatment, such as the heat treatment temperature and heating rate [27]. Controlled modification of zeolite acidity on biosensors can enable the investigation of the changing acidic nature of this material on the biosensor applications. Several zeolite properties which can potentially influence the biomolecule adsorption have been identified; these include the zeolite framework structure and its chemical composition, the crystal size, morphology, and defects as well as presence of mesopores. These properties determine the zeolite pore size(s), internal and external specific surface area, hydrophobicity/hydrophilicity, ion exchange capacity, the amount and strength of Brønsted acid sites, i.e., bridging hydroxyl Si–(OH)–Al groups associated with framework aluminum in tetrahedral coordination, and the amount of non-/weakly acidic silanol Si–OH groups that are present at the external crystal surface and at structural defects [28-30.]. The effects of zeolite acidity on the adsorption of biomolecules were examined using either series of different types of zeolites such as Na-Y, H-Y, H-USY, Na-BEA, etc., with various Si/Al ratios or different samples of the same zeolite type with different Si/Al ratios [31-34]. Because of this, the variation in the crystal Si/Al ratio and the associated acidity was also accompanied by the changes in the zeolite crystal structure, size, and/or morphology. Thus, the sole effect of zeolite acidity on the biomolecule adsorption was in fact not examined in these investigations.

It is well established that adjustment in the chemical composition and the framework of the zeolite has a strong influence on the surface acidic groups [35-37]. In fact, it is well known that the number and types of bridging hydroxyl groups Al–(OH)–Si (Brønsted acid sites) and surface silanol groups (OH)-Si (i.e., isolated, vicinal, etc) (Figure 1.3) which can be characterized by their strong OH

stretching bands in the 3610 and 3745 cm^{-1} region measured by IR Specroscopy respectively, can lead to higher or lower activities in many different catalytic reactions and adsorption processes [38].

(A)

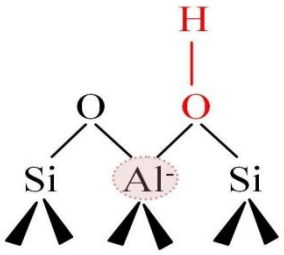

(B)

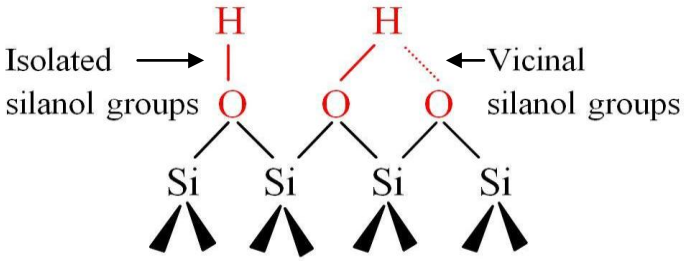

Figure 1.3: Shematic representation of Brønsted acid sites (A) and silanol groups (B) of zeolite.

1.2 Importance of Protein Monitoring in Biotechnology

In the last few decades, protein monitoring has gained more attention for the direct quantification of environmental pollutants and concentration of fundamental products in human metabolism. Urea, glucose and butyrylcholine are three crucial proteins commonly used for the determination of pollutants in the environment and numerous disorders in the human body.

Urea, an important product of an organism's vital activity, is present in water environment at considerable concentrations. It can occur from sewers of industrial and sanitary water as well as from surface drainage in the regions where urea is used as nitric fertilizers. Urea accumulation in water can also result from natural biochemical processes, metabolism of aquatic species and be produced by plants, fungi, bacteria because of ammonia binding during protein degradation. Enzymatic processes in water environment also have an effect on urea concentration. Increase in urea concentration can indicate to pollution of the water object with agricultural and domestic sewage. Usually it is accompanied with intensification of processes of urea utilization by aquatic organisms and oxygen consumption which results in deficient oxygen condition. In uncontaminated river water urea concentration is 60-300 $\mu g/dm^3$, in lakes and other ponds 40-250 $\mu g/dm^3$; the highest levels are observed in summer and autumn [39].

Furthermore, glucose is another important product of fundamental activity of organism, and plays a crucial role in sugar metabolism. Determination of glucose concentration in blood is essential since insulin deficiency and hyperglycemia cause one of the important diseases, diabetes. This metabolic disorder is observed by blood glucose concentrations higher or lower than the normal range of 80-120

mg/dL (4.4-6.6 mM) [40]. The diabetes is one of the leading causes of death and disability around the world. For this reason, continuous and rapid monitoring of sugar level in the human blood is essential.

Moreover, BuChE is commonly used for the detection of several kinds of organophosphorous pesticides [41]. These kinds of pesticides are among the most toxic of all substances that cause serious poisoning in animals and humans, thus rapid measurement of toxicity level is a crucial step before the clinical treatment.

Above-stated consideration causes a challenge of permanent monitoring of urea, glucose and butyrylcholinesterase concentrations in environment and human body. Novel bioanalytical devices, i.e. biosensors, seem to be promising for this purpose since they have high sensitivity, rapid selectivity and wide measurable range.

1.3 Protein Immobilization

Nowadays, it is well established that the many technologies require protein immobilization on different kinds of substrates. This can allow proteins to be easily reused for several times in the application process by increasing their half life, stability and resistance to changes in conditions (i.e. pH, temperature…) [42]. Furthermore, immobilization of proteins on substrates allows development of multienzyme reaction systems which are widely used in biotechnological applications and industry [43]. These benefits of immobilized proteins make them highly applicable to a range of evolving biotechnologies.

1.3.1 Protein Immobilization Techniques

Immobilization of proteins onto support materials can be performed by using different approaches (Figure 1.4). The proteins can be cross linked to the support material by applying several cross linkers such as GA or they can be entrapped without employing any cross-linker but in this case most of the time the matrix needs to be functionalized before the immobilization [42]. The major disadvantages of these methods are that the applying chemicals into the medium which can leads to formation of covalent bonds and finally cause a number of damage to the enzyme and reduce its stability and activity.

Another approach is the adsorption of proteins onto support surfaces. In this case, weak interactions such as Van-der Waals, hydrogen bond or electrostatic forces occur between the protein and the support surface. The main advantages of this method are that it is simple to perform, cheap and no further treatment of the support is needed [33]. On the other hand, leaching proteins from the support surface or denaturation of proteins according to the surface chemistry of support are the main disadvantages of physical adsorption method.

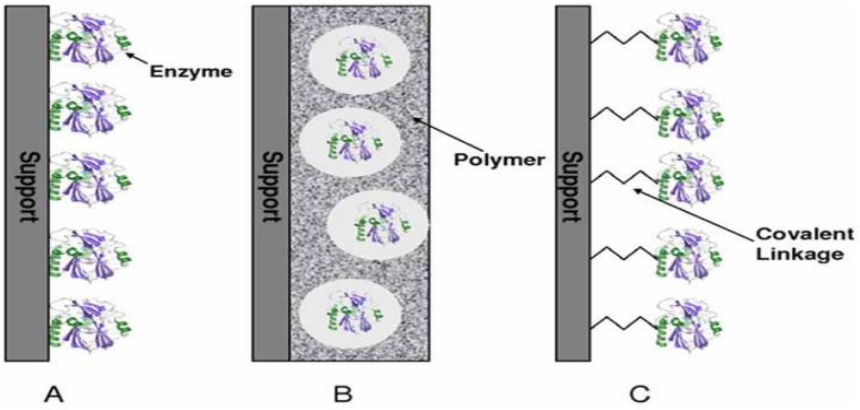

Figure 1.4: Shematic representation of widely used approaches for the immobilization of proteins; physical adsorption (A), entrapment (B), cross linking (C) [44].

Nowadays, immobilization of enzymes on electrodes in the design and optimization of biosensors and incorporation of nanomaterials into the biosensing have attracted great interest. Immobilization is the key-step in biosensor construction, but, regardless their peculiar advantages, the conventional methods for biomolecule immobilization (physical adsorption, covalent binding, cross-linkings and entrapment in gels or membranes) have, in general, low reproducibility and poor spatially controlled deposition, a crucial problem for the development of commercial miniaturized bio-sensors [45]. In the next context, the use of nanomaterials for the construction of biosensing devices constitutes one of the most exciting approaches. The extremely promising prospects of these devices accrue from the unique properties of nanomaterials, i.e., high surface area, local chemical environment, tailorable surface groups.

1.3.2 Immobilization on Support

Application of nanomaterials in biosensors allows the use of many new signal transduction technologies in their manufacture. Nanomaterials can be used in a variety of electrochemical biosensing schemes thereby enhancing the performance of these devices and opening new horizons in their applications. The success of immobilization of enzymes depends strongly on the properties of the carriers employed. The carrier material should have a high capacity to bind enzyme, should be mechanically stable and must not have reduced the enzymatic activity.

The organic supports like polymers lead to a number of problems such as poor stability and disposal issues [46]. In contrast, inorganic materials such as silica and alumina are thermally and mechanically stable and strong [47-48]. Among different types of nanomaterials, zeolites have proven to be excellent alternatives for use in selective adsorption of biopolymers, like proteins, DNA, and RNA. According to the literature, zeolite crystals and membranes are widely used as adsorbent materials for the immobilization of various proteins, cells, and nucleic acids. Various types of interactions such as hydrophilic and hydrophobic, electrostatic, and structural have been observed between the biomolecules and the zeolite support [32, 50-54]. Some of the principal advantages of zeolites are their large specific surface areas, tunable surface properties, adjustable surface charge, and dispersibility in aqueous solutions. Furthermore, adjustable hydrophilicity of zeolites, which is a function of crystal Si/Al ratio, plays an important role in the immobilization of biomolecules [49, 31]. These properties make zeolites promising alternative candidates for the immobilization of enzymes and incorporation into biosensing devices. A sensor prepared by incorporating zeolites into the electrode coating has the potential to exhibit all the advantages governed

by the zeolite properties. Thus, the research in the field of zeolites introduced into the electrode coatings has been pursued by a number of groups who are actively working in this area [55-59].

1.4 Principles of Electrochemical Biosensors

Quantification of biochemical reactions are one of the most important process for all kinds of medical, chemical, and biotechnological applications. In order to monitor those reactions, different kinds of devices have been developed worldwide which can be capable of converting the biological signal directly into an electronic signal whose amplitude depends on the concentration of defined analytes in the analyte solution. Due to their unique advantages such as easiness, fastness and inexpensiveness and ability to analyze the biological content as electric signal, electrochemical biosensors have gained more and more attraction in the last few decades.

Functionally, an electrochemical biosensor is a device that contains two basic components; a biomatrix, i.e., immobilized layer of bioelements (proteins, cells, and organalles) and a tranducer (conductometric, amperometric or potentiometric…) which is capable of transferring the output signal of biomatrix to electric signal. Details of the principles of conductometric and ISFET type biosensor will be given in the following section.

1.3.1 Conductometric Biosensors

Compared to other types of electrochemical biosensors, not much work has been done about the conductometric biosensors. Biosensors based on the conductometric principle present a number of advantages: a) thin-film electrodes are suitable for miniaturisation and large scale production using inexpensive technology, b) they do not require any reference electrode, c) transducers are not light sensitive, d) the driving voltage can be sufficiently low to decrease significantly the power consumption, e) large spectrum of compounds of different nature can be determined on the basis of various reactions and mechanisms.

Conductometric biosensors are based on the fact that almost all enzymatic reactions involve either consumption or production of charged species and, therefore, lead to a global change in the ionic composition of the tested sample [60].

The conductometric transducer is an interdigitated two-electrode device which is capable of quantifying the conductivity of the biomatrix layer adjacent to the electrode surface. The enzymatically produced ions are able to provide a significant change of conductivity which is quantified by the ionic difference between two parallel electrodes, i.e., one with enzyme and identical one without enzyme, in the working solution. The enzyme is immobilized on the working electrode through cross-linking with BSA (bovine serum albumin) by glutaraldehyde while only BSA is cross linked on the reference electrode. Design of the interdigitated conductometric transducer (with a reference and a working electrode) and of the experimental set-up for conductometric measurements is shown in Figure 1.5.

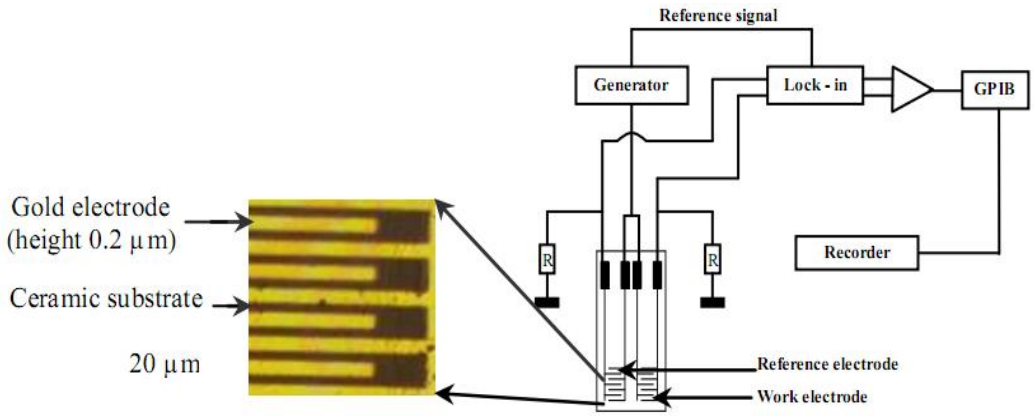

Figure 1.5: Design of the conductometric transducer (with a reference and a working electrode) and of the experimental set-up for conductometric measurements [60].

Conductometric measurement can be done with a simple set-up shown in Figure 1.5. Conductometric measurements with each pair of interdigitated electrodes were performed by applying a small-amplitude alternating voltage of 100 kHz generated by a low-frequency wave-form generator. The reason for choosing the low frequency indeed, at frequencies higher than 10 kHz, the impedance of diffusion can be neglected. The differential output signal between working and reference sensor was recorded using a lock-in amplifier and the data of the biosensor were recorded as a function of substrate concentration. Acquired data can be stored and analyzed by the computer or data plotter.

1.3.1 ISFET Biosensors

ISFETs are miniaturized silicon-based semi-conductor devices used to quantify ion concentrations in the analyte solution. In general, a field-effect transistor (FET) contains three components, the source, drain, and gate. Current flow in the gate voltage is adjusted by the voltage between the drain and source. Voltage affects the electrical field of the transistor by extending or reducing the conductivity of the electron flow from source to drain. In order to configure the FET device as a biosensor, gate terminal has to be modified with molecular receptors or ion-selective membranes for the analyte of interest (i.e., EnFET, ISFET, etc).

One of the most popular methods for the construction of FET-based biosensing devices is the creating a biochemically sensitive surface by immobilization of enzymes at the gate surface of pH-sensitive ISFET devices, and such devices are named as EnFET. Exclusively, enzymatic reactions result in changes of H^+ concentration leading to alteration of solution pH in the gate terminal, which allows the usage of pH-sensitive field-effect transistors as tranducers in ENFET type biosensors. Among various types of biosensors, ion-sensitive field-effect transistors (EnFETs) are among the most attractive selections due to their extensive advantages such as simplicity of use, potential miniaturization, portability, and low cost. Such biosensors are powerful sensing tools provide various opportunities for developing a new generation of biosensor technologies.

The sequence of ISFET line production included the following basic operations: thermal oxidization of silicon plate to oxide thickness of 0.6 micrometer; opening of window in oxide for forming of n+-area for the contact to substrate with next

two-stage diffusion of phosphorus; opening of windows in oxide for diffusion buses of ISFET source and drain with next two-stage diffusion of boron; opening in the oxide of gate window and forming of two-layer gate dielectric: at first thermal oxidization of silicon is conducted in dry oxygen at the temperature of 1000^{o}C to thickness of 50 nm, then deposition of Si_3N_4 film of 50 nm thick in the reactor of reduced pressure from mixture of dichlorsilane and ammonia at the temperature of 800^{o}C; after opening in the oxide of windows to diffusion area the evaporation of aluminium is conducted for forming of electric contacts to the transistor outlets and substrate. With the purpose of improvement of sensor stability the operations of the high temperature annealing of silicon crystals were entered in a technological cycle in the atmosphere of hydrogen.

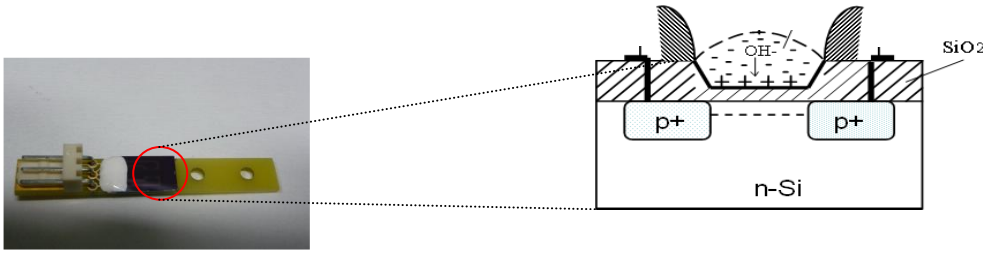

Figure 1.6: Schematic picture of separated p-channel ISFET, its gate is coming to contact with electrolyte solution.

EnFET measurement can be done with a simple transducer shown in Figure 1.6. The EnFET sensor chip contains two identical p-channel transistors on the same crystal. The diffusion p^+-buses with contacts to the drain and source of each transistor are coming out on the edge of the chip along with an outlet to the built-in reference microelectrode. To prevent formation of a parasitic conductivity channel between p^+-areas of two transistors, the chip has a 50 μm wide protecting division n^+-line with a contact to the substrate. Zigzag geometry of the transistor gate area with the width-to-length ratio 100:1 ensures sufficient steep slope of the transfer characteristic. A window etched in an oxide layer for growing gate dielectric replicates the channel geometry with a 7 μm overlapping. A "saturated calomel" reference electrode is used to maintain the potential between the back contact of the ISFET and the solution. The output signal of the biosensor was recorded as a function of substrate concentration. Acquired data can be stored and analyzed by the computer.

CHAPTER 2

LITERATURE REVIEW

2.1 The Role of Adding Zeolite and Zeo-Type Materials on Enzymatic Studies

Over the last few decades numerous researches into enzyme immobilization technology concentrated on using nanoparticles as potential carriers [61-63]. Immobilization of enzymes on a solid support is definitely the most important difficulty in biotechnology. The success of immobilization of enzymes depends strongly on the properties of the carriers employed. The carrier material should have a high capability to bind protein, should be thermally and mechanically stable, reusable and must not have reduced the enzymatic activity. The organic supports like polymers generally suffer from poor stability and reusability. On the contrary, inorganic materials such as silica and alumina are strong and stable even in extreme conditions [64].

Among different types of nanomaterials, zeolites have proven to be excellent alternatives for use in selective adsorption of biopolymers, like aminoacids, proteins, and nucleic acids, due to their increased surface area, tunable hydrophilic/hydrophobic properties and Brønsted acidity by controlling the Si/Al ratio as well as their thermal and mechanical stabilities [32, 50-51]. In this way higher stability and increased activity of the enzyme can be obtained [65].

In general, the presence of zeolite leads to increased enzyme activity [66], however the exact reason behind such enzymatic activities and the nature of zeolite-protein interactions are still under a lot of debate. In fact, with case of zeolite crystals and membranes it is observed that varied types of interactions exist between the biomolecule and the zeolite support. The interaction between biomolecules and surfaces is complicated since forces such as hydrophilic and hydrophobic, electrostatic and structural interactions are involved to a greater or lesser extent [53-54, 67]. In the literature, zeolite Y and silicalite are the commonly used potential carriers for immobilization of different types of proteins like lipase [60, 66], albumin [68], and trypsin [69] in biotechnological processes. In such studies, which used zeolites as potential carriers for protein immobilization, higher stability, reusability, and productivity were observed. Furthermore, hydrophobicity, pore size, particle size and acidity are the mostly discussed properties that are shown to affect the adsorption and biosensor performances.

2.1.1 Effect of Hydrophobicity

Commonly, the parameters that affect the immobilization of biomolecules on zeolites were examined using different types of zeolites such as Na-Y, H-Y, H-USY, Na-BEA, etc., with various Si/Al ratios, and thus various acidic and hydrophilic properties [70-71]. However, because different zeolites were used in these investigations, the variation in the crystal Si/Al ratio and acidity was also accompanied by the changes in the zeolite morphology. However, studying varying factors like pore size and/or Si/Al ratio using different zeolite types of different morphologies may lead to more complications to draw some conclusions

For instance, comparing enzymatic activities using different types of zeolites (i.e., comparing the effect of Si/Al ratio by utilizing zeolite Na-Y and zeolite Na-Beta with Si/Al = 5.7 and 27.4 respectively [32] can be misleading because once the morphologies change, a lot of other factors, such as surface groups, pore sizes, effect of differing structure directing agents, etc. also effect the interaction of zeolites with the guest molecules. In order to overcome this drawback, zeolites with identical morphologies are used and compared in only some studies in the literature. Krohn and Tsapatsis studied phenylalanine adsorption on zeolite beta crystals with varied Si/Al ratio and they concluded that the higher adsorption at lower Si/Al ratio was observed [72]. The same behavior for the adsorption of tryglycine was also seen in the work of Wijntje [49]. Alternatively, Calgaroto currently published that Si/Al ratio of zeolite MCM-22 has a significant influence on the immobilization yield and enzymatic activity of lipase due to adjusted acidity of zeolite MCM-22 [73].

2.1.2 Effect of Pore Size

The adsorption of biomolecules on zeolite and zeo-type materials offers the potential improvement of the biomolecule activity and stability even under excessive conditions. Although microporous nature of zeolite and zeo-type materials is commonly used as adsorbents for a number of chemical reactions, they are not capable of adsorb large biomolecules such as proteins, enzymes or nucleic acids, caused by the limitation of microporous size. For this reason, mesoporous molecular sieves are one of the most attractive materials that have been paid much attention in recent years [74-76]. Due to their high capability to bind proteins, thermal and mechanical stability, tunable pore diameters, and high

surface areas, mesoporous molecular sieves with highly regular pore geometries are the ideal candidates for the adsorption processes [77-78]. There have been a number of reports describing the use of mesoporous molecular sieves as biomolecule carriers in the literature [79-84]. Miyahara and Yiu demonstrated that the amount of myoglobin and trypsin molecules adsorbed on MCM-41, SBA-15 and MCM-48 was strongly related with the pore size of the employed molecular sieves [85-86]. Balkus studied SBA-15, MCM-41, and MCM-48 as carriers for the immobilization of enzymes [87-88]. Along with their study, it was proposed that the immobilization of enzymes mainly occurs in the mesoporous structures of the material and adsorbed amount are strongly related with the pore size of the molecular sieves and enzyme molecules retain their activities after adsorption. Moreover, Goradia and Stucky reported that the activity, storage stability and reusability of the trypsin and conalbumin molecules can be increased by using mesoporous sieves as adsorbents [89-90].

2.1.3 Effect of Particle Size

In the literature, various studies can be found about the effect of particle size on the immobilization of biomolecules. Lundqvist [91] stated that the surface curvature of silica particles has a strong influence on the conformational change of human carbonic anhydrase which may affect its activity. Increased particle size causes a higher degree of conformational change of related protein. The same behavior for the adsorption of lysozyme was also seen in the work of Vertegel [92]. On the other hand, Hu [93] stated that the decreasing particle diameter of zeolite L crystals causes an increase in adsorption of cytocrom c, transferring, and myoglobin due to increasing surface area.

2.1.4 Effect of Zeolite Acidity

Different hydrophobic/hydrophilic characters can be created by simply changing Si/Al ratio of zeolite and zeo-type materials. On the other hand, increasing Al content also decreases the hydrophobic behavior of the zeolite. Because of this further effect, a change in aluminum content is responsible for both hydrophobicity and acidity of zeolitic material.

In the literature, numerous acidity studies were done by eliminating the differences through employing the zeolite with same morphology such as Krohn et al. [19] and Wijntje et al. [49]. They compared the effect of Si/Al ratio of zeolite BEA and FAU, respectively. In the study of Wijntje et al., as Si/Al decreases, adsorbed amount of tryglycine molecules increases as a result of increasing acid sites of the zeolite FAU. They also stated that the Ca^{2+} and H^{+} exchanged FAU particles adsorbed more triglycerin than as-synthesized Na-FAU due to altered acidity and electrostatic field on the zeolite surface. Likewise, similar type of behavior was observed in the study of Krohn et al.

2.2 Enzyme Immobilization on Zeolite Surfaces

The use of zeolites in combination with enzymes have been of interest for a while due to some of their particular properties, such as tailorable surface groups, controlled hydrophilic/hydrophobic properties, shape, charge, and size selectivity, and their ability to regulate acidity for bi-functional enzymatic-acid catalysis. Furthermore, they are stable at high temperatures, insoluble in organic solvents,

and resistant to harsh experimental conditions. Thus, they have been used to control the micro-environment of enzymes [94]. With such interesting properties, zeolites can offer themselves as alternative materials to be used for functionalizing solid substrates in a controlled manner.

2.3 Zeolite and Zeo-Type Materials in Biosensor Applications

Development of biosensors based on immobilized enzymes solves several problems such as loss of enzyme, reduced enzyme stability, and sensitivity. Nowadays, immobilization of enzymes on electrodes in the design and optimization of biosensors and incorporation of nanomaterials into the biosensing devices have attracted great interest [64, 95].

In the literature, there are various reports about immobilization of enzymes on the transducer solid substrates with some supporting materials such as sol-gels [96-97], polymeric membranes [98, 60], and microcapsules [99-100]. These approaches can increase the adsorption capability of the solid substrate, but also reduce the catalytic activity [101] with an increased response time [102].

The aim in biosensor research is to improve the performance and long-term stability of enzyme transducers. Such developments can be attained by the modification of transducer surfaces by zeolitic materials. However, in order to use zeolites as alternative materials for enzyme immobilization and integrate them into such biosensor devices, the possibility to develop a simple and general technique to engineer the transducer surfaces for immobilization of biomolecules should be investigated [68-69]. In this way, the potential advantageous roles for

integrating zeolites can be explored by adsorbing enzymes on the surface of appropriate zeolites to obtain microdevices with high-sensitive biocatalytic function and long life biosensor property. Liu et al. described the new approach to construct an amperometric biosensor based on glucose oxidase by using dealuminized Y zeolite (DAY) modified platinum electrodes. Constructed sensors exhibited high sensitivity, stability, reproducibility and selectivity according to the framework properties of zeolite Y (i.e., surface area, pore size distribution, acidity…) [70]. Alain Walcarius made an attempt to classify the wide range of different fabrication procedures into 7 classes in his review [103]. These methodologies basically consist of adding/mixing zeolite particles with different composite materials, such as polymers and carbon paste and covalently tethering clay particles to the electrode surfaces.

CHAPTER 3

EXPERIMENTAL

3.1 Synthesis of Zeolite and Zeo-Type Materials

3.1.1 Zeolite A (LTA) with Varying Particle Size

Zeolite A crystals were hydrothermally synthesized using molar composition 1.94 Na_2O : Al_2O_3 : 0.84 SiO_2 : 194 H_2O : 0.5-4 TEA. In this preparation, sodium hydroxide and sodium aluminate were dissolved in deionized water in a 120 mL high-density polyethylene (HDPE) bottle. After dissolving these components, solution were stirred for 40 min and kept statically at 100 °C in a conventional oven, forming the Al precursor solution. The mixture then removed from the oven after 50 min. Then, in order to obtain varying particle diamaters of Zeolite A crystals, different concentrations (0.5, 1, 1.5, 2, and 4) of tetraethanolamin solution (TEA), which is the structure directing agent (SDA) for Zeolite A synthesis, was added and the prepared precursor solution was stirred thoroughly. For preparation of the Si precursor solution, sodium metasilicate pentahydrate was added to deionized water in another 120 mL HDPE bottle and hand-shaken for 5 min. Then Si precursor solution was poured into Al precursor solution. The resulting mixture (white, viscous gel) was hand-shaken for 5 min. The static synthesis was carried out for 1-4 days at 100 °C; the products were cooled to

room temperature, filtered, washed with deionized water, and dried overnight in ambient air at ~70 °C.

3.1.2 Zeolite Beta (BEA) with Varying Si/Al Ratio

Sub-micron Zeolite Beta crystals were hydrothermally synthesized using molar composition 1.92 Na_2O : Al_2O_3 : 30-120 SiO_2 : 444 H_2O : 4.6 $(TEA)_2O$. In this preparation, sodium hydroxide and sodium aluminate were dissolved in deionized water in a 120 mL high-density polyethylene (HDPE) bottle. After dissolving these components, solution were stirred for 40 min and kept statically at 100 °C in a conventional oven, forming the Al precursor solution. The mixture then removed from the oven after 50 min. Then tetraethyl ammonium hydroxide solution (TEAOH), which is the structure directing agent (SDA) for zeolite Beta synthesis [104], was added and the prepared precursor solution was stirred thoroughly. For preparation of the Si precursor solution, in order to obtain varied Si/Al ratio of Beta crystals, different concentration of Ludox® HS-40 colloidal silica solution (30, 50, 60, and 120) was added into aluminate precursor and hand shaken for 5 min. The resulting mixture (white, viscous gel) was transferred into 10 mL Teflon-lined stainless steel autoclaves. The static synthesis was carried out for 7 days at 393 K; the products were cooled to room temperature, filtered, washed with deionized water, and dried overnight in ambient air at ~70 °C.

Nano sized Zeolite Beta crystals were hydrothermally synthesized using molar composition 0.25-0.50 Al_2O_3 : 25 SiO_2 : 490 H_2O : 9 TEAOH [105]. In this preparation, aluminum isopropoxide and tetraethyl ammonium hydroxide (TEAOH) were dissolved in deionized water in a 120 mL high-density

polyethylene (HDPE) bottle with stirring. After dissolving the component, in order to obtain varied Si/Al ratio of Zeolite Beta crystals, different concentration of Si precursor solution (0.25, 0.35, and 0.50), tetraethoxy silane (TEOS), was added and the prepared precursor solution was stirred thoroughly. The static synthesis was carried out for 14 days at 100 °C; the products were cooled to room temperature, centrifuged at 13000 rpm, washed with deionized water, and dried overnight in ambient air at ~70 °C.

3.1.3 Silicalite and SBA-15 Synthesis

Silicalite crystals were hydrothermally synthesized using molar composition 1 TPAOH : 4 TEOS : 350 H_2O. In this preparation, tetraethylorthosilicate (TEOS) and tetrapropyl ammonium hydroxide (TPAOH), which is the structure directing agent (SDA) for silicalite synthesis, were dissolved in deionized water and hand shaken for 5 min. The resulting mixture (white, viscous gel) was transferred into 10 mL Teflon-lined stainless steel autoclaves. The static synthesis was carried out for 1 day at 403 K; the products were cooled to room temperature, filtered, washed with deionized water, and dried overnight in ambient air at ~70 °C.

SBA-15 particles were hydrothermally synthesized using molar composition 1 TEOS : 0.017 P123 : 0.6 Mesitylene : 1 KCl : 5.85 HCl : 165 H_2O [106]. In this preparation, potassium chloride, hydroxyl chloride, mesitylene and tetraethylorthosilicate (TEOS) were dissolved in deionized water and hand shaken for 5 min. The resulting mixture (white, viscous gel) was transferred into 10 mL Teflon autoclaves and kept statically in 35 °C for 24 h. After 24 h, the temperature was raised to 100 °C and the static synthesis was carried out for an additional 24

h; the products were cooled to room temperature, filtered, washed with deionized water, and dried overnight in ambient air at ~70 °C.

3.2 Modification of Zeolite and Zeo-type Materials

3.2.1 Functionalization of Zeolite BEA and SBA-15

Post-synthetic functionalization procedure of zeolite Beta and SBA-15 particles were carried out in a reflux system (Figure 3.1) at ~100 °C. In order to examine the influence of surface charge of zeolite Beta and SBA-15 on the protein adsorption process and analytical characteristics of ISFET based biosensors, two different approaches were used to attain high degree of functionalization.

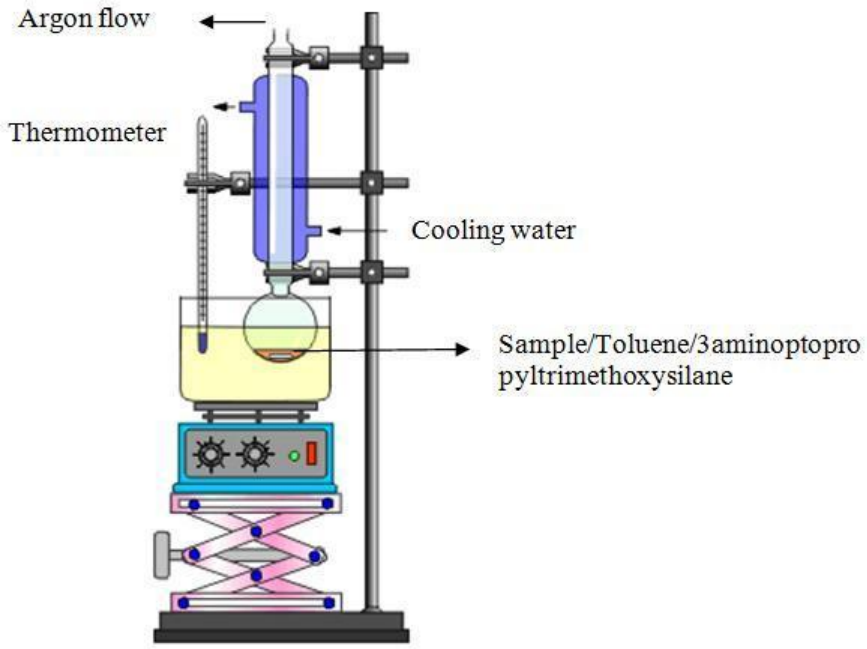

Figure 3.1: Shematic presentation of reflux system [107].

In the first functionalization process, 5 g zeolite Beta samples were placed in a 250 mL toluene solution containing 18 mL 3-aminoptopropyltrimethoxysilane (3-APTES) and refluxed under argon for 18 hours at 100 ºC. The products were cooled to room temperature, filtered, washed with 200 ml toluene and ethanol, and dried overnight in ambient air at ~70 °C. [108]. In the second procedure, 134 mg zeolite Beta or SBA-15 samples were refluxed in a 20 mL toluene solution containing 1.6 mL APTES for under argon for 2 hours at 100 ºC. After being cooled to room temperature, zeolite BEA powders were collected by filtration and dried in an overnight in ambient air at ~70 °C. [109]. The procedure shows the highest functionalization were then used for the functionalization of SBA-15 particles.

3.2.2 Ion Exchange of Zeolite Beta

Sub-micron zeolite Beta crystals were ion exchanged with calcium, cobalt, copper, manganese, ammonium, magnesium and iron ions by using liquid phase ion exchange procedure. In this procedure, as-synthesized zeolite Beta crystals were calcinated at 550 °C in air for 24 h and used as starting materials for ion exchange experiments. Calcined zeolite Beta crystals (10 mL nitrates/g zeolite) were then suspended in an aqueous solution of 1 M calcium, cobalt, copper, manganese, ammonium, magnesium and iron nitrates and stirred for 3 h at 80 °C. The proton forms were made by calcinations of ammonium exchanged zeolite Beta crystals at 550 °C [110]. Each experiment was repeated three times to achieve a high degree of ion exchange. The products were then cooled to room temperature, filtered, washed with deionized water, and dried overnight in ambient air at ~70 °C

3.2.3 Heat Treatment of Zeolite Beta

Sub-micron zeolite Beta crystals were subjected to different heat-treatment protocols which the TEA^+ cations were removed and H^+ forms of zeolites were formed with varying acidity as a function of the harshness of the heat treatment. The H^+ forms of these samples were named as BEA-1, BEA-2, and BEA-3. In these procedures, ammonium exchanged zeolite Beta crystals were used as starting materials. In the first procedure, 0.2 g of parent material, NH_4-BEA, was placed into crucible and heat-treated in a conventional furnace under ambient air. Then sample was heated from 25 to 500 °C at a rate of 1 °C/min, maintaining 500

°C for 6 h, and then cooled to 25 °C. In the second procedure, NH_4-BEA samples were heated from 25 to 700 °C at a rate of 10 °C / min, maintaining 700 °C for 6 h, and cooled to 25 °C. In the final procedure, NH_4-BEA samples were heated from 25 to 700 °C at a rate of 1 °C/min, maintaining 700 °C for 6 h, and cooled to 25 °C [111].

3.3 Material Characterization

3.3.1 X-Ray Diffraction

Phase identification of the zeolite A (LTA), zeolite Beta (BEA), and silicalite particles were done by powder X-Ray diffraction analysis (XRD) using Ni filtered Cu-Kα radiation (Philips PW 1729). The voltage and current were 40 kV / 30 mA, respectively. The diffraction peaks were scanned between 5-40° 2θ degrees with step size of 0.03° and 0.1°/s. Time constant was 1s, and slit was 0.2 mm (CAMMP Laboratory, Northeastern University, Boston, USA).

Small-angle X-ray scattering (SAXS) patterns of the SBA-15 samples were acquired on a Nanostar U small-angle X-ray scattering system using Cu-K radiation. The d-spacings were calculated directly from the scattering patterns by d = 2/q.

3.3.2 Scanning Electron Microscopy

The field emission scanning electron microscope (FE-SEM) images of zeolite A, Beta, Silicalite and SBA-15 were acquired for AuPb coated samples using a Hitachi S-4700 FESEM (accelerating voltage 2 kV, beam current 10 μA) in the secondary electron imaging mode (CAMMP Laboratory, Northeastern University, Boston, USA). Crystal morphology/texture/surface features of all zeolites were also examined by scanning electron microscopy (FE-SEM) (400 Quanta FEI) (Central Laboratory, METU, Ankara, TURKEY). The energy dispersive X-ray spectroscopy (EDX) analysis of the all samples was carried out to determine crystal Si/Al ratios utilizing a Phoenix EDAX X-ray analyzer equipped with Sapphire super ultrathin window detector attached to the Hitachi S-4700 FE-SEM (accelerating voltage 12 kV, beam current 10 μA).

3.3.3 Surface and Pore Size Analysis

To investigate the difference of pore openings and surface areas of zeolite and zeo-type materials, surface and pore size analysis were carried out. The nitrogen adsorption/desorption experiments were carried out by Autosorb 6 series (Quantachrome Instruments) instrument. Surface area of the samples was obtained by Multipoint BET, while external surface area was obtained by t-plot method. P/P_0 of microporous (zeolite A and Beta) and mesoporous (silicalite, SBA-15) materials were 0.01-0.1 and 0.05-0.3, respectively. Sample preparation method includes outgassing samples under vacuum at 27 °C for 5 h before analysis (Central Laboratory, METU, Ankara, TURKEY).

3.3.4 Zeta Potential

The zeta potential of zeolite Beta, Silicalite, and SBA-15 particles were obtained by a zeta potential measurement system (Malvern, Nano ZS90) at 25°C (Central Laboratory, METU, Ankara, TURKEY). The particles were dispersed in deionized water (solid load is 1 wt %) and ultrasonicated for 1 h. After the ultrasonication, zeta potential was measured as a function of pH by titration with 0.1 M HCl or 0.1 M NaOH.

3.3.5 Fourier Transform Infrared Spectroscopy

For the analysis of the OH-stretching region (4000–3200 cm^{-1}), diffuse reflectance infrared Fourier-transform (DRIFT) spectra were acquired at 100 ◦C on a Nicolet Magna-IR 560 spectrometer supplied with a DTGS KBr detector and a Spectra-Tech diffuse reflectance high-temperature/vacuum chamber with KBr windows (CAMMP Laboratory, Northeastern University, Boston, USA). The samples were under dry nitrogen (99.9% purity with < 10 ppm moisture content) flowing at 33 mL/min (STP) during the heat treatment in the chamber and during spectra acquisition. For the dehydration of the samples, the cell was heated to 350 ◦C for 2 h. Subsequently, the spectra were collected after the samples were cooled to 100 ◦C, at 10 min. Potassium bromide was used as the background and the catalyst samples were analyzed neat. Before collection of the IR spectrum, nitrogen was purged through the beam path at 14 L/min (NTP). The spectra were collected with resolution of 2 cm^{-1} using 128 scans.

3.4 Protein Adsorption

Materials

Bovine serum albumin (BSA), Concanavalin A, Butyrylcholinesterase, Glucose oxidase, Hemoglobin, Lysozyme, and Soybean Urease, were purchased from Sigma-Aldrich Chemie. Phosphate solution (KH_2PO_4-NaOH) and acetate solution ($C_2H_4O_2$ - $C_2H_3NaO_2$) were chosen as working buffers. The compounds for buffer preparation as well as other inorganic compounds used were of analytical grade.

Method

Adsorption experiments were carried out by contacting the 0.2 mg/ml of zeolite A, zeolite Beta, Silicalite, and SBA-15 particles with 0.2 mg/ml proteins in 20 mM of appropriate buffer. The adsorbent zeolites and protein solution were stirred at 120 rpm for 2 h. The equilibrated samples were centrifuged for 20 min then the supernatants were analyzed by UV-Vis Spectroscopy.

3.4.1 UV-VIS Measurement

The UV-visible spectra of the adsorbed proteins in diffuse reflectance mode were recorded on a Carry 5000 UV-VIS spectrophotometer from at 280 nm (CAMMP

Laboratory, Northeastern University, Boston, USA). Spectra were recorded in the liquid form by squeezing a small amount of liquid in a holder. A mass balance then was applied to calculate the protein adsorbed on the zeolite crystals. To calculate the adsorption amounts accurately, a standard curve at λ: 280 nm was done by using a series of protein solutions with different concentrations. A blank run was performed with each experiment for good control in experimental conditions.

3.5 Biosensor Measurement

Materials

The frozen-dried preparations of enzymes used in the experiments were as follows: glucose oxidase (GOD) from Penicillium vitale (EC 1.1.3.4) with specific activity of 130 U/mg from Diagnosticum (L‟viv, Ukraine); urease from soybeans (EC 3.5.1.5, type B) with activity of 22 U/mg, Butyrylcholinesterase (activity index of 22 U/mg), Bovine serum albumin (BSA) (V fraction) and 50 % aqueous solution of glutaraldehyde (GA) were obtained from Sigma-Aldrich Chemie. Glucose, urea, and Butyrylcholine were used as a substrate and analyzed substance, potassium-phosphate solution (KH2P04-NaOH), pH 7.4 from Merc was used as a buffer. All chemicals were of analytical reagent grade and used as received without additional purification.

Enzymatic Reactions

The key enzymatic reactions used for glucose, urea and butyrylcholine determination by biosensor based on immobilized glucose oxidase, urease and butyrylcholinesterase are shown below.

Substrate enzymatic transformation results in generating substances such as gluconolactone and hydrogen peroxide, causes change in conductivity measurable by conductometric transducer.

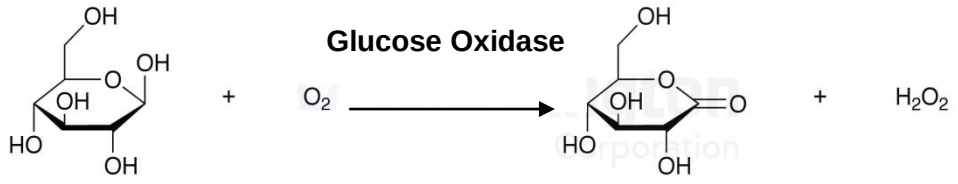

β-D-Glucose D-Glucono-1,5-lactone (1)

The key enzymatic reaction employed for urea determination by conductometric and ISFET biosensors based on immobilized urease is shown below. Generated substances such as ammonia and carbonate result in changes of conductivity, which allows the usage of conductometric transistors as transducers.

On the other hand, urease and butyrylcholinesterase reactions result in changes of H^+ concentration leading to alteration of solution pH in the bio-membrane, which allows the usage of pH-sensitive field-effect transistors as transducers.

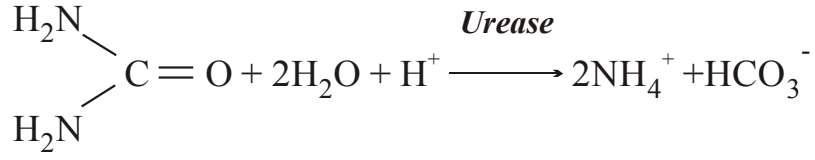

(2)

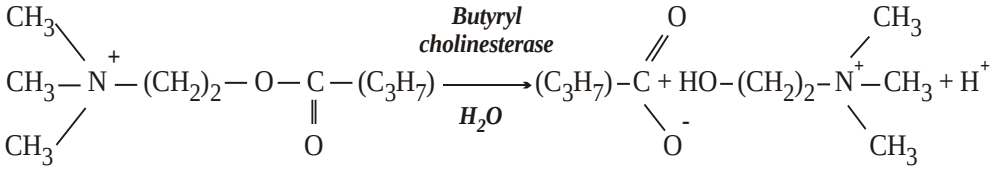

(3)

Zeolite Modified Transducers

Zeolite modified electrodes were attained by simply adding zeolite and zeo-type particles with desired concentrations into standard membrane transducers (Figure 3.2).

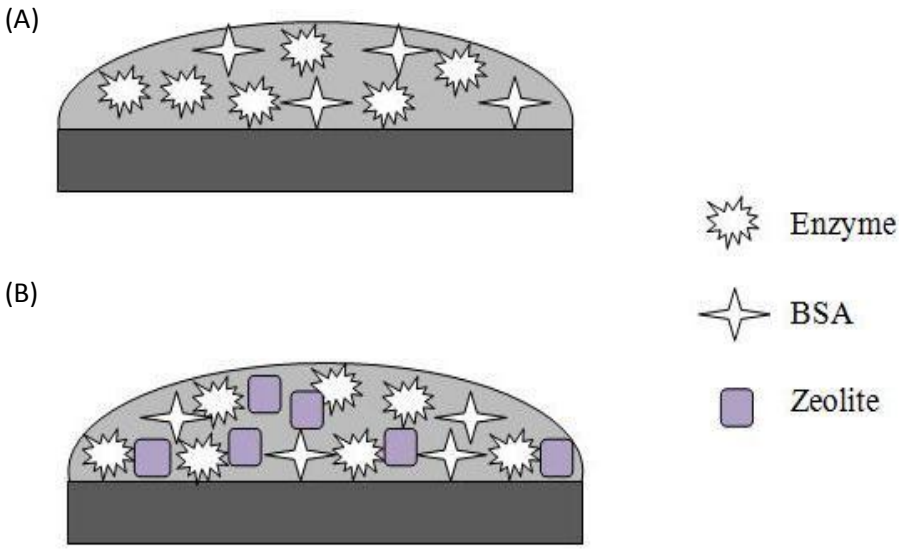

Figure 3.2 Schematic presentation of standard membrane transducer-SMT (A) and zeolite modified transducer-ZMT (B).

3.5.1 Conductometric Biosensor

Sensor Structure and Measurement Setup

The conductometric transducers were produced in Lashkarev Institute of Semiconductor Physics of National Academy of Sciences of Ukraine (Kyiv, Ukraine). They were consisted of two identical pairs of gold interdigitated electrodes made by gold vacuum evaporation onto pyroceramic substrate (5 x 40 mm). The surface of sensitive area of each electrode pair was about 1.0 x 1.5 mm. The width of each of interdigital spaces and digits was 20 μm. Measurements

were done by using the setup produced in CNRS Laboratory in Lyon. A Stanford Research System (SR510) model Lock-in Amplifier, a Shlumbereger Generator 4431 model AC Signal Generator and appropriate connections are used and data are acquired and stored with the help of a Recorder.

Zeolite Modified Transducer Production

To produce working bioselective elements based on enzyme and zeolites, the mixture of 5 % enzyme, 5 % BSA, and 20 % glycerol in 10 mM phosphate buffer at pH 7.2 was prepared. The solution obtained upon mixing was deposited immediately on the transducers using eppendorf micro sampler (total volume 1 µl) and the working surfaces were fully covered. The volume of each membrane was about 0.1 µl. The reference membrane mixture was prepared using the same mixture as above with the exception of enzyme. All membranes contained the same total amount of protein and zeolite. After deposition, the membranes were dried in Glutaraldehyde (GA) vapour for 15 minutes and air at room temperature for another 15 min to allow the cross-linking. Prior to using the membranes; they were washed in the buffer solution to get rid of the excess of unbound GA.

Measurement Procedure

The measurements were carried out in an open cell at room temperature. The 10 mM phosphate buffers at different pH values were intensively stirred. The necessary substrate concentration in the working buffer was achieved by adding

given portions of the stock substrate solution. The experiments were repeated at least three times sequentially. The effect of nonspecific variations of output signal owing to temperature and pH changes and electric interferences was avoided by operating in the differential mode.

3.2.2 ISFET Measurements

Sensor Structure and Measurement Setup

The ISFET transducers were produced in Lashkarev Institute of Semiconductor Physics of National Academy of Sciences of Ukraine (Kyiv, Ukraine). The ISFET sensor chip contains two identical p-channel transistors on the same crystal. The diffusion p^+-buses with contacts to the drain and source of each transistor are coming out on the edge of the chip along with an outlet to the built-in reference microelectrode. To prevent formation of a parasitic conductivity channel between p^+-areas of two transistors, the chip has a 50 μm wide protecting division n^+-line with a contact to the substrate. Zigzag geometry of the transistor gate area with the width-to-length ratio 100:1 ensures sufficient steep slope of the transfer characteristic. A window etched in an oxide layer for growing gate dielectric replicates the channel geometry with a 7 μm overlapping. A “saturated calomel” reference electrode is used to maintain the potential between the back contact of the ISFET and the solution. The output signal of the biosensor was recorded as a function of substrate concentration. Acquired data can be stored and analyzed by the computer.

Zeolite Modified Transducer Production

To produce working bioselective elements based on enzyme and zeolites, the mixture of 5 % enzyme, 5 % BSA, and 20 % glycerol in 5 mM phosphate buffer at pH 7.4 was prepared. The solution obtained upon mixing was deposited immediately on the transducers using eppendorf micro sampler (total volume 1 µl) and the working surfaces were fully covered. The volume of each membrane was about 0.1 µl. The reference membrane mixture was prepared using the same mixture as above with the exception of enzyme. All membranes contained the same total amount of protein and zeolite. After deposition, the membranes were dried in GA vapour for 15 minutes and air at room temperature for another 15 min to allow the cross-linking. Prior to using the membranes; they were washed in the buffer solution to get rid of the excess of unbound GA.

Measurement Procedure

The measurements were performed in daylight at room temperature in an open glass vessel filled with a vigorously stirred 5 mM phosphate buffer solution at pH 7.4. The substrate concentrations were varied by addition of portions of standard stock solutions of the substrates into the working buffer. The experiments were repeated at least three times sequentially.

CHAPTER 4

RESULT AND DISCUSSION

4.1 Protein Immobilization by Physical Adsorption

4.1.1 Synthesis of Zeolite and Zeo-type Materials

4.1.1.1 Zeolite A with Varying Particle Diameter

The first step was to investigate the influence of particle diameter on the physical adsorption of proteins. For this purpose, zeolite A was chosen by considering the particle diameters approximately 2, 3.8, and 5 μm. Varying particle diameters of zeolite A (LTA) micro crystals were hydrothermally synthesized by changing the template concentration in the synthesis formula. Thus three optimized gel synthesis formulas, i.e., formula I: 1.94 Na_2O : Al_2O_3 : 0.84 SiO_2 : 194 H_2O : 0.5 TEA (LTA-2), formula II: 1.94 Na_2O : Al_2O_3 : 0.84 SiO_2 : 194 H_2O : 1 TEA (LTA-3.8), formula III: 1.94 Na_2O : Al_2O_3 : 0.84 SiO_2 : 194 H_2O : 1.5 TEA (LTA-5) were used to examine the effect of particle diameters on the immobilization behavior of proteins.

The XRD patterns of the synthesized zeolite A crystals are shown in Figure 4.1. Zeolite A structure was expected from each XRD pattern. All of them showed Zeolite A structure. All peaks observed in the synthesized samples matched the literature zeolite A XRD peak positions [112], and thus indicated that the products were pure material.

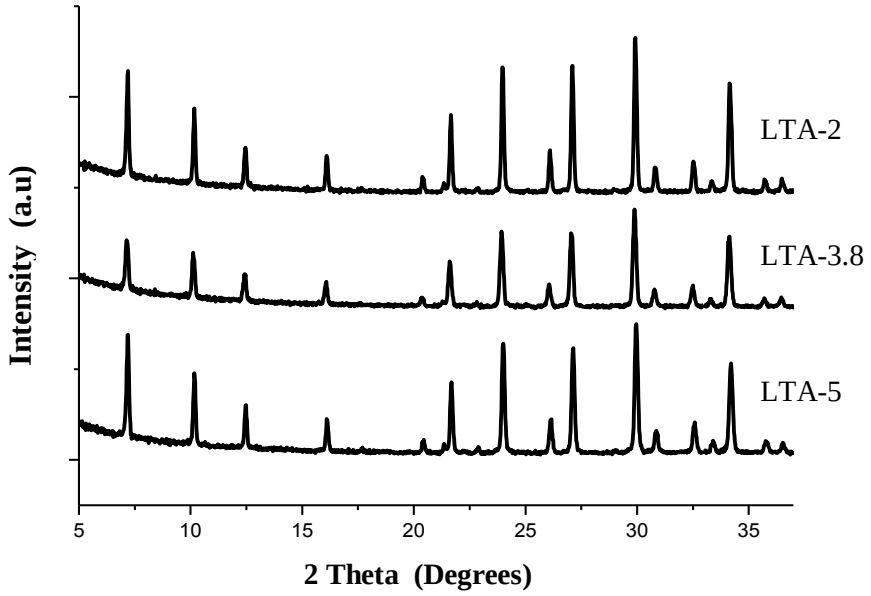

Figure 4.1: XRD patterns of Zeolite A micro crystals with varying particle size.

Figure 4.2 shows FE-SEM images of synthesized zeolite A products. The images revealed the simple cubic morphology of the synthesized zeolite A particles. These particles were predominantly in the 2-5 μm size range, in agreement with the particle size distribution analysis data shown in Figure 4.3.

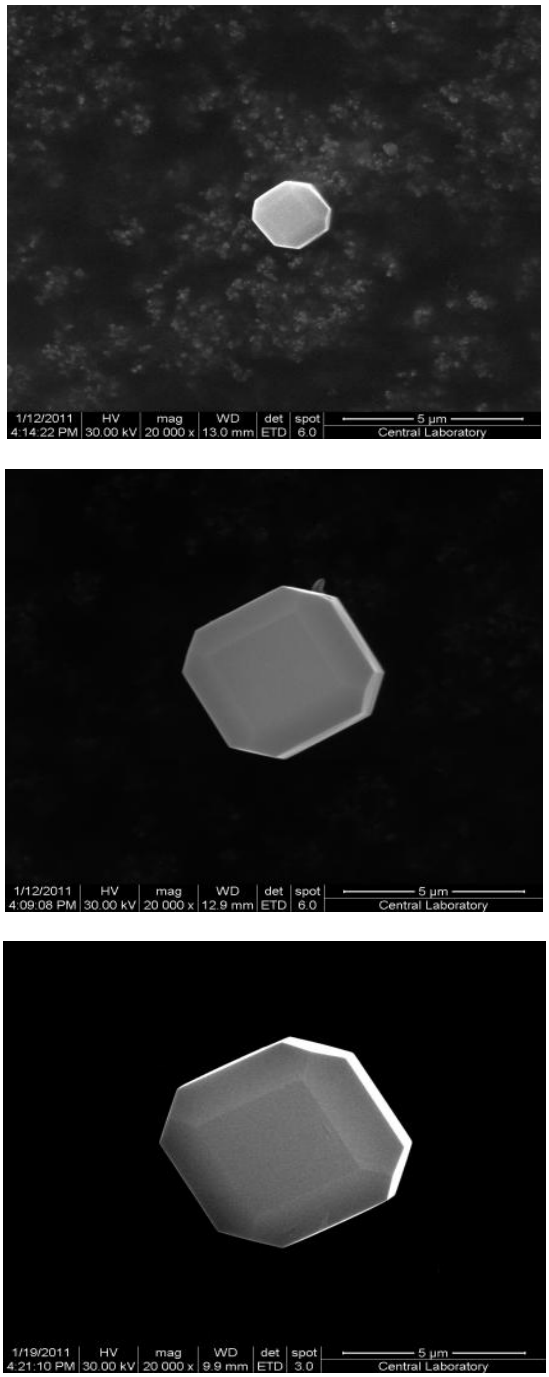

Figure 4.2: FE-SEM images of zeolite A micro crystals with varying particle size.

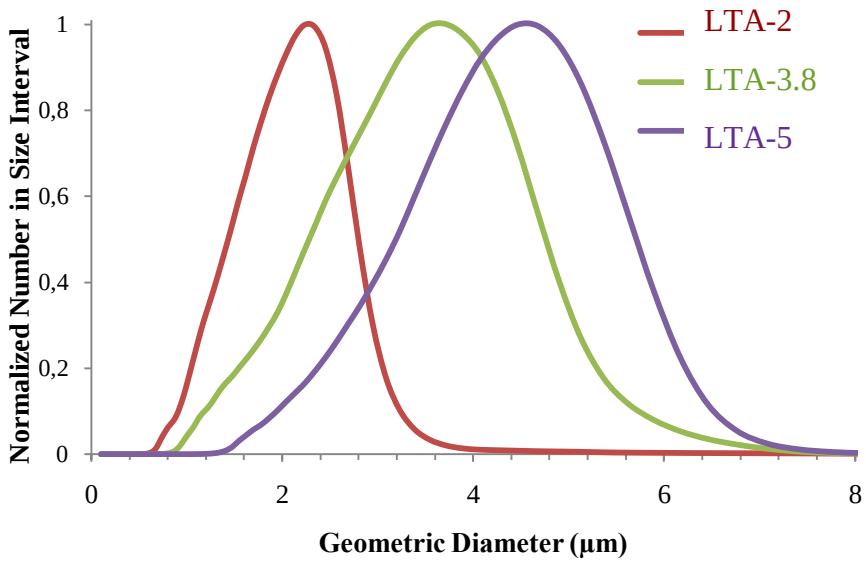

Figure 4.3: Particle Size Distribution result of Zeolite A micro crystals with varying particle size.

According to the Figure 4.2 and 4.3, the average particle size of zeolite A crystals increased from 2 µm to 3.8 and 5 µm upon changing the synthesis formula from I to II and III, respectively. Furthermore, different combinations of synthesis formula didn't induce any significant changes in sample morphology as it was seen in Figure 4.1 and 4.2.These results along with their textural properties are summarized in Table 4.1.

Table 4.1: Summary of textural properties of zeolite A micro crystals.

Formula	Sample Name	Si/Al[a]	Part. Size (μm)[b]	S_{total} (m^2/g)[c]	S_{EXT} (m^2/g)[d]	Pore Volume (cc/g)[e]	Surf. Charge (mV)[f]
I	LTA-2	~1	2	557	192	0.23	-10.5
II	LTA-3.8	~1	3.8	550	188	0.23	-16
III	LTA-5	~1	5	513	193	0.22	-22.2

[a] Measured by EDX.

[b] Measured by API Aerosizer LD.

[c] Measured by Multipoint BET .

[d] Measured by t-plot Method.

[e] Measured by Saito-Foley (SF) Method.

[f] Measured by Zeta potential at pH 7.

According to the results shown in Table 4.1, none of the zeolite A samples showed a considerable change in sample Si/Al ratio, external surface area, pore size, pore volume, and surface charge after using different synthesis procedures. However, the total surface area decreased from 557 m^2/g to 513 m^2/g upon changing the synthesis formula from I to III, respectively. In contrast to the increased external area, the observed decrease in the total surface area could be due to the decrease in the pore volume of the zeolite A samples upon changing the synthesis formula.

4.1.1.2 Zeolite Beta with Varying Si/Al Ratio

The second step was to investigate the effect of hydrophobicity of zeolite crystals on the adsorption behavior of proteins. For this purpose, zeolite Beta was chosen by considering the Si/Al ratio of 30, 50, 60, 120 for sub-micron sized (0.7 μm-1.2 μm) by simply changing the Si and Al concentration in the synthesis formulas. Thus four optimized gel synthesis formulas, i.e., formula IV: 1.92 Na_2O : Al_2O_3 : 30 SiO_2 : 4.6 $(TEA)_2O$: 444 H_2O (BEA-30), formula V: 1.92 Na_2O : Al_2O_3 : 50 SiO_2 : 4.6 $(TEA)_2O$: 444 H_2O (BEA-50), formula VI: 1.92 Na_2O : 0.5 Al_2O_3 : 30 SiO_2 : 4.6 $(TEA)_2O$: 444 H_2O (BEA-60), and formula VII: 1.92 Na_2O : 0.25 Al_2O_3 : 30 SiO_2 : 4.6 $(TEA)_2O$: 444 H_2O (BEA-120) were used for the synthesis of sub-micron sized Beta crystals.

The XRD patterns of synthesized zeolite Beta samples are shown in Figure 4.4. All peaks observed in the as-synthesized sample matched the literature zeolite Beta XRD peak positions [113], and thus indicated that the product was pure material. Table 4.2 summarizes the textural properties of the synthesized sub-micron zeolite Beta crystals obtained upon varying concentration of the Si and Al sources.

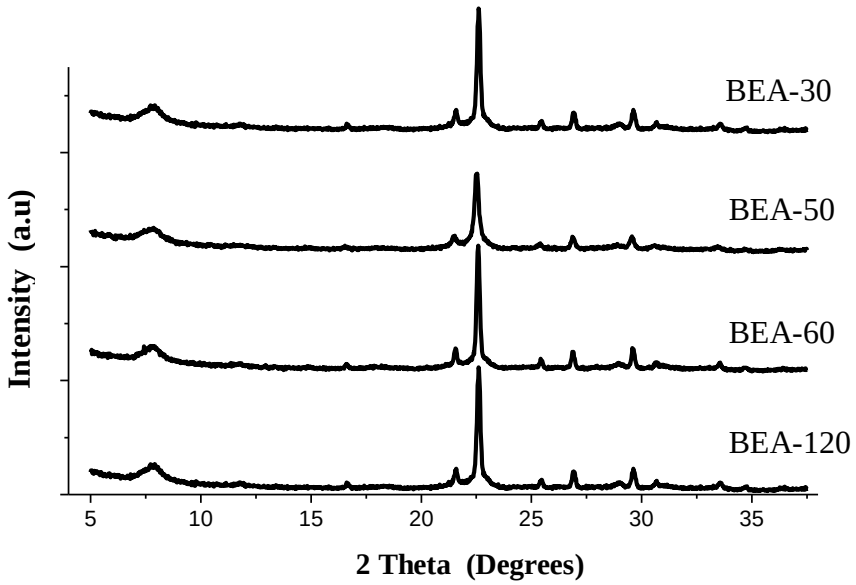

Figure 4.4: XRD patterns of sub micron zeolite Beta crystals with varying Si/Al ratio.

Figure 4.5 shows FE-SEM images of synthesized sub-micron zeolite Beta product. The images revealed the spheroidal and truncated square bipyramidal morphology of the synthesized zeolite Beta particles. These particles were predominantly in the 0.7-1.2 μm size range in agreement with the particle size distribution analysis data shown in Figure 4.6.

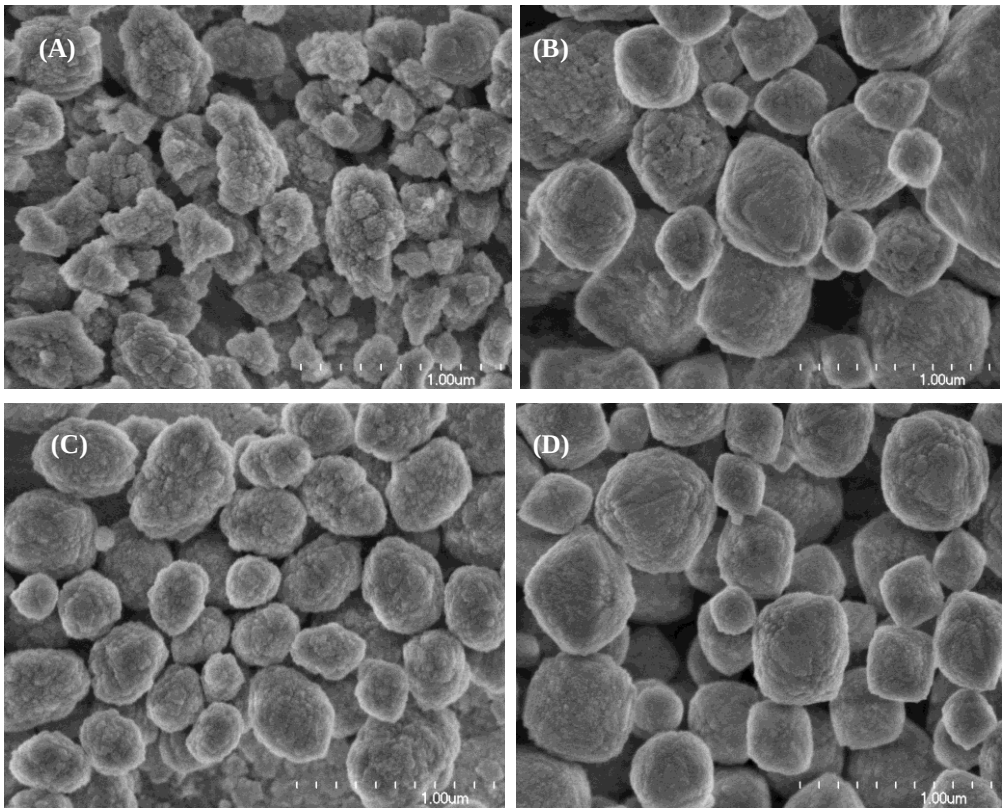

Figure 4.5: FE-SEM micrographs of sub-micron zeolite Beta crystals with varying Si/Al ratio BEA-30 (A), BEA-50 (B), BEA-60 (C), and BEA-120 (D).

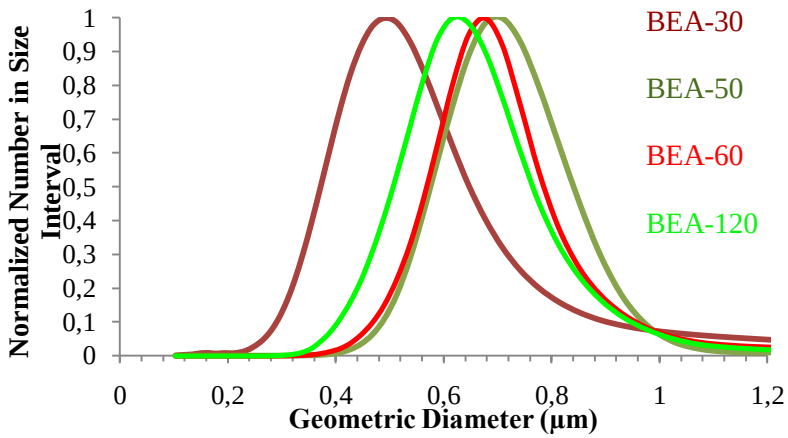

Figure 4.6: Particle size distribution results of sub-micron zeolite Beta crystals with varying Si/Al ratio.

Table 4.2: Summary of textural properties of sub-micron zeolite Beta crystals.

Formula	Sample Name	Si/Al[a]	Part. Size (nm)[b]	S_{BET} (m^2/g)[c]	S_{EXT} (m^2/g)[d]	Pore Volume (cc/g)[e]	Surf. Charge (mV)[f]
IV	BEA-30	9.7 ± 1.0	450	260	144	0.11	-62
V	BEA-50	17.7 ± 1.8	700	460	579	0.19	-89
VI	BEA-60	14.8 ± 1.5	600	360	703	0.15	-65
VII	BEA-120	20.3 ± 2	650	495	726	0.2	-70

[a] Measured by EDX.

[b] Measured by API Aerosizer LD.

[c] Measured by Multipoint BET .

[d] Measured by t-plot Method.

[e] Measured by Saito-Foley (SF) Method.

[f] Measured by Zeta potential at pH 7.

As shown in Table 4.2, although a large variation of gel composition formulas were investigated to obtain different Si/Al ratios, the lowest and highest Si/Al ratio attained were 9.7 and 20.3, respectively. However, the external surface area changed from 144 m^2/g to 7260m^2/g, while particle size changed from 450 nm to 750 nm. Furthermore, none of the sample exhibits significant change in the pore size and surface charge after using different synthesis formulas.

4.1.1.3 Silicalite and SBA-15

The next step was to investigate the effect of pore diameter on the immobilization of proteins. For this purpose, microporous Silicalite and mesoporous SBA-15 were chosen by considering the pore diameters of approximately 1 and 8 nm. Thus two optimized gel synthesis formulas, i.e., formula VIII: 1 TPAOH : 4 TEOS : 350 H_2O (Silicalite) and formula IX: 1 TEOS : 0.017 P123 : 0.6 Mesitylene : 1 KCl : 5,85 HCl : 165 H_2O (SBA-15) were used to examine the effect of pore diameter on the immobilization of proteins. The XRD patterns of Silicalite and SBA-15 particles are shown in Figure 4.7.

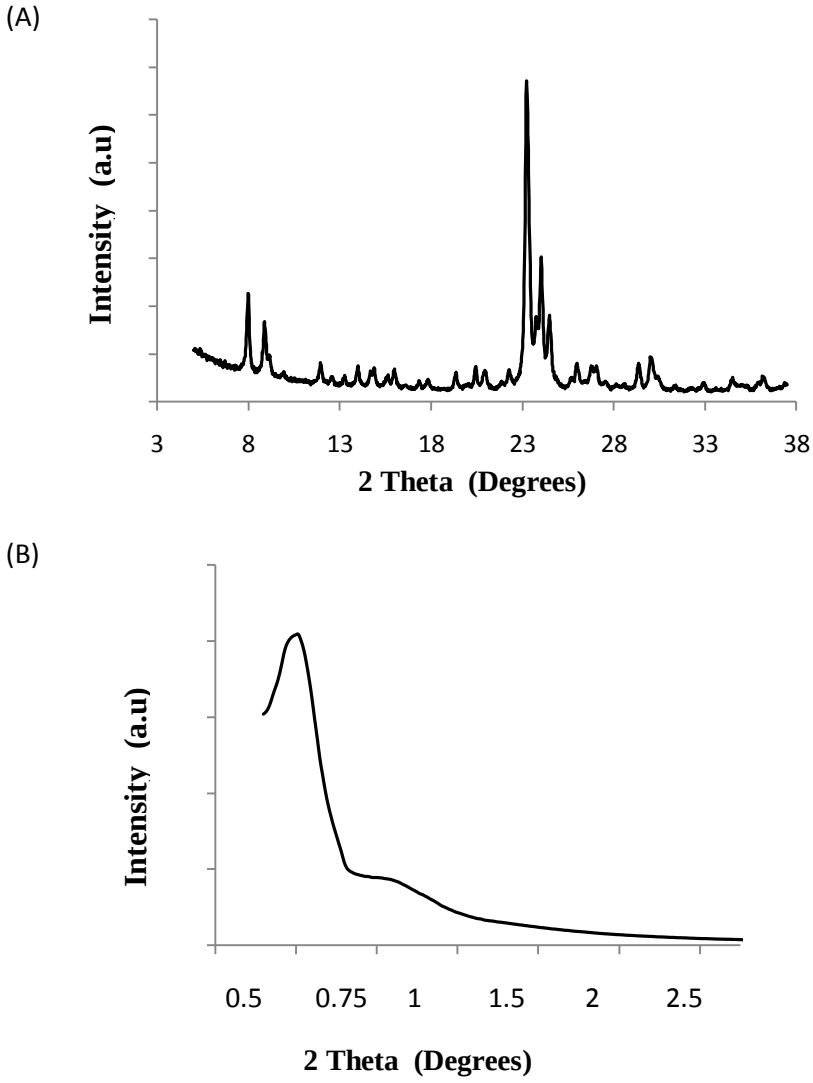

Figure 4.7: XRD patterns of Silicalite (A) and SBA-15 (B) particles.

All peaks observed correspond completely to those of the silicalite and SBA-15 material reported previously [106, 115]. Moreover, powder XRD patterns reveal that all silica samples employed in the present study exhibit reflections that are characteristic of high quality Silicalite and SBA-15.

The obtained silicalite and SBA-15 particles are shown in Figure 4.8. The FE-SEM images indicated the silicalite with coffin-like structure and highly ordered spherical SBA-15 particles were obtained. Silicalite particles were predominantly in the 1 um while SBA-15 particles were in 2.5 um size range. Table 4.3 summarizes the textural properties of the Silicalite and SBA-15 particles obtained upon varying pore sizes.

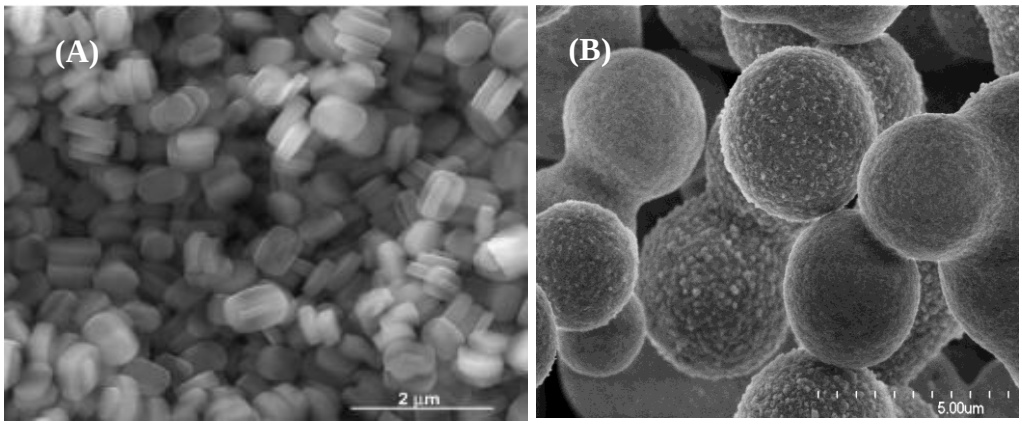

Figure 4.8: FE-SEM images of silicalite and SBA-15 particles using Formula XI (A) and XII (B).

Table 4.3: Summary of the textural properties of silicalite and SBA-15 particles.

Formula	Sample Name	Si/Al[a]	Part. Size (μm)[b]	S_{total} (m2/g)[c]	S_{EXT} (m2/g)[D]	Pore Volume (cc/g)[E]	Surf. Charge (mV)[F]
VIII	Silicalite	No Al.	~1	288	202	0.12	-43
IX	SBA-15	No Al.	~2,5	800	693	2.4	-33

[a] Measured by EDX.

[b] Measured by API Aerosizer LD.

[c] Measured by Multipoint BET .

[d] Measured by t-plot Method.

[e] Measured by Saito-Foley (SF) Method.

[f] Measured by Zeta potential at pH 7.

As shown in Table 4.3, the pore and particle size, pore volume, total, and external surface area was quite higher for the SBA-15 than silicalite particles depending on the synthesis conditions. However, all samples were pure silica materials and surface charge did not considerably change from silicalite to SBA-15.

4.1.2 Modification of Zeolite and Zeo-type Materials

4.1.2.1 Surface Functionalization

Surface functionalization of zeolite and zeo-type materials is important since most of the reactions are taking place on the surfaces. Therefore, protein

immobilization can be adjusted by simply changing the surface properties of the employed materials.

In the current study, the desired surface groups controlled by employing functionalization process. For this reason, two different approaches were used to attain high degree of functionalization and obtained results were shown in Figure 4.9.

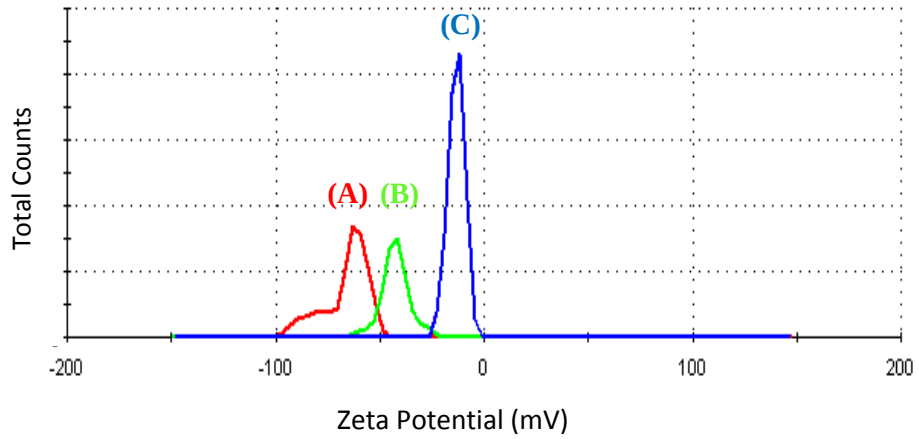

Figure 4.9: Zeta potential distribution of functionalized zeolite Beta samples by using two different experimental procedures; non-functionalized zeolite Beta (A), functionalized zeolite Beta by using procedure 1 (B) [108], and procedure 2 (C) [109].

Functionalized zeolite Beta samples obtained by different approaches are shown in Figure 4.9. Comparing to the non-functionalized zeolite surface, more positively charged surfaces were expected from each procedure. Although there were still negative groups on the surface, larger quantities of positive groups were

obtained in the case of procedure 2 (C) than procedure 1 (B). For this purpose, procedure 2 was used for the surface functionalization of zeolite and zeo-type materials in the current report. Table 4.4 summarizes the textural properties of the functionalized and non-functionalized zeolite Beta (BEA-120) and SBA-15 particles.

Table 4.4: Textural properties of the functionalized and non-functionalized zeolite Beta and SBA-15 particles.

Sample Name	Surface Groups	Si/Al [a]	Part. Size (μm) [b]	S_{total} (m^2/g) [c]	Pore Size [d]	Pore Volume (cc/g) [d]	Surf. Charge (mV) [e]
Funct-BEA-120	OH^-, NH_2^+	20.3	0.7	450	0.3	0.25	10
BEA-120	OH^-	20.3	0.7	400	1.03	0.2	-70
Funct-SBA-15	OH^-, NH_2^+	No Al.	2	790	6.8	1.5	-7
SBA-15	OH^-	No Al.	2	800	7.9	2.4	-33

[a] Measured by EDX.

[b] Measured by API Aerosizer LD.

[c] Measured by Multipoint BET.

[d] Measured by BJH and Saito-Foley (SF) Method.

[e] Measured by Zeta potential at pH 7.

As shown in Table 4.4, surface charge of the samples was changed from -70 to +10 and -33 to -7 for the zeolite Beta (BEA-120) and SBA-15, respectively. However, there was a small decrease of the pore size were observed after the functionalization process. This can be related with the attachment of a layer of functional moiety on the pore walls.

4.1.2.2 Ion Exchange

The tetrahedral framework structure of zeolite Beta consists of ordered and disordered poly-types that have three dimensional networks of 12-ring channels. This structure is consistent with the known properties such as ion exchange [116]. In order to investigate the influence of extra framework cations on the immobilization of proteins, Beta type zeolite was chosen due to their exclusive catalytic and adsorbent properties. Zeolite Beta in as-prepared and ion modified forms have been characterized using, FE-SEM and EDX (Table 4.5).

Table 4.5: Summary of the properties of ion exchanged sub-micron zeolite Beta crystals.

Sample Name	Exchanged with	Si/Al Ratio	Exchange Level (%) [a]
Na-BEA-120	As-synthesized	~14	-
Ca-BEA-120	$Ca(NO_3)_2$	~14	94
Co-BEA-120	$Co(NO_3)_2$	~14	76
Cu-BEA-120	$Cu(NO_3)_2$	~14	92
Mn-BEA-120	$Mn(NO_3)_2$	~14	75
Mg-BEA-120	$Mg(NO_3)_2$	~14	75

According to the Table 4.5, high levels of ion exchange were achieved by using related nitrates of preferred ions. Overall, ion-exchange was accomplished above 75%. Furthermore, as-synthesized Na-BEA crystals had Si/Al ratio of 14,

spherical morphology and uniform size of 0.7 μm, which remained unchanged after ion-exchange procedures.

4.1.3 UV-VIS Measurements

In this study, to gain more insight about the interaction between zeolites and proteins, zeolite A (LTA) and zeolite Beta (BEA) were chosen by considering the particle diameter, Si/Al ratio, surface charge, and extra-framework cations of the same type zeolite. Additionaly, proteins with varying diameters and isoelectric points (GOx, hemoglobin and lysozyme) were chosen in order to investigate the influence of pH on the adsorption behavior of proteins. Furthermore, silicalite and SBA-15 particles with varying pore sizes and surface charges were used for the adsorption of proteins Molecular weights (MW) and isoelectric points (pI) of employed proteins listed in Table 4.6.

Table 4.6: Molecular weights and isoelectric points of proteins.

Protein	MW (kD)	Isoelectric point
BSA	66	4.9
Concanavalin A	104	~5
Hemoglobin	64.5	6.8
Lysozyme	14.5	11.4
GOx	160	4.2
Urease	480	5.2
Butyrylcholinesterase (BuChE)	440	5

Understanding the protein-zeolite interaction in more detail paves the way for generating ideal surfaces for potential biotechnological applications by designing the conformation and orientation of the surface and framework species of zeolites. For this purpose, physical adsorption methods were preferred to eliminate the other factors that come into play when employing chemicals and reagents. Table 4.7 summarizes the adsorption of proteins onto zeolite A and as-synthesized, functionalized, and ion exchanged zeolite Beta crystals at pH 7.4.

Table 4.7: Adsorption of proteins onto zeolite A and Beta crystals. [1]

Samples	BSA	Con.A	Hem	Lys	GOx	Urease	BuChE
LTA-2	-	-	-	+	-	+	-
LTA-3.8	-	+	+	+	+	+	+
LTA-5	+	+	+ +	+ +	+ +	+ +	+ +
BEA-30	-	-	-	+	- -	-	-
BEA-50	-	+	+	+	-	+ +	+
BEA-60	+ +	+	+	+	-	+	+
BEA-120	+	+	+	+	-	+	+
Func.-BEA-120	-	-	+ +	+	+	+ +	+ +
Ca-BEA-120	-	+++	+ +	+	++	+ +	+ +
Co-BEA-120	-	+ +	+ +	+++	+	+	+
Cu-BEA-120	- -	+ +	+++	+	+	+	+
Mn-BEA-120	-	+++	+ +	+	+	+ +	+ +
Mg-BEA-120	+	n/a[2]	++	+++	++	+ +	+ +

[1] (- -) 0-20 %, (-) 20-40 %, (+) 40-60 %, (+ +) 60-80 %, (+ + +) 80-100 %.

[2] n/a; not applicable.

4.1.3.1 Effect of Particle Diameter

Table 4.7 shows the amounts of proteins adsorbed onto three different zeolite A (LTA) crystals with increasing particle diameter in the order of LTA-2< LTA-3.8< LTA-5. Since all zeolite A crystals were microporous and average diameters of employed proteins was about 3-15 nm range, the immobilization of proteins occurred only on the external surface of the zeolite A as also suggested by Ismail and Yiu et al. [117-118]. Thus higher immobilization amounts were expected for zeolite A crystal with the largest particle diameter which should presents a wide area for the immobilization of proteins.

According to Table 4.7, all proteins were highly bound to largest zeolite A crystals and adsorptions increased in the order of LTA-2< LTA-3.8< LTA-5. As a result, it was concluded that the wide external surface area provided suitable regions for the attachment of proteins with their several domains and increased their stabilization on the zeolite surface. Thus, desorption could be prevented during the adsorption process. This phenomenon is illustrated in Figure 4.10 by visualizing the possible arrangement of proteins on the crystals.

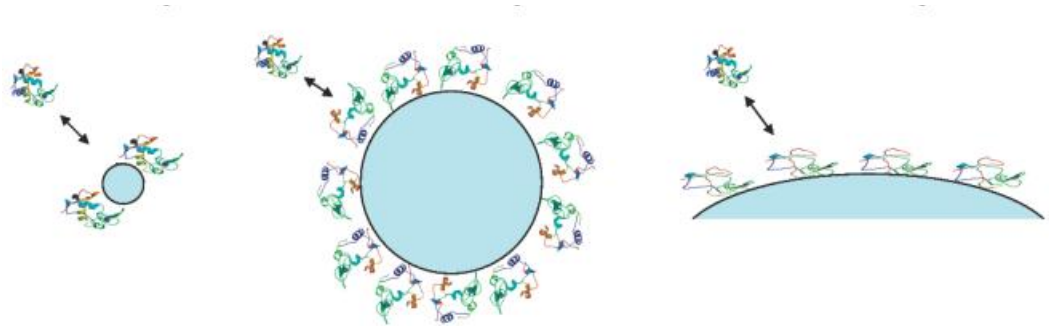

Figure 4.10: Schematic representation of protein adsorption onto Zeolite A crystals with varying particle diameters. Larger surface area provided by larger Zeolite A crystals leads proteins to elongate through the surface and partially unfold, which results in more interaction between proteins and crystal [92].

4.1.3.2 Effect of Si/Al Ratio

Table 4.7 illustrates amounts of proteins adsorbed onto four different BEA samples with increasing Si/Al ratio in the order of BEA-30< BEA-60< BEA-50< BEA-120 according to EDX results (Table 4.2). Because of the varying Si/Al ratio it was assumed that the surfaces of zeolites had different amounts of hydrophobic and acidic regions, which would result in different proteins adsorption levels by hydrophobic forces. In addition to the hydrophobic regions on the zeolite surface, the presence of different amounts of aluminum atoms in the zeolite framework generated different amounts of negative charges, which may have assisted proteins to be adsorbed through electrostatic forces. While all acidic regions and electrostatic interactions contributed to the adsorption process, varying protein adsorption levels would be expected.

According to the results shown in Table 4.7, nearly all proteins with acidic and neutral pI, bound to each zeolite Beta species in high amounts except Na-BEA-30 which had the lowest Si/Al ratio and hydrophobicity. On the other hand, Na-BEA-30 samples displayed highest surface negativity due to high amount of aluminum atoms in the framework. Since acidic proteins contain negative charges above their isoelectric points and charge of the zeolites themselves is negative, repulsion should have occured between protein molecules and Na-BEA-30 surface. On the other hand, since nearly 10% low adsorption amounts were obtained by more hydrophilic Na-BEA-30, candidates of the main driving forces for the immobilization of proteins by physical adsorption may include hydrophobic interactions either. Moreover, acidity of proteins is another parameter which influences the attraction and repulsion between zeolite Beta crystals and protein molecules at varying pH. Additionally, since low external surface area of the Na-BEA-30 samples adsorbed less protein than other zeolite Beta samples, external surface area could be another driving force for the adsorption of proteins.

Moreover, according to the Table 4.7, only basic protein, lysozyme, bound to all zeolite Beta species with nearly same efficiency. Since lysozyme had the smallest diameter in all protein species, it looked like lysozyme could easily interact with any kind of zeolites and molecular weight of the proteins seemed to be related to the interaction. In the light of these findings, it could be concluded that the immobilization of proteins by physical adsorption was influenced by the Si/Al ratio of the zeolite Beta crystals. Hydrophobic and electrostatic nature of the particles increases the protein adsorption by almost 10 %. Furthermore, in order to increase the protein immobilization on zeolite surfaces, molecular weight and acidic/basic properties of the proteins can be tuned. Proteins with low molecular weights adsorbed easily on all zeolite Beta species with varying hydrophobicity and surface charge.

4.1.3.3 Effect of Surface Charge

Table 4.7 shows that the immobilization of proteins by physical adsorption was clearly influenced by the surface properties of the carrier such as surface charge and surface groups. When all electrostatic interactions contribute to the immobilization process, varying amounts of protein adsorption would be expected due to different surface properties of the proteins and zeolite A crystals.

According to the Table 4.7, all acidic and neutral proteins highly bounded to functionalized (positively charged) surfaces with the exception of BSA and Concanavalin A. Since acidic proteins contain net negative charges at pH 7.4, surface charge seemed to be a factor that influences adsorption of proteins on zeolite crystals. Therefore we concluded that the physical adsorption of proteins can be increased by the functionalization of zeolite surfaces with 3-APTES due to changing of the electrostatic nature of the particles. Furthermore, the basic protein lysozyme, highly bound to all zeolite species as it was stated in the previous section. Since small diameter of lysozyme molecules had an influence on the adsorption, it could be concluded that the molecular weight and surface charge of proteins had to be considered as potential parameters which influences the immobilization of proteins by physical adsorption.

4.1.3.4 Effect of pH

Since the data in preceding sections show a substantial relationship between adsorption and the acidity of employed proteins, pH dependency of the adsorption

process was examined and discussed in the next content. Figure 4.11 shows adsorption of glucose oxidase (acidic), hemoglobin (neutral), and lysozyme (basic) at various pH values. Various amounts of adsorption were expected due to varying acidic properties of proteins.

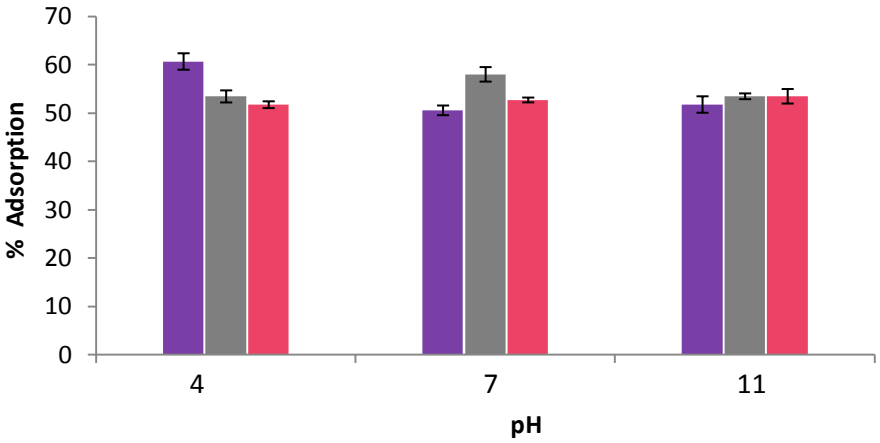

Figure 4.11: Adsorption of glucose oxidase (■), hemoglobin (■), and lysozyme (■) onto zeolite Beta crystals under different pH conditions.

Figure 4.11 illustrates the effect of pH on the adsorption capacity of proteins onto zeolite Beta crystals (Na-BEA-60). The adsorbed amounts of acidic and neutral proteins, glucose oxidase and hemoglobin, were the highest at their isoelectric points, pH 4 and 7 respectively. This increase was most likely the result of the localization of surface charges on the protein surface and agglomeration behavior of proteins around their isoelectric points. Therefore we concluded that the immobilization of proteins can be increased by tunning the acidic/basic properties of the medium. Nevertheless, lysozyme behaved differently, probably because of

very small diameter of the molecule as it was discussed in the previous sections. Consequently, in the light of our findings we concluded that the adsorption of proteins was a complicated phenomenon since adsorption occurred through a combination of several forces and rearrangement behavior of proteins on the zeolitic surface.

4.1.3.5 Effect of Extra-Framework Cations

In addition to effect of other zeolitic properties, presence of extra framework ions is another parameter that may influence the adsorption of proteins as it was studied by numerous researchers due to altered acidity and electrostatic field on the zeolite surface Wijntje et al. [31], Sakaguchi et al. [50]. When all acidic and electrostatic interactions contribute to the adsorption process, varying amount of protein adsorption would be expected according to the varying surface properties of the employed ion exchanged zeolite particles. According to the Table 4.7, all acidic, neutral and basic proteins with the exception of BSA, tend the adsorbed ion exchanged zeolite Beta crystals rather than non-exchanged Beta crystals (Na-BEA). Furthermore, Mg exchanged zeolite Beta crystals were highly preferred for all types of proteins with the exception of acidic protein concanavalin A. Proteins with acidic and neutral properties highly bound to Ca and Cu exchanged crystals, respectively. On the other hand, basic protein lysozyme selectively bound to Co exchanged crystals as well as Mg exchanged ones. Some exceptions, however, were also confirmed (Table 4.7). Additionally, these results strongly suggested that the adsorption of proteins is zeolite specific and ideal surfaces for the immobilization of proteins can be generated by using zeolites with varying physicochemical properties

4.1.3.6 Effect of Pore Size

Pore diameter of zeolite and zeo-type materials greatly influences the adsorption of proteins. It was believed that porous structure would satisfy the requirements in practical uses of protein carriers in micro-scale dimension [119]. Furthermore, when microporous materials are used as adsorbent, the protein adsorption occur only on the external surface which may cause weak interaction between proteins and zeolite surfaces as illustrated by Figure 4.12. On the other hand, using mesoporous materials avoids protein leaching from the zeolite surface and .increase the activity, storage stability and reusability of proteins [120-122].

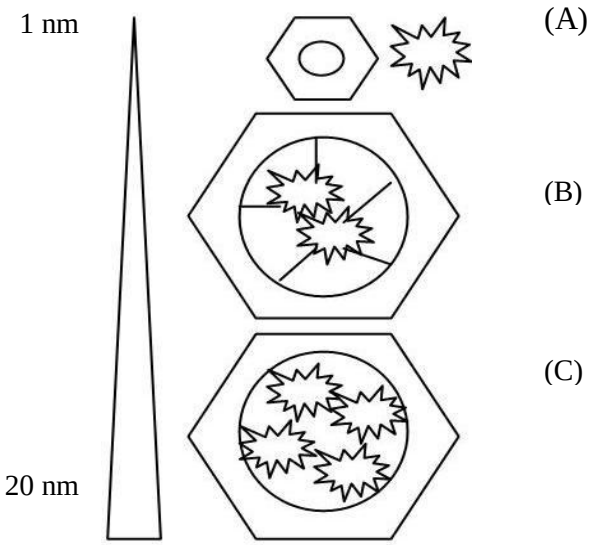

Figure 4.12: Illustration of adsorption behaviors of proteins (✹) according to pore diameters of silicalite (A), functionalized SBA-15, and SBA-15 (C).

For this purpose, immobilization of proteins to varying pore sizes of silicalite and SBA-15 were investigated. In order to obtain intermediate pore size, SBA-15 was functionalized by 3-APTES. Lysozyme (3.2 nm) [123], hemoglobin (5.5 nm) [124], and glucose oxidase (less than 10 nm) [125] were chosen as model proteins due to their varying molecular dimensions. Different amounts of adsorption would be expected depending on different molecular sizes of employed proteins. Figure 4.13 shows the adsorption amounts of lysozyme, glucose oxidase and hemoglobin on silicalite and SBA-15 particles.

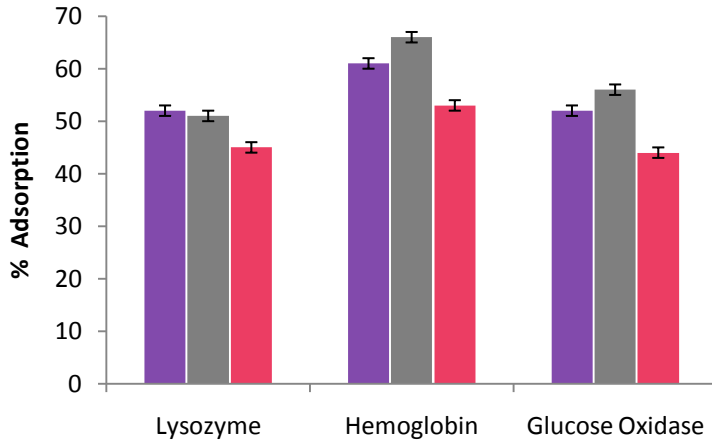

Figure 4.13: Adsorption of glucose oxidase, hemoglobin and lysozyme molecules onto silicalite (■), SBA-15 (■) and functionalized SBA-15 (■) particles.

Figure 4.13 shows the amounts of lysozyme, hemoglobin and glucose oxidase biomolecules adsorbed on silica particles with varying pore size and surface properties. All proteins showed much higher preference in binding to mesoporous SBA-15 than microporous silicalite particles. However, increased adsorption of proteins could be due to the high surface area of SBA-15. On the other hand,

comparison of the two SBA-15 particles with varying surface charge and pore diameter suggest that the functionalized SBA-15 with intermediate pore diameter, adsorbed proteins more efficiently than the non-functionalized SBA-15 as it was convenient with the results at Table 4.7. Thus it can be concluded that the surface charge is the main driving force when pore and particle diameter come into play upon adsorption.

4.2 Biosensor Measurements

4.2.1 Conductometric Urea and Glucose Biosensors

Conductometric biosensors which were produced by immobilizing urease and glucose oxidase on different types of commercial zeolites have been investigated and compared. Commercial zeolite A, zeolite Y, Silicalite-1, Silicalite-2, H^+ exchanged zeolite Beta with Si/Al ratio 150 and 300, and NH_4^+ exchanged zeolite Beta with Si/Al ratio 25 were compared as potential carriers for enzyme immobilization for the first time (Table 4.8).

Table 4.8: Summary of the textural properties of zeolites.

	Particle Size (μm)	Pore Size (A) *	Si/Al Ratio
Zeolite A	0.25	0.41	1.35
Zeolite Y	1.5	0.74	2.4
Silicalite-1	0.8	0.5	No Al.
Silicalite-2	0.4	0.5	No Al.
H^+ BEA-150	1-2	7.6 x 7.4	~150
H^+ BEA-300	1.5-3	7.6 x 7.4	~75
NH_4^+ BEA-25	1-3	7.6 x 7.4	~12.5

According to Table 4.8, particle sizes of the samples were changing between 0.4 and 3 μm. Moreover, pore size of zeolite A, zeolite Y, silicalite, and zeolite Beta was found to be 0.41, 0.74, 0.5, and 7.6, respectively. Silicalite zeolites contain only Si in the framework and Si/Al ratios of the other zeolite samples were changing between 1.3 and 150. In order to investigate the influence of zeolite incorporation into the conductometric electrodes, optimization of the system was further studied.

4.2.1.1 Effect of Zeolite Loading into Bioselective Membranes

Initially the effect of the zeolite loading in immobilization mixture on biosensor response was investigated. Different concentrations of silicalites in the zeolite modified electrodes (ZMTs) were tested to optimize the amount of zeolite loading with the sensor response (Figure 4.14).

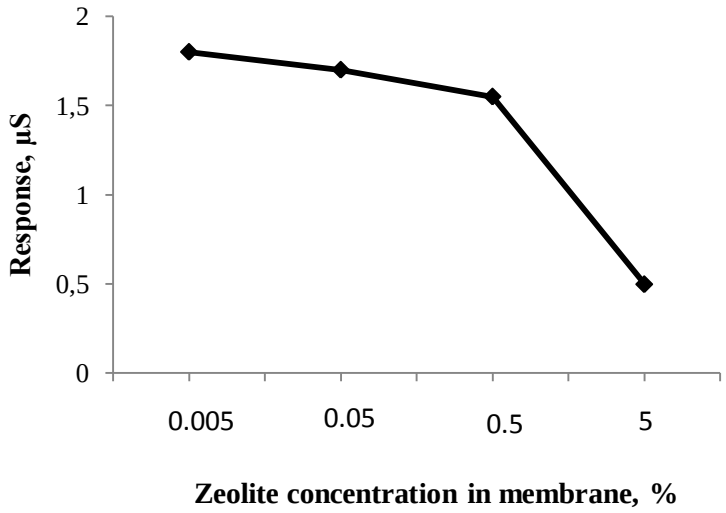

Figure 4.14: The dependence of responses of biosensors on weight percent of ZMTs at pH 7.5.

According to Figure 4.14, responses of biosensors with 5% silicalite were relatively low compared to responses with lower amount of silicalite. The level of saturation of biosensors also differs depending on concentration of silicalite particles in the membranes. It can be attributed to the high concentration of

silicalite particles in the bioselective membrane can cause a damage of the enzyme structure or act as a barrier and avoid the access of substrate to the active site of the immobilized enzyme. For this purpose, biosensors utilizing 0.5% silicalite loadings were used for further experimental work.

4.2.1.2 Effect of Cross-Linking Time

In order to optimize the cross-linking time for the enhanced sensor performance, zeolite modified electrodes (ZMTs) were kept in GA vapor for various periods and results were shown in Figure 4.15.

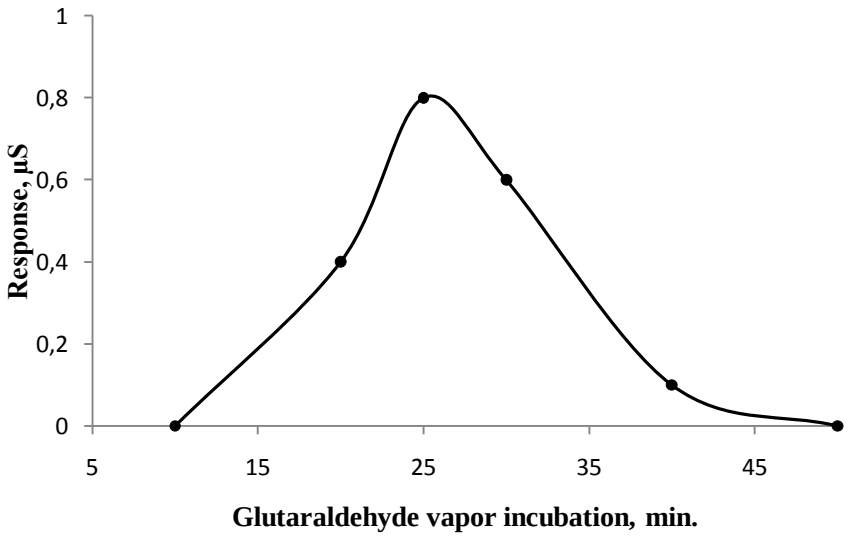

Figure 4.15: The dependence of responses of conductometric biosensors on cross-linking time in glutaraldehyde vapor for ZMTs.

According to the Figure 4.15, 25 minutes exposure time in GA vapor ,lead to the highest response and thus the optimum time for cross-linking of urease. In fact, if the exposure time was kept short for immobilization, enzyme leakage through the membrane took place because of insufficient bonding. This led to poor stability of the biosensors and the responses of the sensors decreased accordingly. On the other hand, if the exposure time for immobilization was longer than the optimum value, a decrease of response was observed. This can be related to the formation of a large number of bonds between glutaraldehyde and the enzyme molecules, which resulted in a compact structure of the membrane. This compact formation made the active site of the enzyme inaccessible.

4.2.1.3 Effect of Buffer Concentration and pH

It was well known that the choice of buffer strongly influenced the enzymatic activity and conductivity of the medium. The most commonly used buffer in similar systems was phosphate buffer saline (PBS) solution. Figure 4.16 illustrates the variation in the enzymatic response at different concentrations of PBS and different pH values. The results showed that the optimum sensor response was in 5 mM phosphate buffer with pH 7.5.

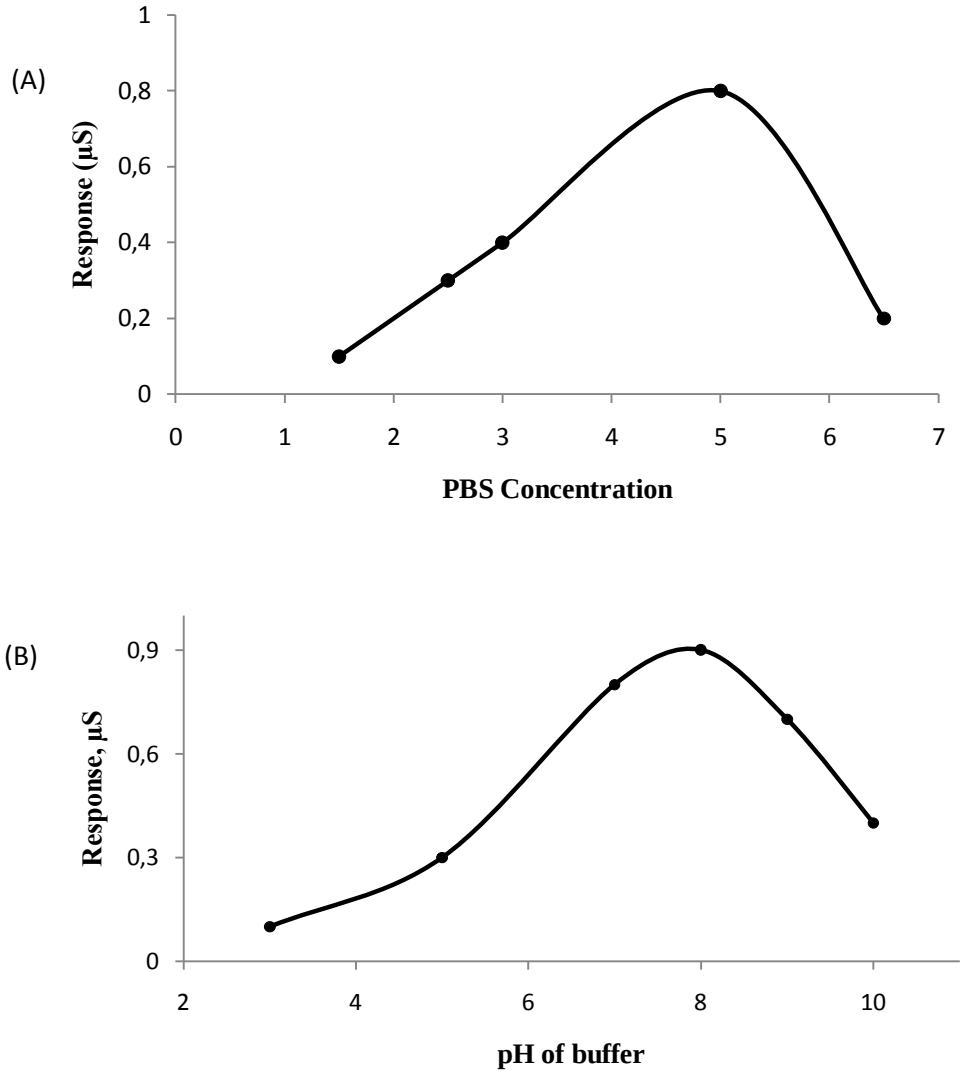

Figure 4.16: The dependence of responses of conductometric biosensors on concentration (A) and pH (B) of phosphate buffer for ZMTs.

4.2.1.4 Effect of Zeolite Morphology

For testing the influence of zeolite morphology on the sensitivity of ZMTs, Silicalite-2, zeolite A, and zeolite Y modified electrodes were studied and compared with SMTs (Figure 4.17).

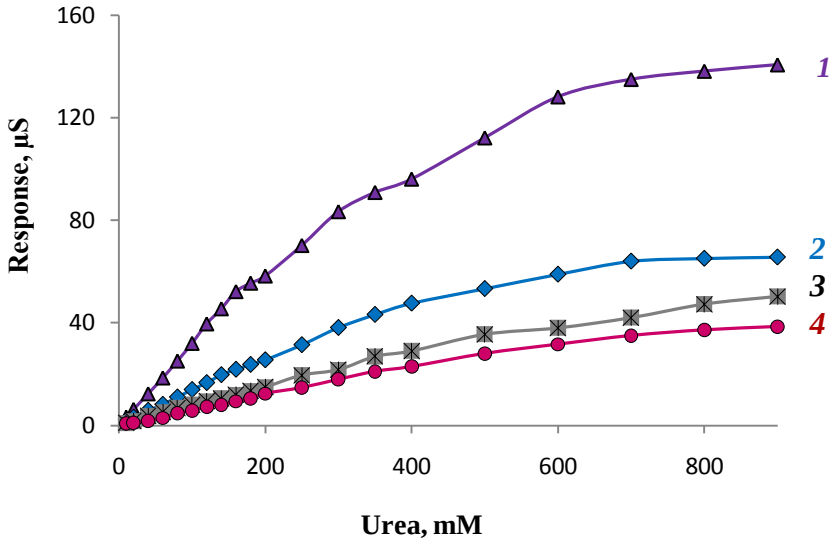

Figure 4.17: Calibration curves of biosensors based on immobilized urease with silicalite-2 (1), SMT (without zeolite) (2), zeolite Y (3), and zeolite A (4) modified sensors.

As seen in Figure 4.17, silicalite-2 modified sensors showed the highest response compared to other zeolite species and also relatively higher than the SMT based on urease immobilized without zeolite. Silicalite-2 had no aluminum, and thus it

was the most hydrophobic material among all samples investigated. Furthermore, zeolite Y showed slightly higher response than zeolite A. This could be related to the relatively higher pore size and Si/Al ratio and surface area of zeolite Y with respect to zeolite A crystals.

Furthermore, calibration curves of the laboratory prototypes of conductometric glucose transducers, ZMTs and SMTs are shown in Figure 4.18.

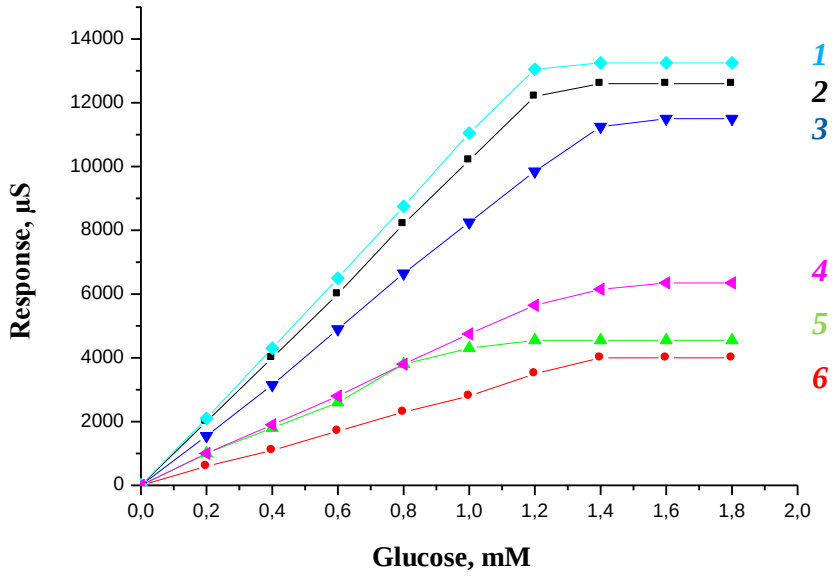

Figure 4.18: Calibration curves of biosensors based on immobilized glucose oxidase with NH_4^+ Beta 25 (2), Silicalite-1 (3), Silicalite-2 (4), H^+ Beta 300 (5), H+Beta 150 (6) and SMT (1).

According to Figure 4.18, the linear dynamic range of glucose determination was until 1-1.5 mM in 10 mM phosphate buffer solution with the detection limit of 200 nM. Analysis of working characteristics of developed biosensors demonstrated linear response to glucose for ZMTs in almost the same concentration range as SMTs. As can be seen from Figure 4.18, $NH4^+$ Beta-25 modified sensor based on glucose oxidase demonstrated the best working characteristics: low detection limit and high level of response. Furthermore, all $NH4^+$ Beta-25 modified sensors exhibited good storage and operational stability as well.

4.2.2 Ion Sensitive Field Effect Transistor (ISFET) Based Urea and Butyrylcholine Biosensors

4.2.2.1 Effect of Surface Silanol Groups and Brønsted Acidity of Heat Treated Zeolite Beta on the Analytical Characteristics of ISFET Biosensors

4.2.2.1.1 Synthesis and Modification of Zeolites

The sensitivities of urease and butyrylcholinesterase biosensors, prepared by the incorporation of zeolite Beta crystals with varying acidity into the membrane on the surface of pH-sensitive field-effect transistors (pH-FETs), have been studied and compared. In order to study exclusively the effect of zeolite acidity, highly crystalline pure zeolite Beta sample with Si/Al ratio of 17 (BEA-50) was

synthesized as it was explained in Chapter 4.1.1.2. Then zeolite Beta samples subjected to different heat treatment protocols and named as BEA-1 (heated from 25 to 500 °C at a rate of 1 °C/min, maintaining 500 °C for 6 h, and then cooled to 25 °C), BEA-2 (heated from 25 to 700 °C at a rate of 10 °C / min, maintaining 700 °C for 6 h, and cooled to 25 °C), and BEA-3 (heated from 25 to 700 °C at a rate of 1 °C/min, maintaining 700 °C for 6 h, and cooled to 25 °C).

4.2.2.1.1.1 Heat Treatment

Zeolite Beta attracts much attention due to its high specific surface area, large available micropore volume, large pore channel system, and adsorption ability. This material can be prepared to have different concentration of active acid sites by dealumination via thermal treatment at different conditions [126-128]. This should enable the investigation of the effect of changing acidic nature of this material on the biosensor characteristics. So far, the effect of acidic properties of zeolite matrices on the performance of biosensors is not clear. For this purpose, in order to induce a change in only the acidic properties of zeolite Beta and not the structural properties, pure zeolite Beta samples of with Si/Al ratio of 17 (BEA-50) were subjected to different heat-treatment protocols and named as BEA-1 (calcined at 500 °C with the ramp of 1 °C/min), BEA-2 (calcined at 700 °C with the ramp of 10 °C/min), and BEA-3 (calcined at 700 °C with the ramp of 1 °C/min). In this way, the surface acidic groups were controllably altered without changing any other zeolitic properties as confirmed by FTIR results. The aim of this investigation was to ascertain if a correlation existed between the obtained ISFET responses and the Brønsted acid sites, characterized by the 3610 cm^{-1} IR band.

The XRD patterns of as-synthesized and heat-treated zeolite Beta samples are shown in Figure 4.19.

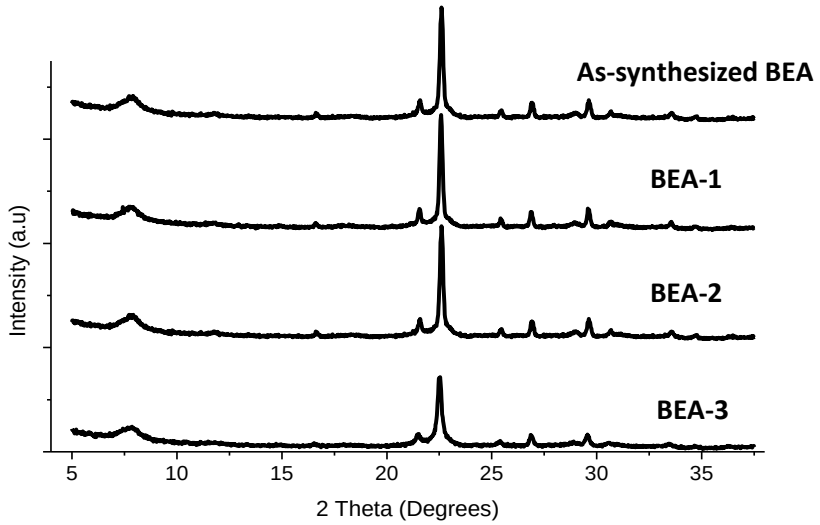

Figure 4.19: XRD patterns of the as-synthesized and heat-treated zeolite Beta samples.

All peaks observed in the as-synthesized sample matched the literature zeolite Beta XRD peak positions [113], and thus indicated that the product was pure material. Furthermore, the XRD patterns of the heat-treated samples confirmed that the long-range order of zeolite Beta was not affected by the heat treatment.

Figure 4.20 shows FE-SEM images of the as-synthesized and heat-treated zeolite Beta samples. The FE-SEM analysis (Figure 4.20, left image) revealed a typical, slightly rounded truncated square bipyramidal zeolite Beta morphology [129] for the as-synthesized zeolite Beta particles. The surfaces of these particles were not

smooth but contained smaller irregularities typically observed for zeolite Beta [130]. These particles were predominantly in the 0.4–1.7 μm size range.

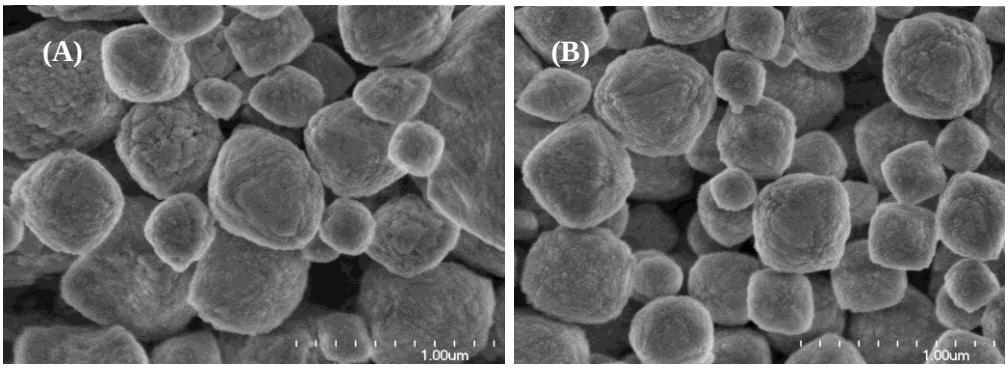

Fig. 4.20: FE-SEM micrographs of as-synthesized zeolite Beta (left image) and BEA-1 (zeolite Beta heat-treated at 500 °C with the ramp of 1 °C min^{-1}; right image) crystals.

According to the FE-SEM (Figure 4.20, right image), and XRD analysis (Figure 4.19) results, heat treatment did not cause any significant changes in zeolite Beta particle morphology, crystallinity, texture/surface features, and size.

Zeolite Beta is easily dealuminated by heat treatment [126, 131], and this methodology is used frequently to modify the acidity, tune the porosity, and improve the stability of zeolites [132]. The extent of acidic and other modifications introduced into the zeolite depends on the harshness of heat treatment, such as the heat treatment temperature and duration, heating rate, etc. [133]. Table 4.9 summarizes the textural properties of the as-synthesized and heat-treated zeolite Beta samples determined from the nitrogen sorption data.

Table 4.9: Properties of as-synthesized and heat treated zeolite Beta samples.

Sample	Si/Al [a]	Particle Size (nm)[b]	S_{total} (m^2/g)[c]	S_{EXT} (m^2/g)[d]	Pore Volume (cc/g)[e]
As-synthesized	17 ± 2	0.7	460	58	0.19
BEA-1	17 ± 2	0.7	666	84	0.28
BEA-2	17 ± 2	0.7	753	101	0.32
BEA-3	17 ± 2	0.7	739	72	0.31

[a] Measured by EDX.

[b] Measured by API Aerosizer LD.

[c] Measured by Multipoint BET .

[d] Measured by t-plot Method.

[e] Measured by Saito-Foley (SF) Method.

The Si/Al ratio of the as-synthesized (parent) zeolite Beta crystals was found to be 17±2 as measured by EDX (Table 4.9). All three heat-treated zeolite samples (i.e., BEA-1, BEA-2, and BEA-3) prepared from the parent material showed the same Si/Al ratios of 17±2 (Table 4.9). Thus, it appears that different calcination procedures did not result in any significant changes in the Si/Al ratio of the resulting materials. This is because aluminum atoms that are taken out of the framework due to heat treatment remain in the zeolite volume in the form of extra-framework aluminum [134]. These changes in the nature of the framework aluminum will likely affect acidic properties of zeolite Beta. Thus, in principle the use of differently heat-treated zeolite Beta samples that come from the same starting batch of material should allow to investigate the sole effect of zeolite acidity on adsorption of biomolecules without additional variation (e.g., different

particle size and morphology,) that may be introduced when using different zeolite types [135-136]. To date, adsorption of proteins, including urease, showed some dependence on the Brønsted acid sites in zeolites [50]. However, these results were obtained using various zeolite types with different Si/Al ratios and pore sizes as well as crystal size and morphology.

As shown in Table 4.9, the BET and external surface area (S_{BET}, i.e., the total surface area and S_{EXT}, i.e., the external surface area) of the heat-treated samples increased with respect to the as-synthesized material. The observed increase in the surface area can be due to an increase in the accessible pore volume of zeolite Beta samples upon the removal of the template after heat treatment (Table 4.9) [137]. This increase was deemed not to affect the adsorption of urease and BuChE on zeolite Beta (i.e., adsorption only on the external zeolite surface is considered), and the biosensor performance because the average diameters of these enzymes (~13 nm for urease [138] and ~6 nm for BuChE [139]) are larger than the pore size of zeolite Beta (~0.5 nm, Table 4.9).

In order to investigate the contribution of Brønsted acid sites to the biosensor activities, Fourier transform infrared (FTIR) spectroscopy was employed for heat-treated samples and the details of the FTIR results are clarified in the next content.

Figure 4.21 demonstrates the IR spectra in the OH-stretching region for three heat-treated zeolite Beta samples. Each sample shows two clear IR bands at ~3745 and ~3610 cm^{-1}. The band at ~3745 cm^{-1} is commonly attributed to the non-/weakly acidic terminal silanol groups (Si–OH) on the external surface of crystals [127]. The band at ~3610 cm^{-1} is assigned to the bridging OH groups in tetrahedrally coordinated Si–(OH)–Al groups (Brønsted acid sites) in the zeolite framework [128]. This band can be affected by heat treatment of zeolite Beta

crystals due to the dealumination process, which leads to lower intensity of the 3610 cm^{-1} band [110-111]. Brønsted acidity is present both on the internal and external surface of zeolite Beta [131]. The silanol groups and Brønsted acid sites in mesoporous silica and microporous zeolites have been investigated for their possible roles in the adsorption of different enzymes [140-142]. In the physical adsorption of enzymes, the NH_2 and C=O groups of the enzyme interact with OH groups of the solid support. The strength of these interactions increases with the increasing acidity of the OH groups [142]. For silanol groups these interactions are not strong enough to prevent the enzyme leaching [140-141].

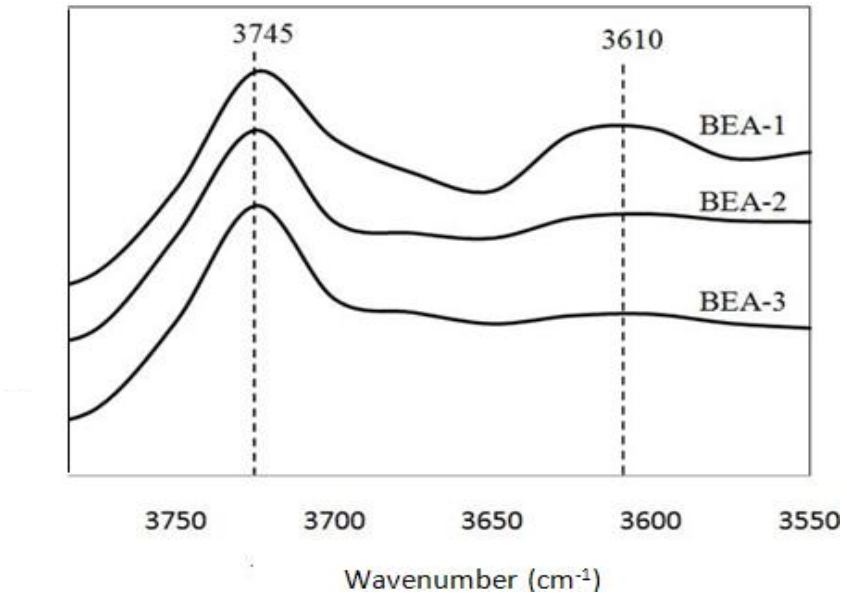

Figure 4.21: Absorbance FTIR spectra in the OH-stretching region of different heat-treated zeolite Beta samples recorded at 100 °C: BEA-1 (heat-treated at 500

°C with the ramp of 1 °C min^{-1}), BEA-2 (heat-treated at 700 °C with the ramp of 10 °C min^{-1}), and BEA-3 (heat-treated at 700 °C with the ramp of 1 °C min^{-1}).

As shown in Figure 4.21, the intensity of the 3745 cm^{-1} IR band did not change significantly; however, the 3610 cm^{-1} IR band significantly decreased in intensity upon applying different heat treatment protocols. When the calcination temperature was increased from 500 °C (sample BEA-1) to 700 °C (sample BEA-2), the integrated intensity of the band at 3745 cm^{-1} decreased slightly (ca. 10%); however, no further changes to this band integrated intensity were observed upon changing the temperature ramp rate (sample BEA-2 versus sample BEA-3). The nearly constant area of the 3745 cm^{-1} band suggests the invariant amount of terminal silanol groups in all heat-treated samples. This is reasonable considering that the intensity of this band is affected by the crystal size [137]; and the FE-SEM (Figure 4.20), data suggested no changes in the morphology/surface features/size of zeolite Beta particles upon heat treatment. The major change observed in the OH-stretching region upon zeolite heat treatment was ca. 85–90% decrease (from sample BEA-1 to sample BEA-3) of the integrated intensity of the band at 3610 cm^{-1}. Furthermore, the integrated intensity of the band at 3610 cm^{-1} progressively decreased from sample BEA-1 to sample BEA-2 and sample BEA-3. This gradual reduction suggests the increasing extent of aluminum removal from the framework for heat-treated zeolite Beta samples. Because of the identical Si/Al ratio measured by EDX for all samples (Table 4.9), the observed decrease in the integrated intensity intensity of 3610 cm^{-1} band suggests that aluminum removed from the zeolite framework upon heat treatment still remains in the zeolite volume in the form of extra-framework aluminum species [134]. The gradual changes to the integrated intensity of the 3610 cm^{-1} band suggested that heat treatment of zeolite Beta resulted in a gradual decrease in the amount of Brønsted acid sites [110].

The framework defects can modify activities of zeolite samples in many different catalytic reactions and adsorption processes. Firstly, in order to investigate the effect of differently heat-treated zeolite Beta samples incorporated into the electrodes on the ISFET performance, ISFET measurement were carried out using urease and BuChE.

4.2.2.1.2 Biosensor Measurements

4.2.2.1.2.1 Sensitivity

The enzymatic response of biosensors based on BuChE and urease were investigated and compared upon modifying the ISFET electrodes with zeolite Beta particles heat-treated differently (i.e., BEA-1, BEA-2, and BEA-3 samples). The obtained biosensor calibration curves based on BuChE and urease immobilized on different zeolite Beta particles are shown in Figure 4.22 (A) and (B), respectively.

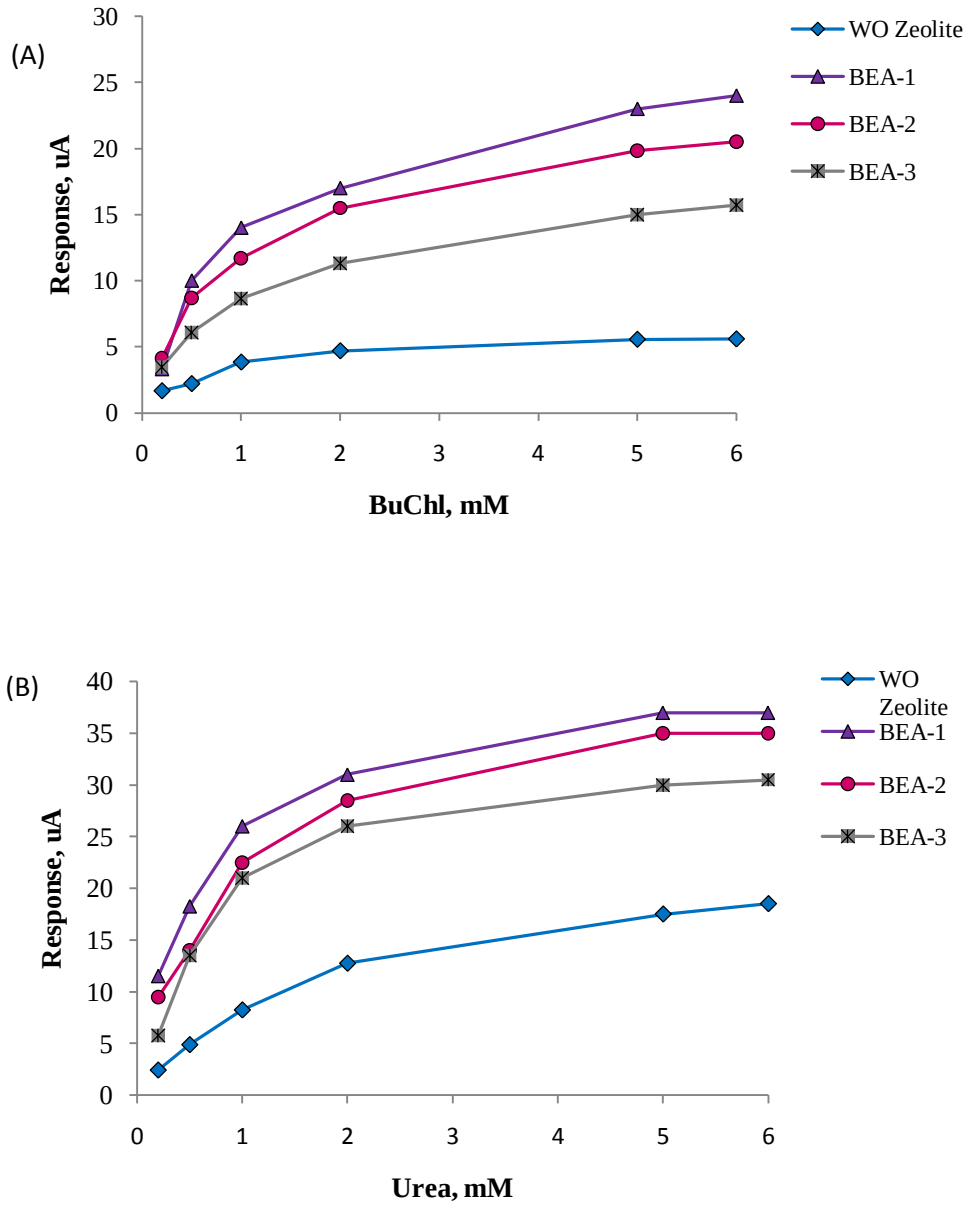

Figure 4.22: Calibration curves of biosensors based on immobilized BuChE (A) and urease (B), with/without heat-treated zeolite Beta samples. Measurements were conducted in 5 mM PBS, pH 7.4.

In general, zeolite addition into the enzymatic membranes increased the responses for both types of biosensors. The response of biosensors modified with BEA-1 sample was the highest among all the zeolite-modified biosensors, and increased approximately 3 times for BuChE and 2 times for urease, as shown in Figure 4.22. The biosensor responses obtained using sample BEA-2 and BEA-3 were lower (Figure 4.22, and the responses measured for all three zeolite Beta samples decreased in the order of BEA-1 > BEA-2 > BEA-3 for both enzymes investigated (Figure 4.22). Thus, removal of aluminum from the zeolite Beta framework, suggested by the decreasing intensity of the 3610 cm^{-1} IR band (Figure 4.21), resulted in a decrease of enzymatic activity likely because the extra-framework aluminum blocked other surface sites. These results show for the first time that it was possible to tailor the electrode surfaces by a simple heat treatment procedure applied to the zeolite incorporated therein, and regulate the ISFET responses for two different enzymatic activities. Furthermore, these results demonstrated a new approach for varying zeolite acidity without simultaneously changing zeolite morphology for biosensor applications.

4.2.2.1.2.2. Operational Stability and Inhibition

Operational stability, an important working characteristic of biosensors, was also studied by modifying the electrodes by heat treated zeolite Beta samples. Obtained results shown in Figure 4.23. Biosensor responses to 5 mM BuChl and urea were determined during one working day with 30-min intervals during which the ISFETs with immobilized bio-membranes were kept in the working buffer solution all the time between measurements.

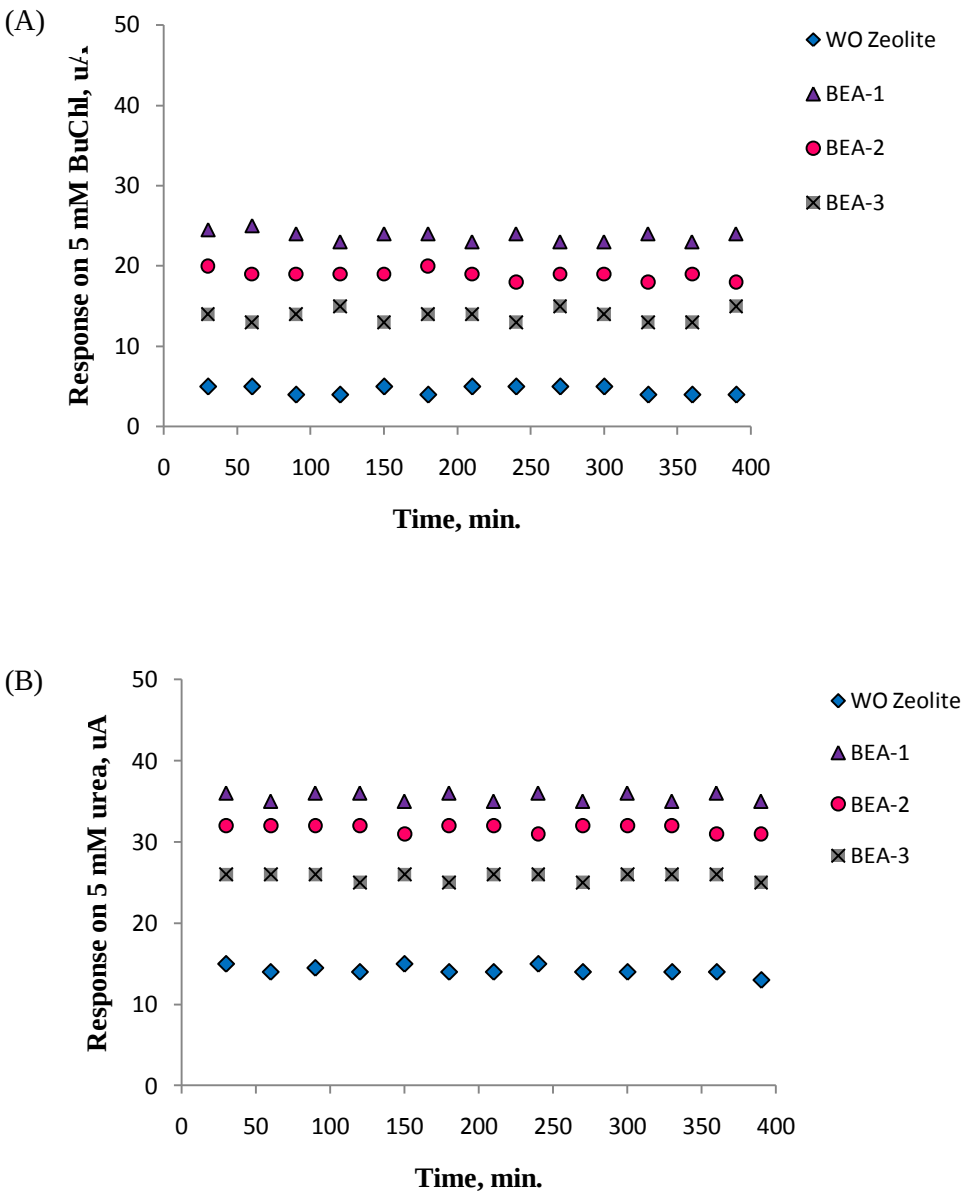

Figure 4.23: Operational stability of biosensors with immobilized BuChE (A) and urease (B). Measurements were conducted in 5 mM PBS, pH 7.4; BuChl and urea concentration was 5 mM.

As shown in Figure 4.23, all biosensors demonstrated high signal reproducibility for both BuChE and urease. Furthermore, storage stability experiments were also performed by storing biosensors in buffer at room temperature, and all sensors modified by heat treated zeolite Beta were stable for more than 5 days.

The inhibition effect due to glycoalkaloids and metal ions was also investigated using BuChl and urea biosensors, respectively. Thus, the effect of different heat treated zeolite Beta samples incorporated in bioselective membrane on biosensor sensitivity to glycoalkaloids and heavy metal ions was examined in the next content. Calibration curves of residual activity of biomembranes based on BuChE and urease as a function of the concentration of glycoalkaloids and mercury ions are presented in Figure 4.24.

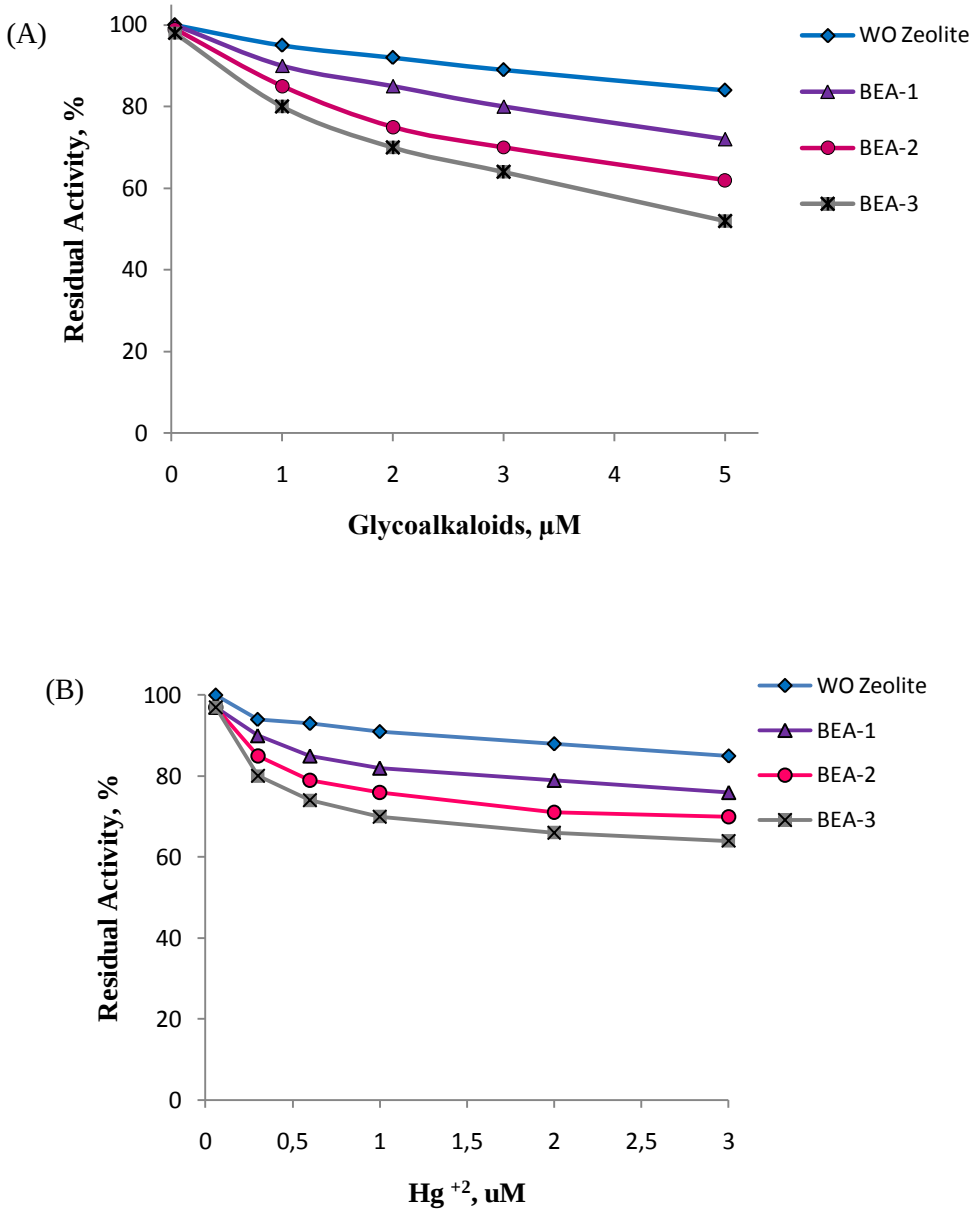

Figure 4.24: Dependence of residual activity of bio-membranes based on BuChE (A) and urease (B) on concentration of glycoalkaloids and mercury ions (Hg^{+2}). Measurements were conducted in 5 mM PBS, pH 7.4.

As shown in Figure 4.24 (A), all BuChl biosensors based on BEA samples showed higher sensitivity to glycoalkoloids than the zeolite-free biosensor, and these sensitivities decreased in the order of BEA-3 > BEA-2 > BEA-1. Similar trends were observed for the mercury ions for urease-based biosensors, i.e., sensitivities to mercury ions were lowest for biosensors without zeolite crystals and decreased in the order of BEA-3 > BEA-2 > BEA-1.

According to the FTIR results and ISFET tests (Figs. 4.21 and 4.22), the responses obtained from the zeolite-modified electrodes (ZMTs) correlated well with the number of Brønsted acid sites created in zeolite Beta samples upon heat treatment. Thus, for both enzymes the highest biosensor response was achieved using sample BEA-1 having the largest amount of Brønsted acid sites characterized by the 3610 cm^{-1} band with the largest integrated intensity, whereas the lowest response was recorded using sample BEA-3 with the smallest number of Brønsted acid sites. Furthermore, the results shown in Figure 4.22, 4.23, and 4.24 indicated that the activities, operational stabilities and inhibition characteristics of BuChE and urease based biosensors were also strongly related to the amount of Brønsted acid sites. In the literature, silanol groups and Brønsted acidity have been investigated for their roles in the immobilization of enzymes [140-142]. However, thus far an ISFET study, which could potentially give the best indication on whether the obtained biosensor data was affected by the changing nature of the modified electrode, related to any of the acid sites observed by FTIR spectroscopy, has not been published. According to the current results, Brønsted acid sites can be hypothesized to be responsible for the obtained ISFET activities. Since the amount of terminal silanols was not affected by the heat treatment protocols used in this study, no conclusion can be made regarding the effect of these non-/weakly acidic OH groups on the ISFET activities. The current results show that the interactions between the enzymes and the Brønsted

acid sites of zeolite support can affect the actual biosensor performances in such a way that the attained responses can be controllably altered. This makes zeolites even stronger candidates for use as electrode modifiers, and for their potential integration into biosensors.

4.2.2.2 Effect of Si/Al, Particle Diameter and Surface Charge of Nano Sized Zeolite Beta on the Analytical Characteristics of ISFET Biosensors

4.2.2.2.1 Synthesis and Modification of Zeolites

In order to investigate the effect of hydrophobicity on the analytical characteristics of ISFET based biosensors, nano sized zeolite Beta was chosen by considering the Si/Al ratio of 50, 75, and 100. Thus three optimized gel synthesis formulas, i.e., formula X: 0.5 Al_2O_3 : 25 SiO_2 : 490 H_2O : 9 TEAOH (N-BEA-50), formula XI: 0.35 Al_2O_3 : 25 SiO_2 : 490 H_2O : 9 TEAOH (N-BEA-75), and formula XII: 0.25 Al_2O_3 : 25 SiO_2 : 490 H_2O : 9 TEAOH (N-BEA-100) were used to examine the effect of Si/Al ratio on the sensitivity, stability and inhibition characteristics of biosensors.

The XRD patterns and FE-SEM images of synthesized nano sized zeolite Beta crystals are shown in Figure 4.25 and Figure 4.26, respectively.

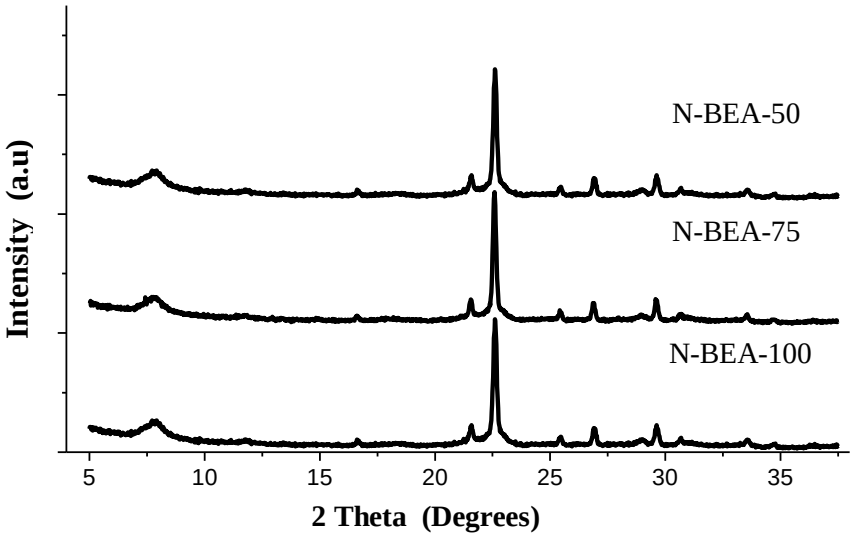

Figure 4.25: XRD patterns of nano sized zeolite Beta crystals with varying Si/Al ratio.

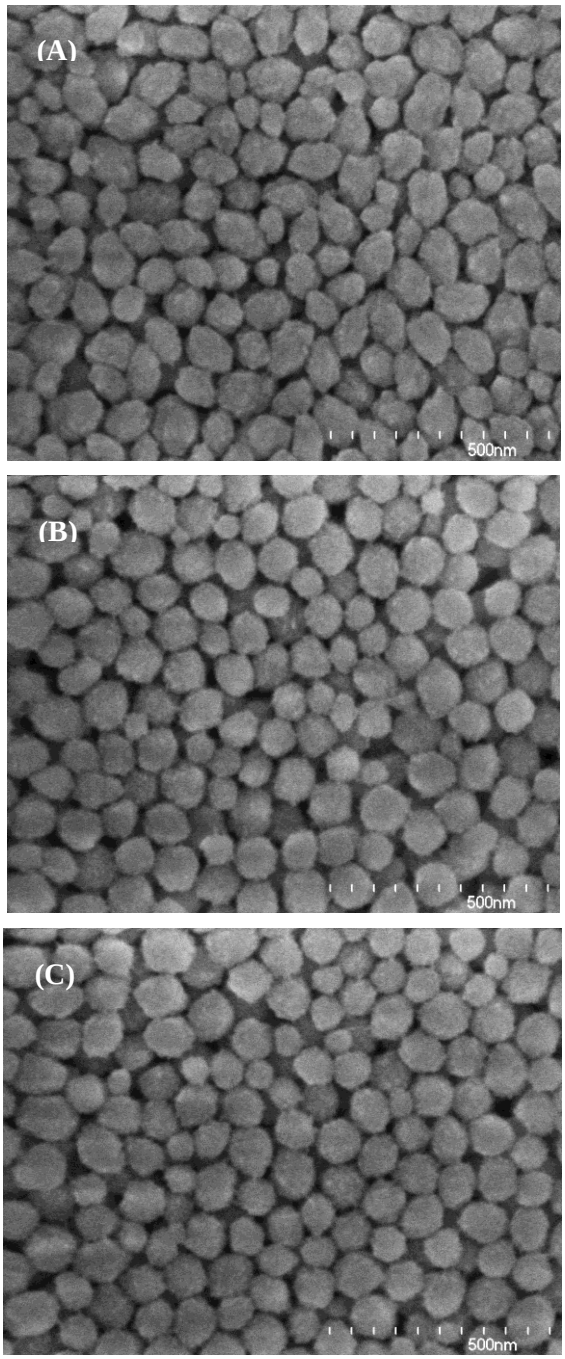

Figure 4.26: FE-SEM images of nano sized zeolite Beta crystals with varying Si/Al ratio, 50 (A), 75 (B), and 100 (C).

All peaks observed in the Figure 4.25, matched the literature zeolite Beta XRD peak positions [114], and thus indicated that the product was pure material. Furthermore, Figure 4.26 shows FE-SEM images of synthesized nano sized zeolite Beta products. The images revealed the spheroidal and truncated square bipyramidal morphology of the zeolite Beta nano particles. These particles were predominantly in the 0.7-1 nm size range.

Table 4.10 summarizes the textural properties of the nano sized zeolite Beta samples obtained upon varying Si/Al ratio.

Table 4.10: Summary of the textural properties of nano sized zeolite Beta crystals.

Formula	Sample Name	Si/Al[a]	Part. Size (nm)[b]	S_{total} (m^2/g)[c]	S_{EXT} (m^2/g)[d]	Pore Volume (cc/g)[e]	Surf. Charge (mV)[f]
IX	N-BEA-50	14.4±1.4	~70	510	252	0.22	-15
X	N-BEA-75	17.4 ±1.5	~70	550	275	0.23	-20
XI	N-BEA-100	22.3 ±2.2	~70	557	303	0.23	-19

[a] Measured by EDX.

[b] Measured by API Aerosizer LD.

[c] Measured by Multipoint BET .

[d] Measured by t-plot Method.

[e] Measured by Saito-Foley (SF) Method.

[f] Measured by Zeta potential at pH 7.

According to the results shown in Table 4.10, although a large variation of gel composition formulas were investigated to obtain different Si/Al ratios, the lowest

and highest Si/Al ratio attained were 14.4 and 22.3, respectively. However, a very small increase in the external surface area was obtained (from 252 m^2/g to 275 and 303 m^2/g) upon changing the synthesis formula from IX to X and XI, respectively. Furthermore, none of the sample exhibits significant change in the pore size, pore volume, and surface charge after using different synthesis formulas.

Furthermore, nano sized zeolite Beta crystals were then subjected to functionalization process with 3-APTES in order to investigate the influence of surface charge of the crystals surfaces on the biosensor performance. Table 4.11 summarizes the textural properties of functionalized and non-functionalized zeolite Beta nano crystals.

Table 4.11: Textural properties of functionalized and non-functionalized zeolite Beta nano crystals.

Sample Name	Surface Group	Si/Al [a]	Particle Size (nm) [b]	S_{total} (m^2/g) [c]	S_{EXT} (m^2/g) [c]	Pore Volume (cc/g) [d]	Surf. Charge (mV) [e]
Funct-N-BEA-50	OH^-, NH_2^+	14.4	~70	550	255	0.25	12
N-BEA-50	OH^-	14.4	~70	510	252	0.22	-15

[a] Measured by EDX.

[b] Measured by API Aerosizer LD.

[c] Measured by Multipoint BET.

[d] Measured by Saito-Foley (SF) Method..

[e] Measured by Zeta potential at pH 7.

As shown in Table 4.11, small increase in the total and external surface area was observed for the functionalized sample. This can be ralted with the attachment of a layer of functional moiety on the pore walls and external surface. Furthermore, surface charge of the samples was changed from -15 to +12.

Furthermore, characteristics of butyrylcholinesterase and urease-based biosensors for direct butyrylcholine and urea determination were investigated and compared upon modifying the ISFET electrodes with synthesized and modified nano sized zeolite Beta particles. Since sensitivity, stability and inhibition were the most important working characteristics of any biosensor, the influence of Si/Al ratio, particle diameter and surface charge of zeolite Beta on these parameters were investigated. Table 4.12 summarizes the zeolite Beta materials used in the following ISFET study.

Table 4.12: Summary of the nano sized zeolite Beta materials used in the ISFET study.

Sample Name	Morphology	Modification	Purpose
N-BEA-100	Nano-sized Zeolite Beta	Varying Si/Al Ratio	Effect of Si/Al Ratio
N-BEA-75	Nano-sized Zeolite Beta	Varying Si/Al Ratio	Effect of Si/Al Ratio
N-BEA-50	Nano-sized Zeolite Beta	Varying Si/Al Ratio	Effect of Si/Al Ratio Effect of Surface Charge Effect of Particle Size
Funct.-N-BEA-50	Nano-sized Zeolite Beta	Varying Surface Charge	Effect of Surface Charge
BEA-50	Sub-micron Zeolite Beta	Particle Size	Effect of Particle Size

4.2.2.2.2 Biosensor Measurements

4.2.2.2.2.1 Sensitivity

The enzymatic response of biosensors based on urease and BuChE was investigated and compared upon modifying the ISFET electrodes with nano sized zeolite Beta particles with varying Si/Al ratio (50, 75, and 100), particle diameter (70 and 700 nm), and surface charge (-OH and -NH_2). The obtained biosensor calibration curves for BuChE and urease based biosensor are shown in Figure 4.27, 4.28, and 4.29, respectively.

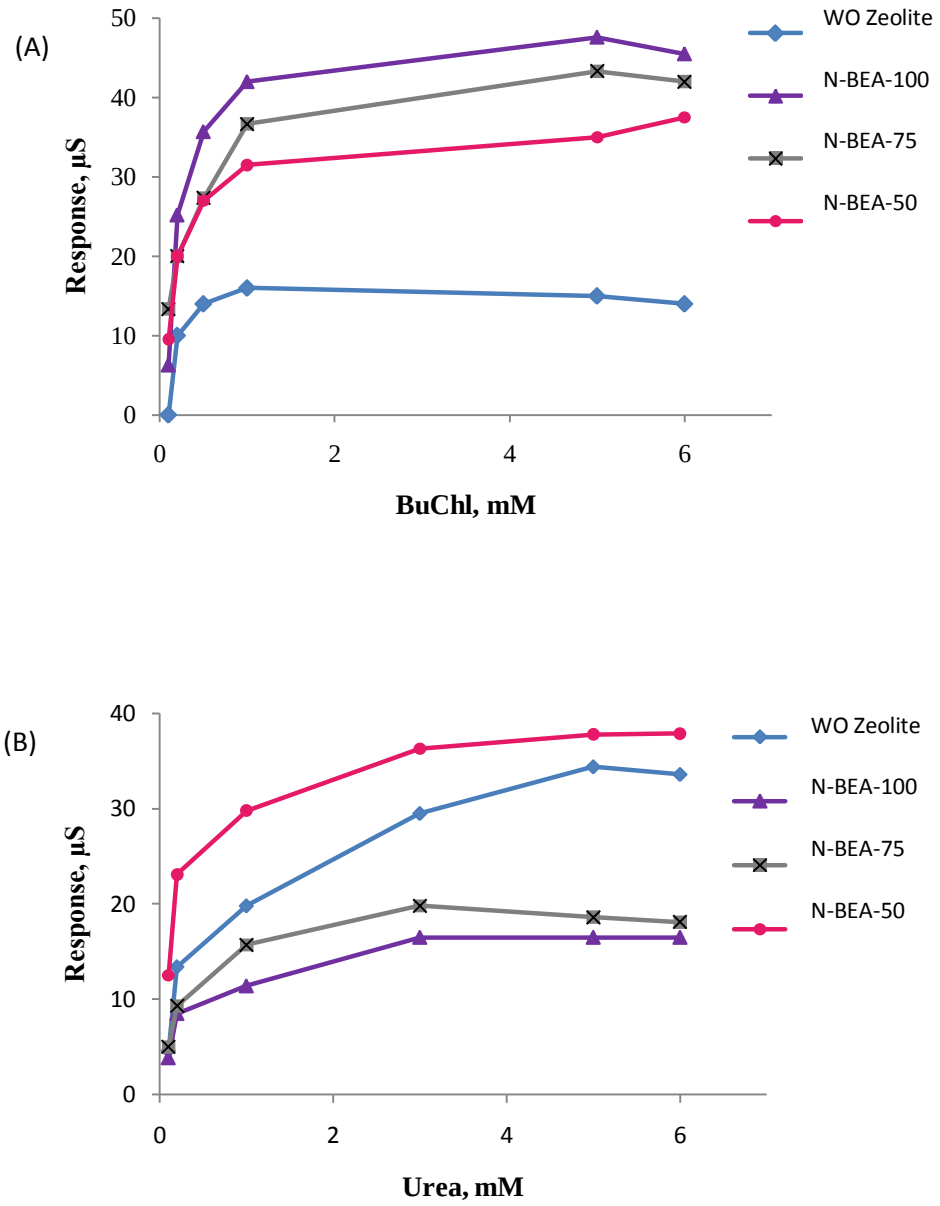

Figure 4.27: Calibration curves of biosensors based on immobilized BuChE (A) and urease (B), with/without nano sized zeolite Beta samples with varying Si/Al ratio. Measurements were conducted in 5 mM PBS, pH 7.4.

According to the obtained results shown in Figure 4.27, biosensor responses were the highest for N-BEA-100 and N-BEA-50 samples for BuChE and urease, respectively. The responses were increasing in the order of N-BEA-100>N-BEA-75>N-BEA-50 for BuChE based biosensors and N-BEA-50>N-BEA-75>N-BEA-100 for urease based biosensors.

In general, aluminum (Al^-) incorporation into the zeolite framework increases the hydrophilicity of the crystal and caused more Brønsted acid sites (proton donors) and negatively charged surfaces. In this way, higher amounts of negative charges and acid sites can be generated. For this reason, aluminum content in the zeolite network should have a strong influence on the enzymatic reactions due to the varying acidity and electrostatic properties of the zeolite surfaces. Figure 4.27 demonstrates that the observed more significant increase in sensitivity to urea upon using N-BEA-50 crystals with respect to N-BEA-75 and N-BEA-100. As a matter of fact, the nature of the reaction of urea catalysis was an example of a hydrolysis system and required proton as a reactant. Thus, increasing aluminum atoms stimulates the urease reaction by increasing proton donor sites of the zeolite network. Additionally, generated negative charges by increased aluminum atoms attract more substrate (urea) molecules which contain two positively charged amine groups in the structure.

On the other hand, BuChE reaction was an example of the "charge relay" system which reveals mobile proton as a product. Thus, proton donors should not have been essential for the BuChE reaction. Furthermore, some electrostatic interactions came into play according to the increased enzymatic activity with N-BEA-100 samples (Figure 4.27). As it was discussed previously, Al addition into the zeolite framework yielded a negative charge per Al atom thus high positivity

would be expected from the high Si/Al ratio. Since BuChl molecules had negative charges due to Cl^- ions, they may have been in close contact with the more positively surfaces (N-BEA-100). Thus, some electrostatic interactions were present between charged BuChl molecules and zeolite surfaces which induced the substrates to reach the immobilized enzymes more efficiently. As a result, an increased activity of BuChE was observed.

Furthermore, surface curvature and surface area are two important parameters that influence the immobilization and activity of the employed proteins. For thispurpose sensitivities of urease and BUChE based biosensors compared by the incorporation of zeolite Beta with two different particle diameters; 70 nm and 700 nm (Figure 4.28). Since diameter of BuChE and urease are larger than the micropores of the employed nano sized zeolite Beta crystals, proteins only interact with the outer surface of zeolite. Thus higher immobilization amounts of proteins on larger zeolite Beta crystals would be expected as it was discussed in the section 4.3.1.2. On the other hand, increased particle size causes to higher degree of conformational change and promote the retention of native enzyme structure and function. Thus reduced activity would be expected for the highly adsorbed enzymes as it was stated by other researchers [40].

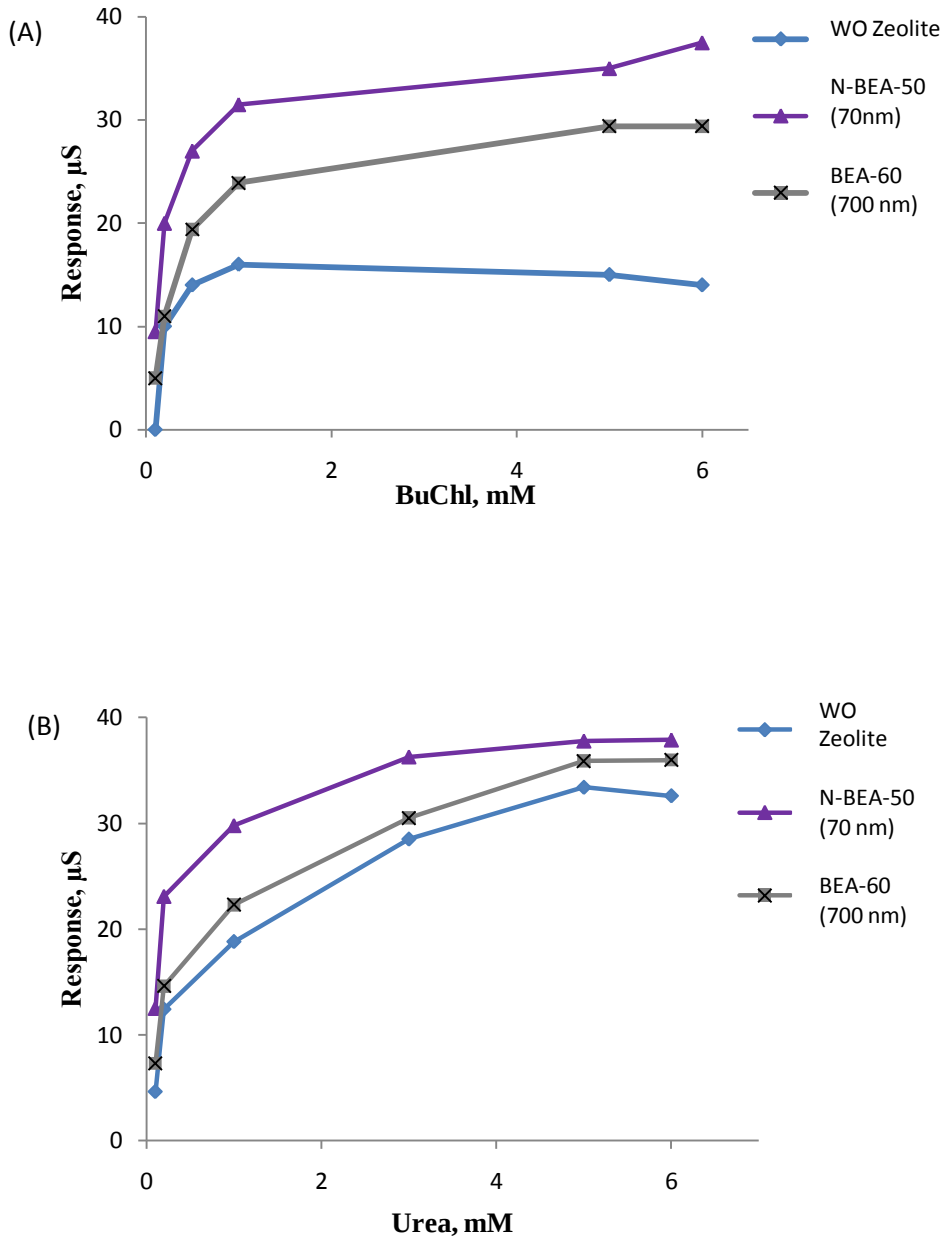

Figure 4.28: Calibration curves of biosensors based on immobilized BuChE (A) and urease (B), with/without nano sized zeolite Beta samples with varying particle diameter. Measurements were conducted in 5 mM PBS, pH 7.4.

As it was shown in Figure 4.28, the observed more significant increase in sensitivity to BuChl and urea upon using nano sized zeolite Beta samples (70 nm) with respect to sub-micron zeolite Beta crystals (700 nm) is due to the wider outer surface provided by larger zeolite A crystals leads proteins to elongate through the surface and partially unfold, which results decrease in enzymatic activity. Additionally, big crystals may act as barriers on the outer surface of the bioselective membrane and blockade the substrate to reach the enzyme more efficiently thus reduced activity of enzymes was observed.

Another factor that was investigated was the effect of surface functionalization of nano sized zeolite Beta samples. The obtained results are shown in Figure 4.29.

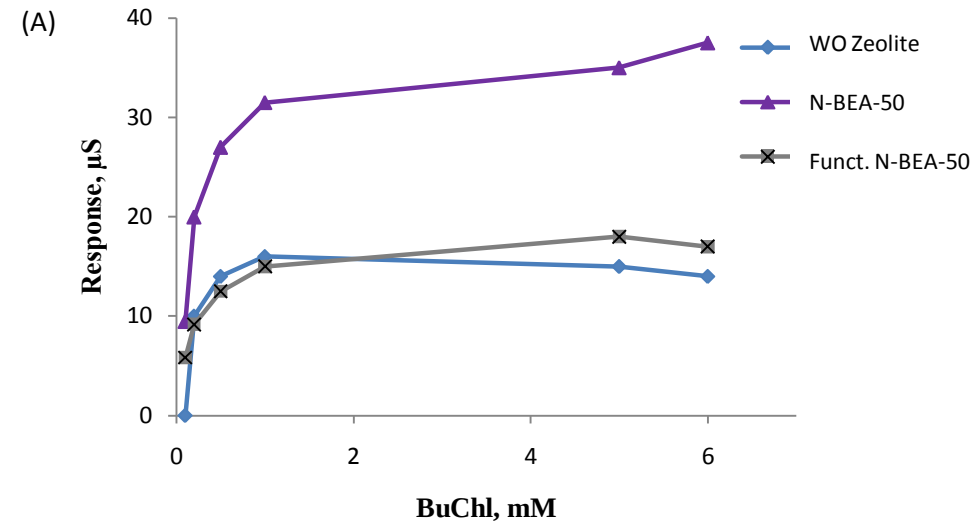

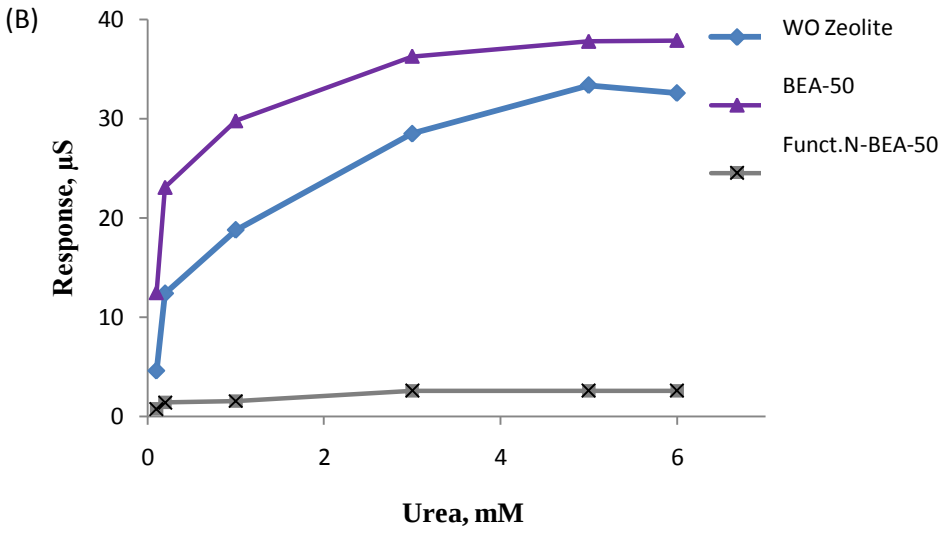

Figure 4.29: Calibration curves of biosensors based on immobilized BuChE (A) and urease (B), with/without nano sized zeolite Beta samples with varying surface charge. Measurements were conducted in 5 mM PBS, pH 7.4.

As shown in Figure 4.29, relatively high sensitivity to BuChl and urea was observed with non-functionalized zeolite Beta with compared to functionalized Beta crystals. This can be related to the formation of a large number of bonds between glutaraldehyde, amine functionalized zeolite surface and enzyme molecules, which might have caused a very compact structure of the biomembrane. Thus the active site of the enzyme was inaccessible.

4.2.2.2.2.2 Operational Stability and Inhibition

Operational stability of BuChE and urease based biosensors were also studied depending on the presence of nano sized zeolite Beta with varying Si/Al ratio. Biosensor responses to 5 mM BuChl and urea were determined for 7 hours with 30-min intervals during which the ion-selective field-effect transistors with immobilized bio-membranes were kept in the working buffer solution all the time between measurements. The results are shown in Figure 4.30.

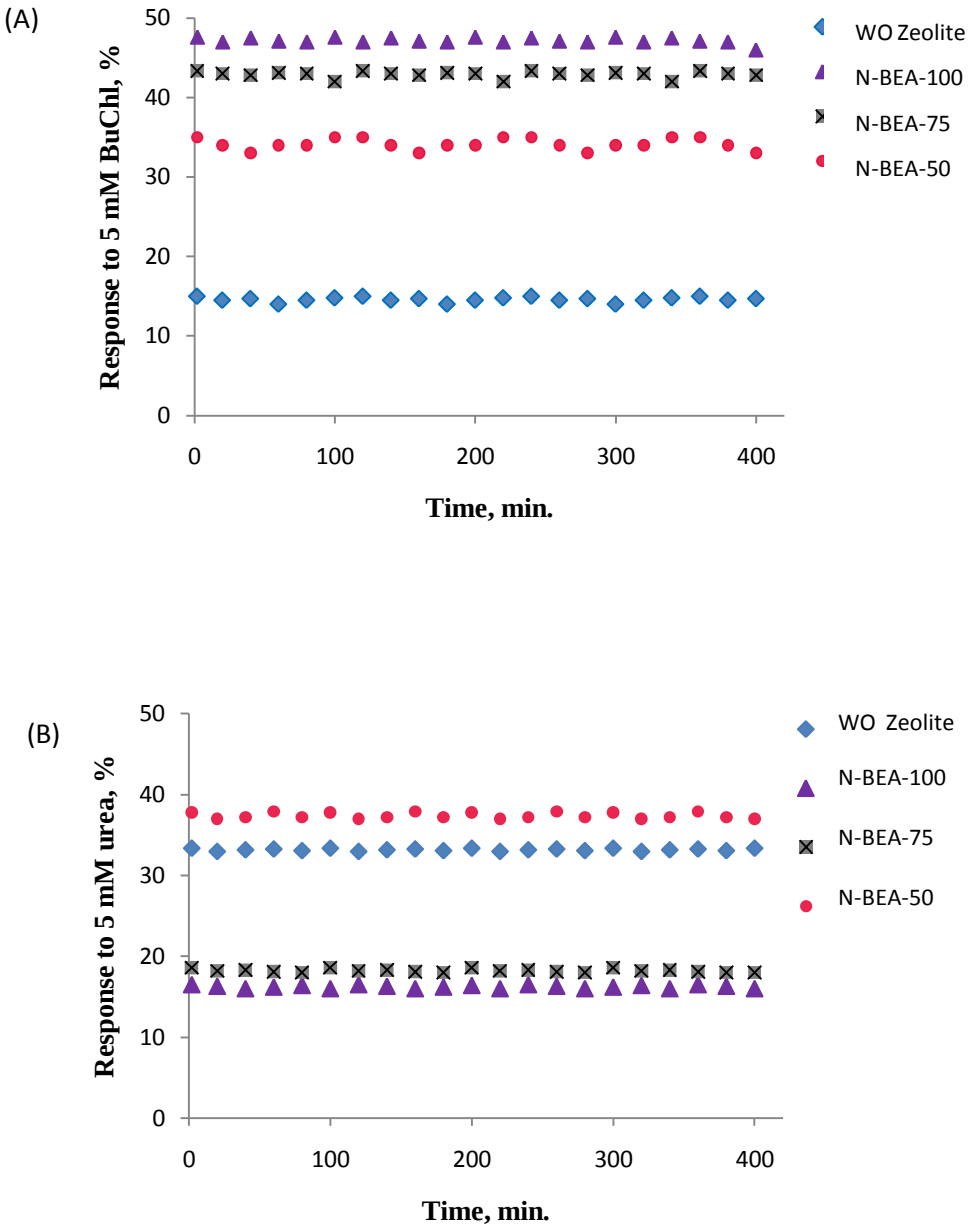

Figure 4.30: Operational stability of biosensors based on immobilized BuChE (A) and urease (B). Measurements were conducted in 5 mM phosphate buffer, pH 7.4, BuChl and urea concentration was 5 mM.

As it can be seen in Figure 4.30, all biosensors showed high signal reproducibility for both BuChE and urease cases. Furthermore, storage stability experiments were performed by storing biosensors in buffer at room temperature and all samples containing nano sized zeolite Beta were stable for more than 7 days.

The inhibition effect due to glycoalkaloids and metal ions was also investigated using BuChl and urea biosensors. For this purpose, nano sized zeolite Beta crystals modified transducers were used in order to clarify the influence of Si/Al ratio on the inhibition characteristics of biosensors. Calibration curves of residual activity of bioselective membranes based on BuChE and urease as a function of the concentration of glycoalkaloids and mercury ions are presented in Figure 4.31.

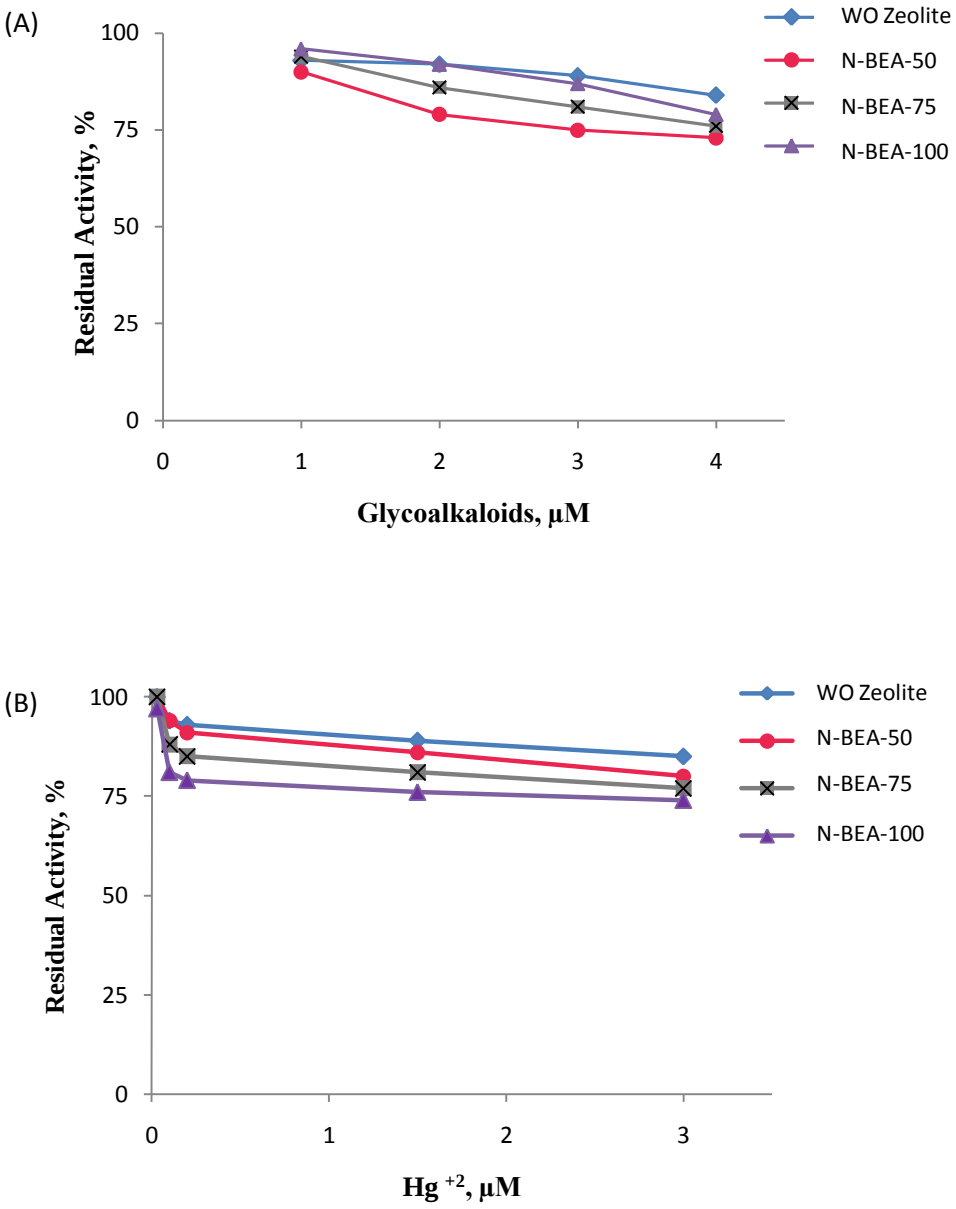

Figure 4.31: Dependence of residue activity of bioselective membranes based BuChE and urease on concentration of glycoalkoloids and mercury ions (Hg^{+2}), respectively. Measurements were conducted in 5 mM PBS, pH 7.4

As shown in Figure 4.31, all BuChl biosensors based on nano sized zeolite Beta samples showed higher sensitivity to glycoalkaloids than the zeolite-free biosensor, and these sensitivities decreased in the order of N-BEA-50 > N-BEA-75 > N-BEA-100. On the other hand, related trends were observed for the mercury ions for urease-based biosensors, i.e., sensitivities to mercury ions were lowest for biosensors without zeolite crystals but decreased in the order of N-BEA-100 > N-BEA-75 > N-BEA-50. The inhibition results correlate with the sensitivity results of biosensors which suggest that the Si/Al ratio has a powerful influence on the analytical characteristics of BuChE and urease based ISFET type biosensors.

Then, influence of silicalite, SBA-15, and functionalizad SBA-15 modified electrodes on the analytical characteristics of ISFET based biosensors were also investigated due to varying pore diameter and surface charge of the silica materials which synthesis conditions and characterizations were discussed in the previous sections.

4.2.2.3 Effect of Pore Size and Surface Charge of Silica Particles on the Analytical Caracteristics of ISFET Biosensors

The sensitivities of urease and butyrylcholinesterase biosensor transducers, prepared by the modification of silica particles with varying pore size and surface charge, have been studied and compared. Sensitivity, stability and inhibition characteristics of each biosensor were investigated.

4.2.2.3.1 Synthesis and Modification of Zeolite and Zeo-type Materials

Synthesis and modification studies of silicalite and SBA-15 particles were explained in the Sections 4.1.1.3 and 4.2.2.1. According to XRD and FE-SEM results, all products were pure silica materials. Functionalization procedure then applied to the SBA-15 particles with the aim of varying surface charge and pore diameter.

4.2.2.3.2 Biosensor Measurements

4.2.2.3.2.1 Sensitivity

The enzymatic response of urease and BuChE based biosensors were investigated and compared upon modifying the ISFET electrodes with silica particles with varying pore diameter (microporous silicalite and mesoporous SBA-15) and surface charge (-OH and -NH_2). The obtained biosensor calibration curves for BuChE and urease based biosensor are shown in Figure 4.32.

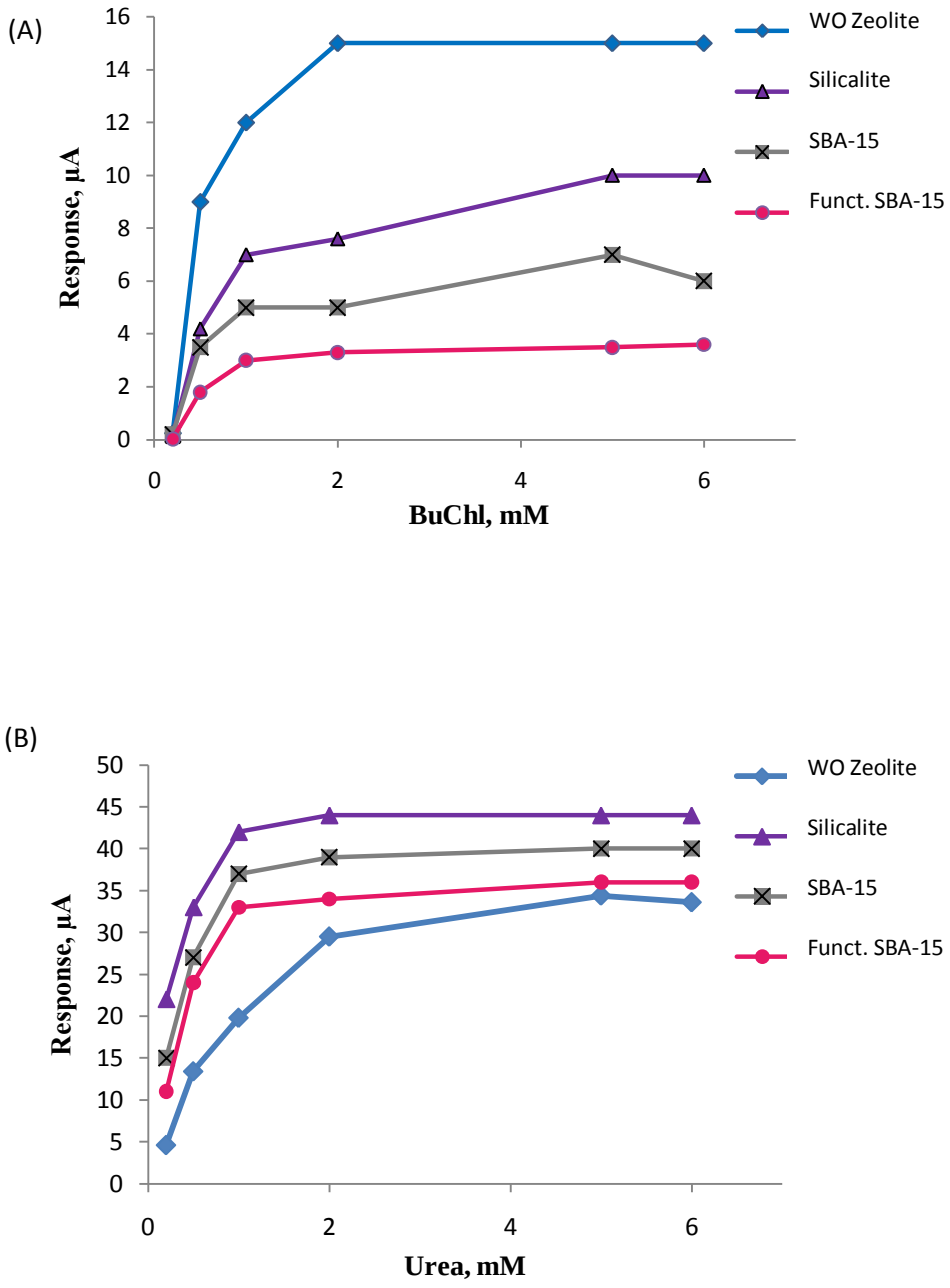

Figure 4.32: Calibration curves of biosensors based on immobilized BuChE (A) and urease (B), with/without silica samples. Measurements were conducted in 5 mM PBS, pH 7.4.

According to Figure 4.32, increased sensitivity of enzymes was obtained by silicalite modified trnsducers based on BuChE and urease sensors. Since physical adsorption of protein was found to be the lowest for silicalite materials (Figure 4.13), we can conclude that the unfolding of protein molecules on the silica surface might have occurred, as it was made clear in the previous sections. Disturbed native structure of enzyme molecules could promote the retention of enzymatic function thus increased activity of enzymes was obtained with the silicalite samples which adsorbed lesser quantities of enzyme molecules than the SBA-15 particles. Additionally, the lowest sensitivities to BuChl and urea were observed with the functionalized SBA-15 particles according to the strong interaction between GA, enzyme, and SBA-15 surface. This can be related to the formation of a large number of bonds between glutaraldehyde, amine functionalized SBA-15 surface and enzyme molecules, which might have caused a very compact structure of the biomembrane. Thus the active site of the enzyme was inaccessible.

4.2.2.3.3.2 Operational Stability and Inhibition

Operational stabilities of BuChl and urea biosensors were further examined upon modifying the electrodes by silicalite, SBA-15, and functionalized SBA-15. Biosensor responses to 5 mM BuChl and urea were determined during for 7 hours with 30-min intervals during which all bio-membranes on the transducer surface were kept in the working buffer solution all the time between measurements. The results are shown in Figure 4.33.

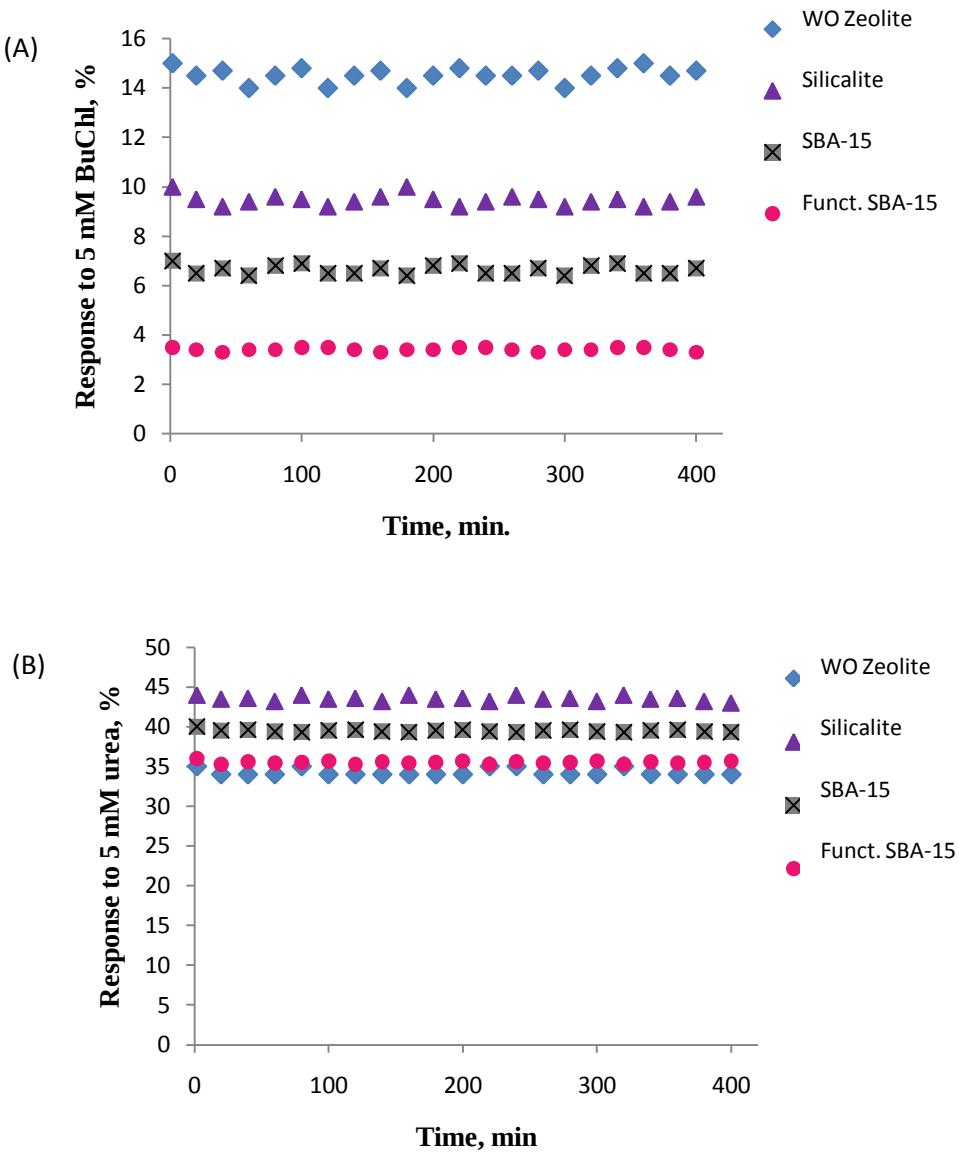

Figure 4.33: Operational stability of biosensors based on immobilized BuChE (A) and urease (B). Measurements were conducted in 5 mM PBS, pH 7.4, BuChCl and urea concentration was 5 mM.

As it can be seen in Figure 4.33, all biosensors displayed high signal reproducibility for each biosensor and all transducers containing silica particles were stable for more than 7 days.

Furthermore, inhibition characteristics of silica modified electrodes based on BuChE and urease were compared with the SMTs. For this purpose, varying concentrations of glycoalkoloids and mercury ions were used and results were shown in Figure 4.34.

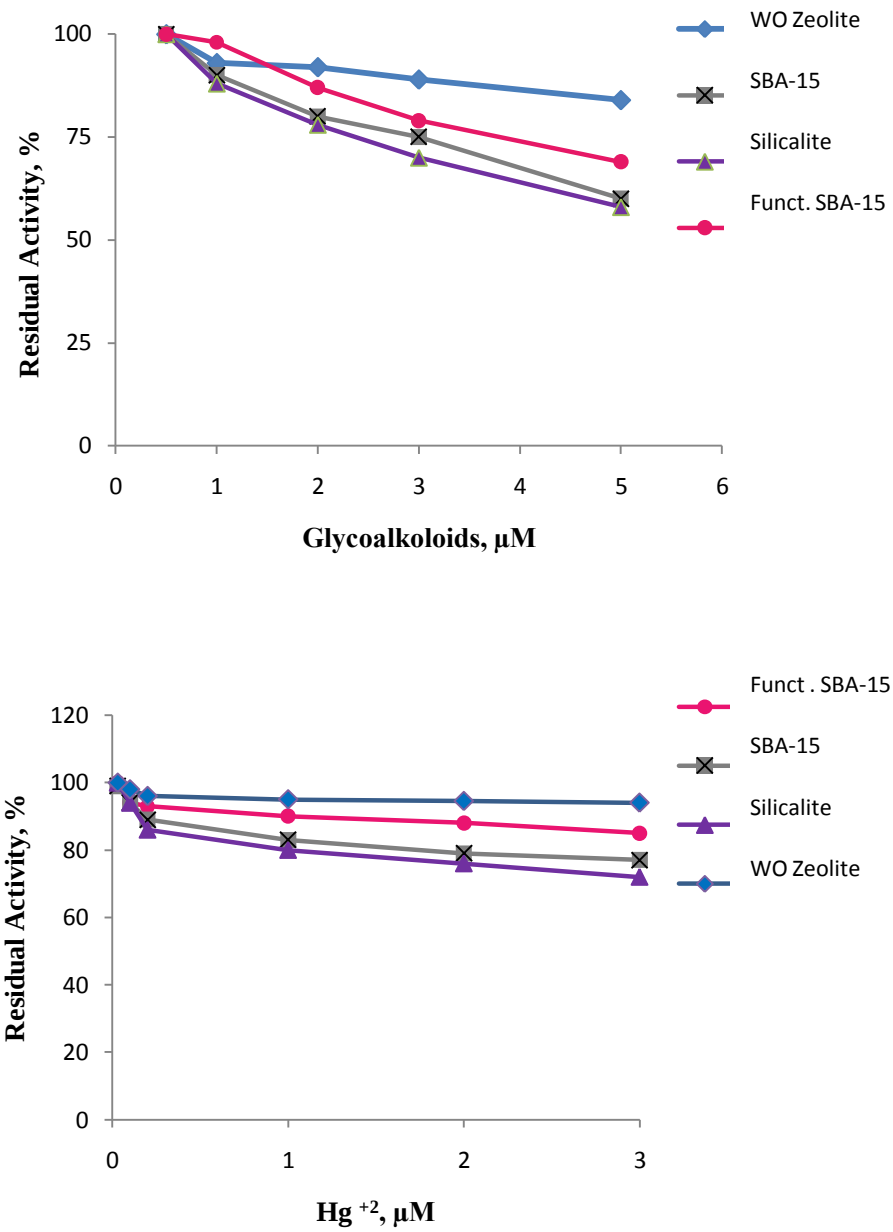

Figure 4.34: Dependence of residue activity of bioselective membranes based BuChE and urease on concentration of glycoalkoloids and mercury ions (Hg^{+2}), respectively. Measurements were conducted in 5 mM phosphate buffer, pH 7.4.

According to the Figure 4.34, highest resistance to the inhibitors was with functionalized SBA-15 modified transducers. According to these results, it can be hypothesized that the compact formation of biomembranes on the transducer surface avoided the inhibitor molecules to make contact with with the enzyme and resulted in resistance to inhibitor molecules.Furthermore, all BuChl and urease biosensors based on silica samples showed higher sensitivity to glycoalkaloids than the zeolite-free biosensor, and these sensitivities decreased in the order of Silicalite > SBA-15 > Funct. SBA-15. The inhibition results suggest that the pore size and surface charge of the silica particles have a powerful influence on the inhibition characteristics of BuChE and urease based ISFET type biosensors.

Eventually, it could be concluded that the effect of the morphology and structure of zeolite and zeo-type materials strongly influences the analytical characteristics of BuChE and urease based ISFET biosensors. Indeed, higher activities with silicalite particles confirmed the potential of application of silicalite as carrier materials for the immobilization of BuChE and urease.

CHAPTER 5

CONCLUSIONS

In this study, zeolite and zeo-type materials with varying physiochemical properties were used for immobilization of proteins with the aim of understanding the nature of interaction. For this purpose, physical adsorption method was chosen for the immobilization of proteins onto zeolite and zeo-type materials due to avoid the side-effects of chemicals on interactions. In the light of our findings, it was concluded that the adsorption of proteins was directly influenced by the Si/Al ratio, particle size, pore diameter, and surface charge of the zeolite and zeo-type materials as well as the molecular weight and acidic/basic properties of the proteins.

Furthermore, conductometric biosensors based on urease and glucose oxidase immobilized with different types of zeolites was constructed by ZMT method. It was seen that silicalite added electrodes lead to increased performances with respect to SMTs. As a result, the zeolite modified urea and glucose biosensors were successfully applied for detecting urea and glucose, which can offer improved possibilities to design biosensors. The results obtained show that zeolites could be used as alternatives for enzyme immobilization in conductometric biosensors development. It was shown for the first time that different zeolites with different characteristics led to different biosensor efficiency and performances.

Moreover, in order to investigate how the number and type of surface -OH groups influence the biosensor performance ISFET type biosensors based on urease and BuChE immobilized with different heat-treated zeolite samples was developed. The gradual changes to the integrated intensity of the 3610 cm^{-1} IR band with a nearly constant integrated intensity of the 3745 cm^{-1} IR band suggested that the employed heat treatment protocols resulted in a gradual decrease in the amount of Brønsted acid sites while preserving the amount of terminal silanols in zeolite Beta. Zeolite addition into the enzymatic membranes increased the sensor sensitivities and demonstrated high signal reproducibility for both types of biosensors. The sensitivities and inhibition characteristics obtained from the zeolite-modified electrodes using ISFET type biosensors were correlated with the FTIR-observed amount of Brønsted acid sites created in zeolite Beta samples upon heat treatment.

Moreover, analytical characteristics of biosensors based on urease and BuChE were investigated and compared upon modifying the ISFET electrodes with nano sized zeolite Beta particles, silicalite and SBA-15 materials with varying Si/Al ratio, particle diameter, surface charge, and pore size. The results suggested that the Si/Al ratio, particle diameter, surface charge, and pore size strongly influenced the biosensor performances as well as nature of the enzymatic reactions. As a result, increased activity of urease and butyrylcholinesterase was observed. These results showed for the first time that it was possible to tailor the electrode surfaces by zeolite and zeo-type materials, and thus regulate the ISFET characteristics for two different enzyme-based biosensors.

Eventually, it can be concluded that the effect of material morphology, structure and framework had very significant effects on the adsorption process and analytical characteristics of conductometric and ISFET based biosensors. Without

a doubt, observed higher adsorption quantities and activities upon zeolite and zeo-type materials confirmed that the potential of application of these materials as carriers for the immobilization of glucose oxidase, urease, and BuChE for the advanced adsorption and biosensor applications.

CHAPTER 6

RECOMMENDATIONS

Zeolite and zeo-type materials are excellent alternatives for use in selective immobilization of biopolymers due to their tunable properties for the desired applications. Thus, further enhancement and improvements are always possible. Based on the findings and conclusions drawn, the following recommendations are offered for future studies.

Zeolite silicalite and SBA-15 used in this study were synthesized according to their varying pore diameter. Since zeolite silicalite and SBA-15 have varying morphologies, comparing pore diameters using different types of materials (i.e., comparing the effect of pore size by utilizing silicalite and SBA-15) can be misleading, because once the morphologies change, a lot of other factors, such as the particle size, pore volume, and the surface area, etc. also change. Hence, comparing materials with same morphologies would be beneficial in the immobilization studies involving physical adsorption and biosensor applications.

FTIR analysis can be varied by studying the conformational change of immobilized proteins. Hence, change in the secondary structure may be measured to determine the protein behaviors on the zeolite surfaces under varying conditions such as pH and temperature. This way, presence of proteins only on the surface of the zeolite is ensured and more distinctive conclusions can be made regarding to behavior of proteins on the zeolite surfaces.

In addition to determination of enzymatic activities by using conductometric biosensors and ion sensitive field effect transistors, UV-VIS Spectroscopy or

Isothermal Titration Calorimetry (ITC) may be used to determine the activities in order to understand the nature of the physical adsorption process.

REFERENCES

[1] W.J. Mortier**,** J. Catal. 55 (1978) 138.

[2] M.A. Camblor**,** A. Corma and S. Valencia**,** Micropor. Mesopor. Mater. 25 (1998) 59.

[3] G. Zhu, S. Qiu, J.Yu, Y. Sakamoto, F. Xiao, R. Xu, and O. Terasaki, Chem. Mater. 10 (1998) 1483.

[4] C.Y. Chen**,** H.X. Li, and M.E. Davis**,** Micropor. Mater. 2 (1993) 17.

[5] R. Ravishankar, C.E.A. Kirschhock, P.P.K. Gerrits, E.J.P. Feijen, P.J. Grobet, P. Vanoppen, F.C. Schryver, G. Miehe, H. Fuess, B.J. Schoeman, P.A. Jacobs, and J.A. Martens, J. Phys. Chem. B 103 (1999) 4960.

[6] A. Corma, F. Rey, S. Valencia, J.L. Jorda, J. Rius, Nature Mater. 2 (2003) 493.

[7] S. Hashimoto, J. Photochem. Photobiol. C 4 (2003) 19.

[8] A. Huczko Appl. Phys. A 70 (2000) *365.*

[9] X. Meng, Y. Zhang, C. Meng, W. Pang, in Proc. 9th Int. Zeolite Conf., Montreal 1992 (Eds: R. Ballmoos, J. B. Higgins, M. M. J. Treacy), Butterworth-Heinemann 1993.

[10] A.P.V. Gonçalves, J.M. Lopes, F.Lemos, R. F. Ramôa, D.M.F. Prazeres, J.M.S. Cabral, M.R. Aires-Barros, J. Mol Catal B: Enzymatic. 1 (1996) 53.

[11] M.J Climent, A. Corma , S. Iborra, J.Catal. 233 (2005) 308.

[12] Y. Wang, F. Caruso, Chem. Mater. 17 (2005) 953.

[13] A.W. Chester, p. Clement, S. Han, US patent 6,136,291A (2000).

[14] S. Ghose, B. Mattiasson, Biotech. Appl. Biochem. 18 (1993) 311.

[15] Y.K. Chang, L. Chu, Biochem. Engin. 35 (2007) 37.

[16] K. Moller, T. Bein, Chem. Mater. 10 (1998) 2950.

[17] M. J. Kim and R. Ryoo, Chem. Mater. 11 (1999) 487.

[18] T.W. Kim, R. Ryoo, M. Kruk, K.P. Gierszal, M. Jaroniec, S. Kamiya, and O. Terasaki, J. Phys. Chem. B 108 (2004) 11480.

[19] E. Prouzet and T.J. Piiinavaia, Angric. Chem. Inr . Ed. Ens. 36 (1997)Yo. 5.

[20] R.B. Borade and A. Clearfield, J. Phys. Chem. 96 (1992) 6729.

[21] K. Yoo, P. G. Smirniotis Appl. Catal. A: General 227 (2002) 171.

[22] S. Mintova, V. Valtchev, T. Onfroy, C. Marichal, H. Knozinger, T. Bein Micropor Mesopor Mater 90 (2006) 237.

[23] S. Namba**,** N. Hosonuma and T. Yashima J. Catal. 72 (1981) 16.

[24] D.R. Rolison, Chem. Rev. 90 (1990) 867.

[25] D. T. Chen, S. B. Sharma, I. Filimonov and J. A. Dumesic, Catal Letters 12 201.

[26] J. Scherzer, Catal. Rev. Sci. Eng. 31 (1989) 215.

[27] P.J. Kunkeler, B.J. Zuurdeeg, J.C. van der Waal, J.A. van Bokhoven, D.C. Koningsberger, and H. van Bekkum, J. Catal. 180 (1998) 234.

[28] J.H.C. van Hooff and J.W. Roelofsen, in: Introduction to zeolite science and practice.

[29] H. van Bekkum, E.M. Flanigen, and J.C. Jansen (eds.), Studies in Surf. Sci. Catal. 58 (1991) 241.

[30] D.W. Breck, Zeolite molecular sieves: structure, chemistry, and use, Wiley & Sons, New York, 1974.

[31] R. Wijntje, H. Bosch, A.B. de Haan, and P.J.T. Bussmann, J. Chrom. A 1142 (2007) 39.

[32] M. Matsui, Y. Kiyozumi, T. Yamamoto, Y. Mizushina, F. Mizukami, and K. Sakaguchi, Chem. Eur. J. 7 (2001) 1555.

[33] A. Tavolaro, P. Tavolaro, and E. Drioli, Colloids Surf. B: Biointerfaces 55 (2007) 67.

[34] P. Tavolaro, A. Tavolaro, and G. Martino, Colloids Surf. B: Biointerfaces 70 (2009) 98.

[35] D. Barthomeuf**,** Mater. Chem. Phys. 17 (1987) 49.

[36] Basab Chakraborty, B. Viswanathan Catal. Today 49 (1999) 253.

[37] G.I. Kapustin**,** T.R.Brueva**,** A.L.Klyachko**,** S.Beran, and B.Wichterlova**,** Appl.Catal.42 (1988) 239.

[38] A. Vimont, F. Thibault-Starzyk, and J.C. Lavalley, J. Phys. Chem. B 104 (2000) 286.

[39] S. Siffert, L. Gaillard, and B.L. Su, J. Mol. Catal. A: Chemical 153 (2000) 267.

[40] J. Wang, Chem. Rev. 108 (2008) 814.

[41] I.M. Abdullat, A.H. Battah, K.A. Hadidi, Forensic Sci. International 162 (2006) 126.

[42] Roger A. Sheldon, Adv. Synth. Catal. 349 (2007) 1289.

[43] A.A. Khan and M.A. Alzohairy, Research J. Biol. Sci. 5 (2010) 565.

[44] C. Spahn and S.D. Minteer, Recent Patents on Engin. 2 (2008) 195.

[45] S.V. Dzyadevych, A.P. Soldatkin, Solid-State Electro-chemical Enz. Biosens. 1 (2008) 222.

[46] Norouzian D., Iranian J of Biotech. 1 (2003) 197.

[47] E. Karakus, S. Pekyardimci, J. Mol. Catal. B: Enzymatic. 56 (2009) 13.

[48] M. Johnson , Z. Li, J. Wang, Y. Yan, Thin Solid Films. 515 (2007) 3164.

[49] R. Wijntje, H. Bosch, A.B. de Haan, and P.J.T. Bussmann, J. Chrom. A, 1142 (2007) 39.

[50] K. Sakaguchi, M. Matsui, and F. Mizukami, Appl. Microbiol. Biotechnol. 67 (2005) 306.

[51] H. Chiku, M. Matsui, S. Murakami, Y. Kiyozumi, F. Mizukami, and K. Sakaguchi, Anal. Biochem. 318 (2003) 80.

[52] H. Chiku, A. Kawai, T. Ishibashi, M. Takehara, T. Yanai, F. Mizukami, and K. Sakaguchi, Anal. Biochem. 348 (2006) 307.

[53] Y.H. Zhang, X.J. Yu, X.Y. Wang, W. Shan, P.Y. Yang, and Y. Tang, Chem. Commun. (2004) 2882.

[54] F. Xu, Y.J .Wang, X.D. Wang, Y.H. Zhang, Y. Tang, and P.Y. Yang, Adv. Mater. 15 (2003) 1751.

[55] A. Walcarius, Electroanalysis 10 (1998) 1217.

[56] A. Walcarius, Anal. Chim. Acta 384 (1999) 1.

[57 B. Liu**,** F. Yan**,** J. Kong, and J. Deng**,** Anal. Chim. Acta 386 (1999) 31.

[58] G. Marko-Varga, E. Burestedt, C.J. Svensson, J. Emneus, L. Gorton, T. Ruzgas, M. Lutz, and K.K. Unger, Electroanalysis 8 (1996) 1121.

[59] D.R. Rolison, Stud. Surf. Sci. Catal. 85 (1994) 28.

[60] N. Jaffrezic-Renault and S.V. Dzyadevych, Sensors 8 (2008) 2569.

[61] S. Phadtare, A. Kumar, V.P. Vinod, C. Dash, D.V. Palaskar, M. Rao, P.G. Shukla, S. Sivaram, and M. Sastry, Chem. Mater. 15 (2003) 1944.

[62] H.R Luckarift, J.C Spain, R.R. Naik, and M.O Stone, Nature Biotech. 22 11 (2004).

[63] H. Tang, J. Chen, S. Yao, L. Nie, G. Deng, and Y. Kuang, Anal. Biochem. 331 (2004) 89.

[64] E. Soy, V. Pyeshkova, V. Arkhypova, B. Khadro, N. Jaffrezic-Renault, A. Sacco Jr., S.V. Dzyadevych, and B. Akata, Sensor Electronics and Microsystem Tech. 1 (2010) 28.

[65] P. Vidinha, V. Augusto, J. Nunes, J, C. Kima, J.M.S. Cabral, S. Barreiros, J. of Biotech. 135 (2008) 181.

[66] R.H. Carvalho, F. Lemos, J.M.S. Cabral, F. Ramoa Ribeiro, J. of Molecular Catal. B: Enzymatic 44 (2007) 39.

[67] H. Chiku, A. Kawai, T. Ishibashi, M. Takehara, T. Yanai, F. Mizukami, and K. Sakaguchi, Anal. Biochem. 348 (2006) 307.

[68] J. Li, G. Calzaferri, J. Eiecrrounal. Chem. 377 (1994) 163.

[69] J. Wang, T. Martinez, Anal. Chim. Acta 207 (1988) 95.

[70] B. Liu, R. Hu, and J. Deng, Anal. Chem. 69 (1997) 2343.

[71] J.C. Jansen, E.J. Creyghton, S.L. Njo, H. van Koningsveld, and H. van Bekkum, Catal. Today 38 (1997) 205.

[72] John E. Krohn and Michael Tsapatsis, Langmuir 21 (2005) 8743.

[73] C. Calgarotoa, R.P. Scherera, S. Calgarotob, J.V. Oliveiraa, D. Oliveiraa, S.B.C. Pergher, Appl. Catal. A: General 394 (2011) 101.

[74] D. Jung, C. Streb, and M. Hartmann, Int. J. Mol. Sci. 11 (2010) 11.

[75] C. Ispas, I. Sokolov, and S. Andreescu, Anal. Bioanal. Chem. 393(2009) 543.

[76] M.C. Rosales-Hernández**,** J.E. Mendieta-Wejebe**,** J. Correa-Basurto**,** J.I. Vázquez-Alcántara**,** E. Terres-Rojas, and J. Trujillo-Ferrara**,** Int. J. Biol. Macromol.40 (2007) 444.

[77] X. Iao, Y. Wang, J. Zhao, and S. Zhu, Chin. J. Chem. Eng., 18 (2010) 493.

[78] A. Katiyar, L. Ji, P. Smirniotis, N.G. Pinto, J. Chromatogr. A, 1069 (2005) 119.

[79] Q. Zhang, K. Ariga, A. Okabe, T. Aida, J. Am. Chem. Soc. 126 (2004) 988.

[80] M. Miyahara, A. Vinu, T. Nakanishi, K. Ariga, Kobunshi Ronbunshu 61(2004) 623.

[81] A. Vinu, V. Murugesan, M. Hartmann, J. Phys. Chem., B 108 (2004) 7323.

[82] A. Vinu, M. Miyahara, K. Ariga, J. Phys. Chem., B 109 (2005) 6436.

[83] M. Hartmann, A. Vinu, G. Chandrasekar, Chem. Mater. 17 (2005) 829.

[84] A. Vinu, K.Z. Hossain, G. Satishkumar, V. Sivamurugan, K. Ariga, Stud.Surf. Sci. Catal.156 (2005) 631.

[85] M. Miyahara, A. Vinu, K. Ariga, Materi. Sci. and Eng. C 27 (2007) 232.

[86] H.H.P. Yiu, P. A. Wright, N.P. Botting, Micropor. Mesopor. Mater. 44-45 (2001) 763.

[87] J.F. Diaz, K.J. Balkus, Jr., J. Mol. Catal. B: Enzymatic 2 (1996), 115.

[88] L. Washmon-Kriel, V.L. Jimenez, K.J. Balkus, Jr., J. Mol. Catal. B: Enzymatic 10 (2000), 453.

[89] D. Goradia, J. Cooney, B.K. Hodnett, E. Magner, J. Molecular. Catal. B: Enzymatic 32 (2005) 231.

[90] Y.J. Hart, G.D. Stucky, A. Butler, J. Am. Chem. Soc. 121 (1999) 9897.

[91] M. Lundqvist, I. Sethson, and B.H. Jonsson, Langmuir 20 (2004) 10639.

[92] A.A. Vertegel, R.W. Siegel, and J. S. Dordick, Langmuir 20 (2004) 6800.

[93] Y.Y. Hu, Y.H. Zhang, N. Ren, and Y. Tang, J. Phys. Chem. C 113 (2009) 18040.

[94] R.H. Carvalho, F. Lemos, J.M.S. Cabral, F. Ramôa Ribeiro, J. Molecular Catal B. 44 (2007) 39.

[95] M.L. Hamlaoui, K. Reybier, M. Marrakchi, N. Jaffrezic-Renault, C. Martelet, R. Kherrat, and A. Walcarius, Anal. Chim. Acta 466 (2002) 39.

[96] W.Y. Lee, K.S. Lee, T.H. Kim, M.C. Shin, J.K. Park, Electroanalysis 12 (2000) 78.

[97] W. Lee, S. Kim, T. Kim, K. S. Lee, M. Shin, J. Park, Anal. Chim. Acta 404 (2000) 195.

[98] B. Adhikari, S. Majumdar, Progress in Polymer Science 29 (2004) 699.

[99] G. Bayramoglu, E. Yalcin, M.Y. Arica, Process Biochem. 40 (2005) 3505.

[100] S. Chinnayelka, M.J. McShane, Anal. Chem. 77 (2005) 5501.

[101] K.Z. Hossain, C.M. Monreal, A. Sayari, Colloids and Surf. B 62 (2008) 42.

[102] W. Lee, S. Kim, T. Kim, K.S. Lee, M. Shin, J. Park, Anal. Chim. Acta 404 (2000) 195.

[103] A. Walcarius, Electroanalysis 8 (1996) 971.

[104] J.M. Newsam, M.M.J. Treacy, W.T. Koetsier, and C.B. de Gruyter, Proc. R. Soc. Lond. A 420 (1988) 375.

[105] P. Prokesova, S. Mintova, J. Cejka, T. Bein, Micropor. Mesopor. Mater. 64 (2003) 165.

[106] L. Wang, T. Qi, Y. Zhang, J. Chu, Micropor. Mesopor. Mater. 91 (2006) 156.

[107] Synthesis of Triacetoxymethylsilane, ‘’http://www.chemiedidaktik.uni-wuppertal.de/disido_cy/en/exp/m_fact03.htm’’, last accessed on 12/07/2011.

[108] X. Zhang **,** E.S.M. Lai**,** R. Martin-Aranda, and K.L. Yeung**,** App. Catal. A: General 261 (1) (2004) 109.

[109] T.W. Pechar, M. Tsapatsis, E. Marand, R. Davis, Desalination 146 (2002) 3.

[110] E.J. Creyghton, S.D. Ganeshie, R.S. Downing, H. Van Bekkum, J. Mol. Catal. A, 115 (1997) 457.

[111] B. Akata, J. Warzywoda, and A. Sacco Jr. J. of Catal. 222 (2004) 397.

[112] G. Zhu, S. Qiu, J. Yu, Y. Sakamoto, F. Xiao, R. Xu, and O. Terasaki, Chem. Mater. 10 (1998) 1483.

[113] K. Narasimharao, M. Hartmann, H.H. Thiel, and S. Ernst, Micropor. Mesopor. Mater. 90 (2006) 377.

[114] P. Prokesova, S. Mintova, J. Cejka, T. Bein, Micropor. Mesopor. Mater. (2003) 165.

[115] Mark C. Lovallo and Michael Tsapatsis AlChE J 42 (1996) 3020.

[116] J.B. Higgins, R.B. LaPierrea, J.L. Schlenker, A.C. Rohrmana, J.D. Wooda, G.T. Kerr, and W.J. Rohrbaugh, Zeolites 8 (1988) 446.

[117] B. Liu**,** F. Yan**,** J. Kong, and J. Deng**,** Anal. Chim. Acta, 386 (1999) 31.

[118] A. Omegna, M. Vasic, J.A. van Bokhoven, G. Pirngruber, and R. Prins, Phys. Chem. Chem. Phys., 2004, 6, 447.

[119] M. Miyahara, A. Vinu, K. Ariga, Mater. Sci. and Engin. C 27 (2007) 232.

[120] Y. Y. Hu, Y. H. Zhang, N. Ren, and Y. Tang, J. Phys. Chem. C 113 (2009) 18040.

[121] H. H. P. Yiu, P. A. Wright, N. P. Botting, Micropor. Mesopor. Mater. 44-45 (2001) 763.

[122] D. Goradia, J. Cooney, B.K. Hodnett, E. Magner, J. of Mol. Catalysis B: Enzymatic 32 (2005) 231.

[123] J. M. Kisler, G. W. Stevens and A. J. O'Connor, Mater. Phys. Mech. 4 (2001) 89.

[124] A. J. Milici, P. W. Bankston, Am J Anat. 165 (1982) 165

[125] H. E. Klei, D. W. Sundstrom, R. Gargan, Biotech. Bioengin. (1978) 611.

[126] N. M. Ismail, L. Y. Fei, L. L. Cheng, C. Y. Yuen, K. Sozana, N. Kamarudin, H. Mat, International Conference of Chemical and Bioprocess Engineering.

[127] S. Siffert, L. Gaillard, and B.L. Su, J. Mol. Catal. A: Chemical 153 (2000) 267.

[128] A. Vimont, F. Thibault-Starzyk, and J.C. Lavalley, J. Phys. Chem. B 104 (2000) 286.

[129] J.M. Newsam, M.M.J. Treacy, W.T. Koetsier, and C.B. de Gruyter, Proc. R. Soc. Lond. A 420 (1988) 375.

[130] B. Akata, B. Yilmaz, S.S. Jirapongphan, J. Warzywoda, and A. Sacco Jr., Micropor. Mesopor. Mater. 71 (2004) 1.

[131] J.C. Jansen, E.J. Creyghton, S.L. Njo, H. van Koningsveld, and H. van Bekkum, Catal. Today 38 (1997) 205.

[132] J. Scherzer, Catal. Rev. Sci. Eng. 31 (1989) 215.

[133] P.J. Kunkeler, B.J. Zuurdeeg, J.C. van der Waal, J.A. van Bokhoven, D.C. Koningsberger, and H. van Bekkum, J. Catal. 180 (1998) 234.

[134] M. Muller, G. Harvey, and R. Prins, Micropor. Mesopor. Mater. 34 (2000) 135.

[135]C.H. Lee, J. Lang, C.W. Yen, P. Shih, T.S. Lin, and C.Y. Mou, J. Phys. Chem. B 109 (2005) 12277.

[136] A. Tavolaro, P. Tavolaro, and E. Drioli, Colloids Surf. B: Biointerfaces 55 (2007) 67.

[137]M.A. Camblor, A. Corma, and S. Valencia, Micropor. Mesopor. Mater. 25 (1998) 59.

[138] N. Sofikiti, N. Chaniotakis, J. Grandal, M. Utrera, M. A. Sanchez-Garcia,E. Calleja, E. Iliopoulos, and A. Georgakilas, App. Phy. Lett. 95 (2009), 113701.

[139] O. Lockridge, E.G. Duysen, and P. Masson, (2011) Butyrylcholinesterase: Overview, Structure, and Function, in Anticholinesterase Pesticides: Metabolism, Neurotoxicity, and Epidemiology (eds T. Satoh and R. C. Gupta), John Wiley & Sons, Inc., Hoboken, NJ, USA.

[140] H.G. Manyar, E. Gianotti, Y. Sakamoto, O. Terasaki, S. Coluccia, and S. Tumbiolo, J. Phys. Chem. C 112 (2008) 18110.

[141] F. Michaux, M. Zoumpanioti, M. Papamentzelopoulou, M.J. Stebe, J.L. Blin, and A. Xenakis, Proc. Biochem. 4 (2010) 39.

[142] P. Tavolaro, A. Tavolaro, and G. Martino, Colloids Surf. B: Biointerfaces 70 (2009) 98.

[143] H. Robson, K.P. Lillerud, “Verified Syntheses of Zeolitic Materials”, Published on behalf of the Synthesis Commission of the International Zeolite Association, 2nd Revised Edition, 2001.

APPENDIX A

CHARACTERISTIC XRD PEAKS OF ZEOLITE A, BETA, SILICALITE, AND SBA-15 IN THE LITERATURE

A.1 Zeolite A (LTA)

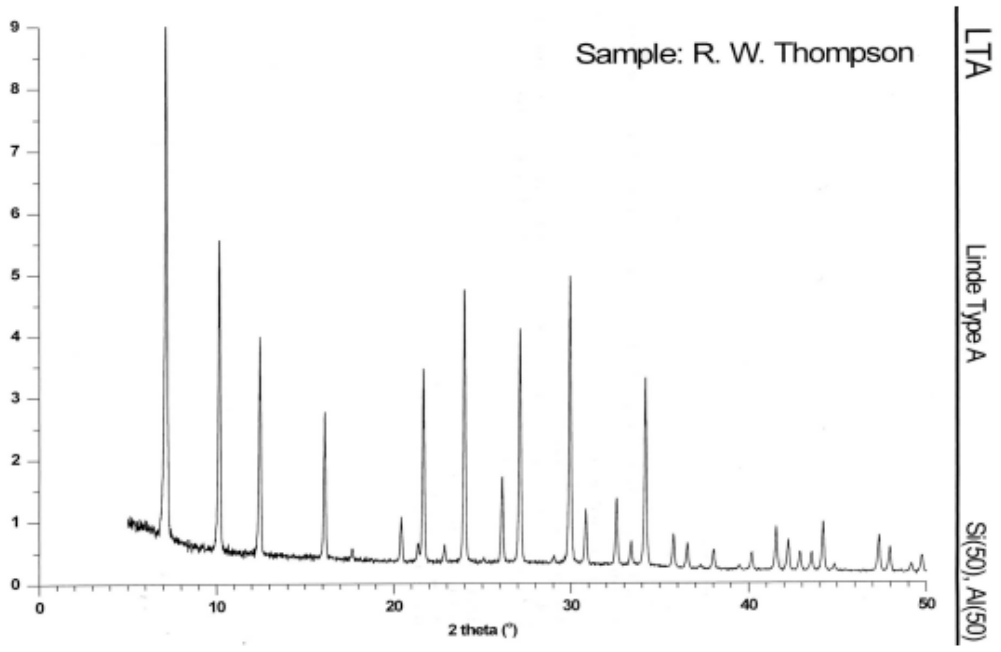

Figure A.1: Characteristic XRD pattern of zeolite A (LTA) [143].

A.2 Zeolite Beta (BEA)

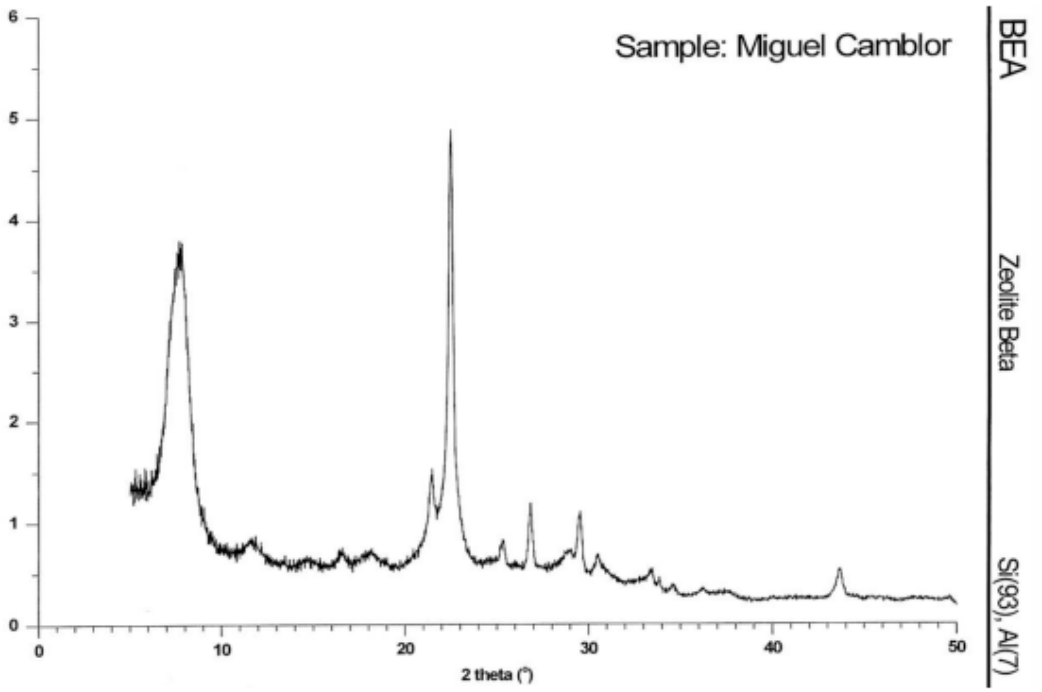

Figure A.2: Characteristic XRD pattern of zeolite Beta (BEA) [143].

A.3 Silicalite

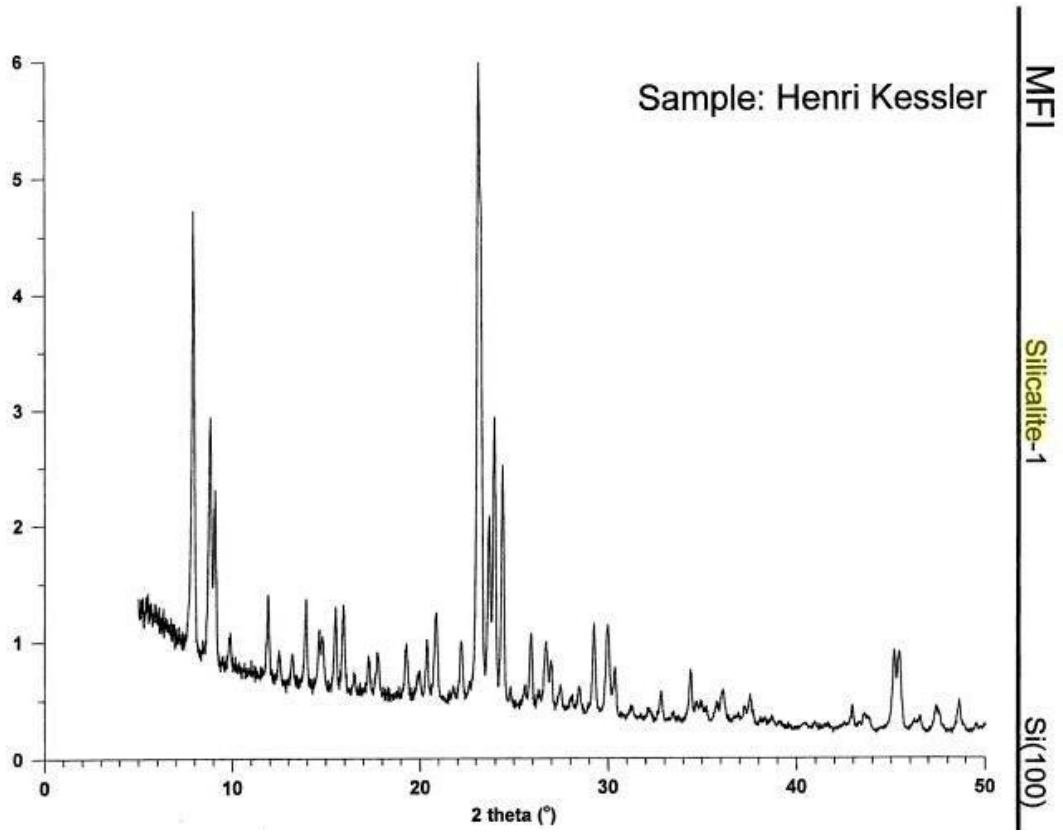

Figure A.3: Characteristic XRD pattern of silicalite [143].

A.4 SBA-15

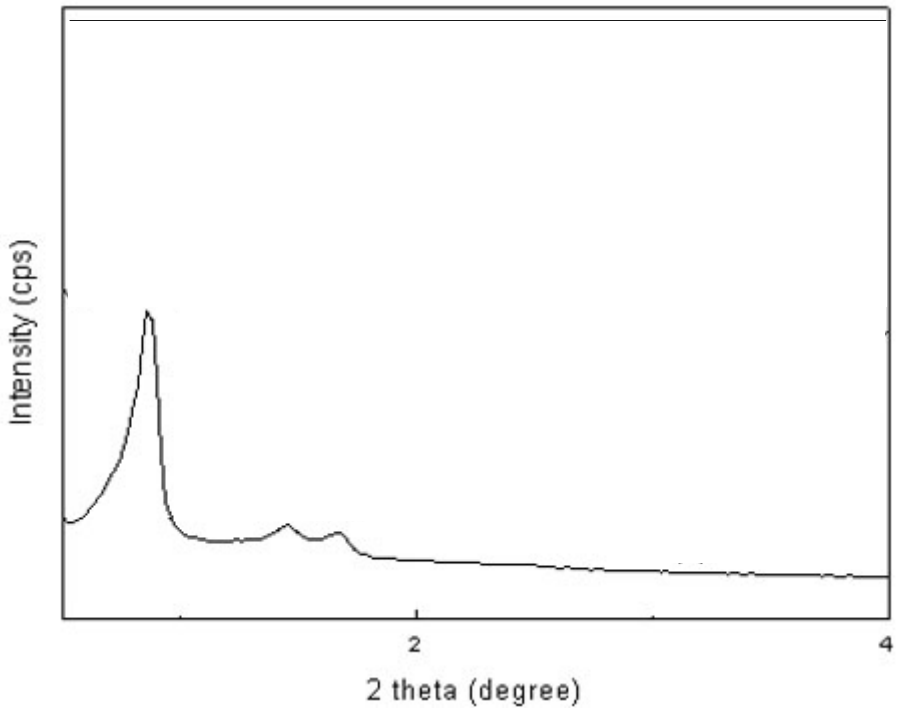

Figure A.4: Characteristic XRD pattern of SBA-15 [106].

APPENDIX B

TABLE OF AS-SYNTHESIZED ZEOLITE SAMPLES

Table B.1: List of as-synthesized zeolite samples.

Formula	Morphology	Sample Name
Formula I	Zeolite A	LTA-2
Formula II	Zeolite A	LTA-3.8
Formula III	Zeolite A	LTA-5
Formula IV	Sub-Micron Zeolite Beta	BEA-30
Formula V	Sub-Micron Zeolite Beta	BEA-50
Formula VI	Sub-Micron Zeolite Beta	BEA-60
Formula VII	Sub-Micron Zeolite Beta	BEA-120
Formula VIII	Nano Sized Zeolite Beta	N-BEA-50
Formula IV	Nano Sized Zeolite Beta	N-BEA-75
Formula X	Nano Sized Zeolite Beta	N-BEA-100
Formula XI	Zeolite Silicalite	Silicalite
Formula XI	Zeo-type SBA-15	SBA-15

APPENDIX C

T-PLOT ANALYSIS OF ZEOLITES

C.1 Zeolite A-LTA-2

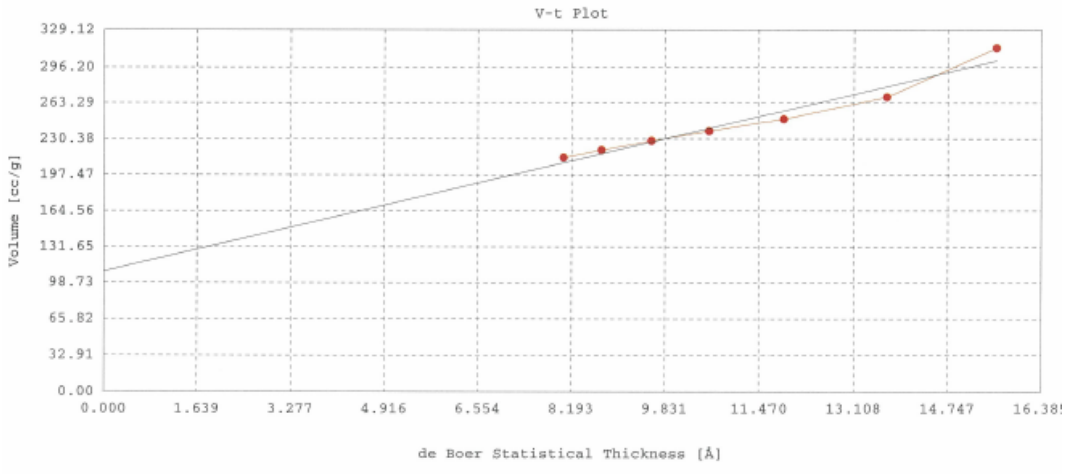

Figure C.1: T-Plot analysis of LTA-2.

C.2 Zeolite A-LTA-3.8

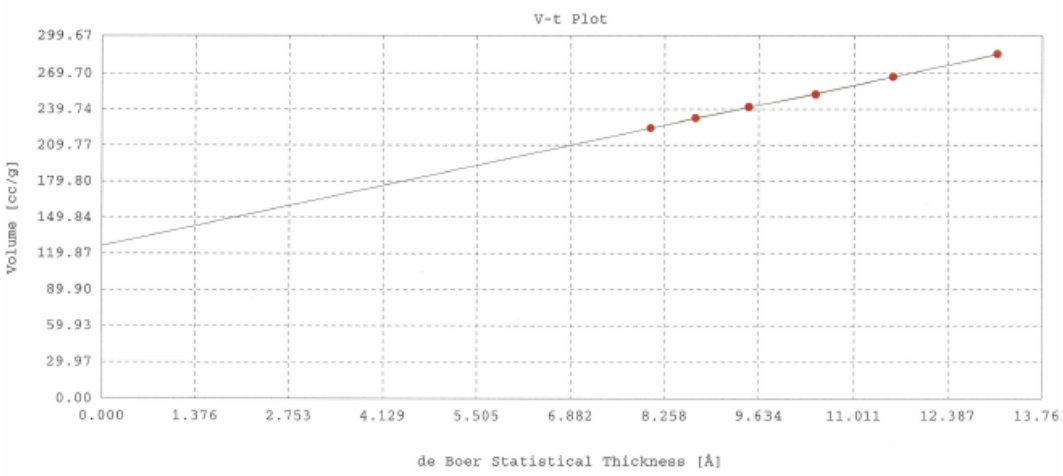

Figure C.2: T-Plot analysis of LTA-3.8.

C.3 Zeolite A-LTA-5

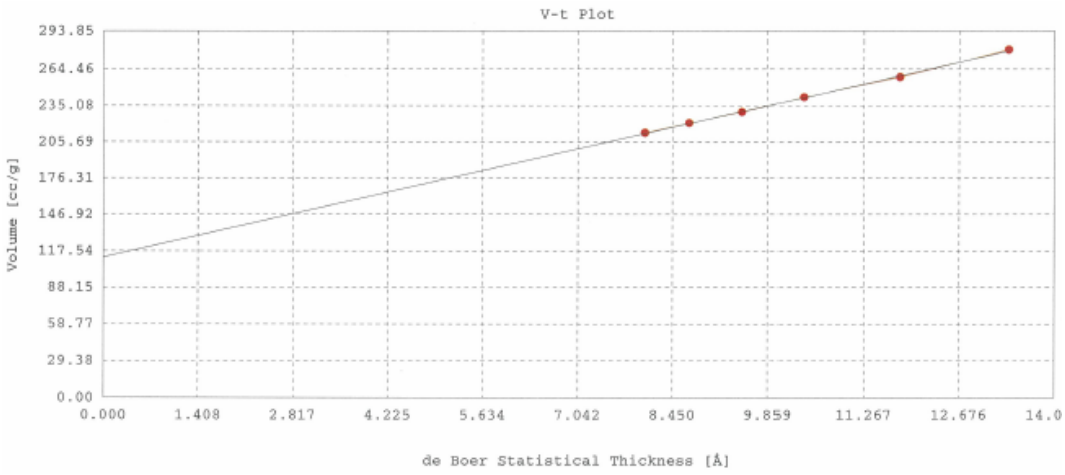

Figure C.3: T-Plot analysis of LTA-5.

C.4 Zeolite Beta-BEA-30

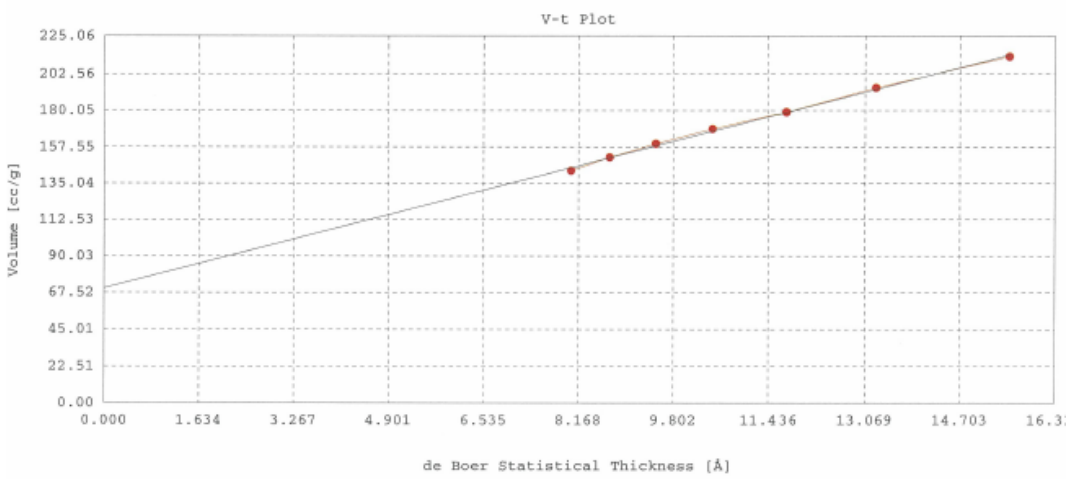

Figure C.4: T-Plot analysis of BEA-30.

C.5 Zeolite Beta-BEA-50

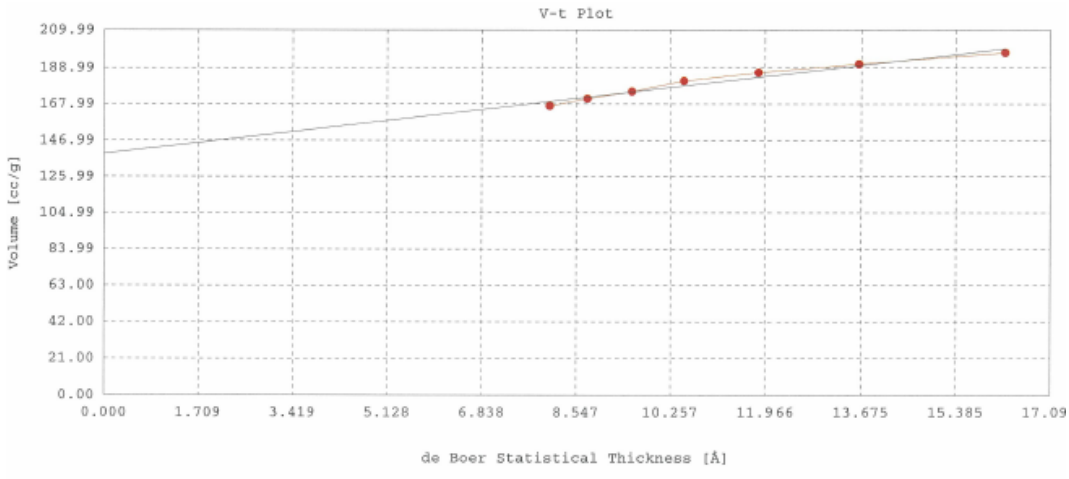

Figure C.5: T-Plot analysis of BEA-50.

C.6 Zeolite Beta-BEA-60

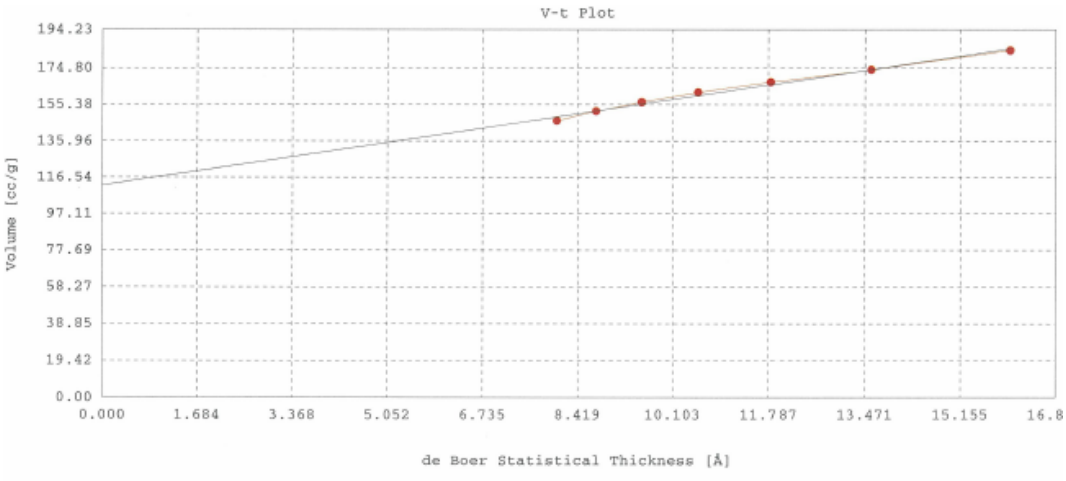

Figure C.6: T-Plot analysis of BEA-60.

C.7 Zeolite Beta -BEA-120

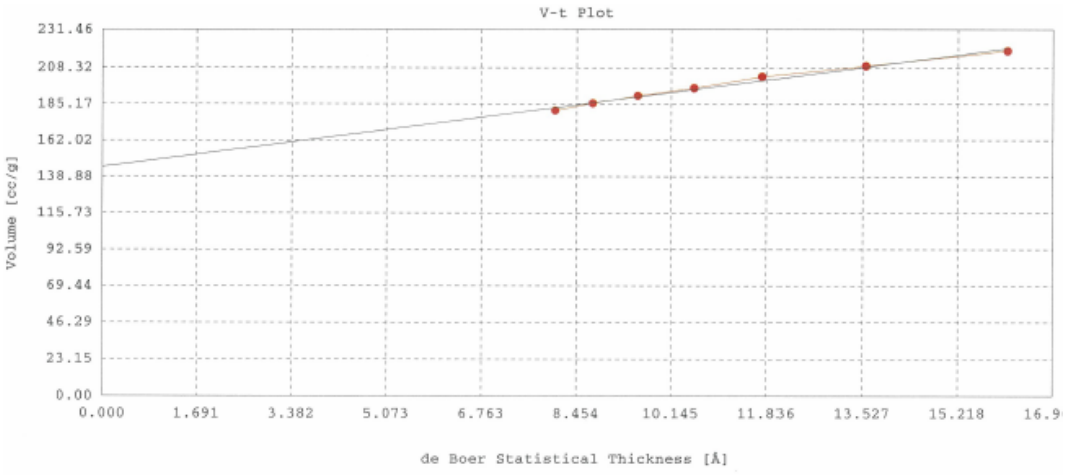

Figure C.7: T-Plot analysis of BEA-120.

C.8 Zeolite Beta-N-BEA-50

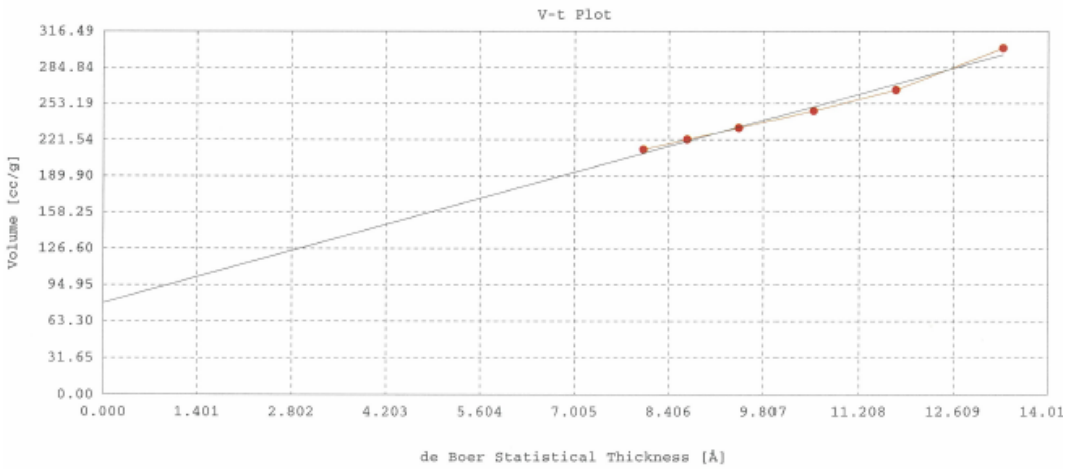

Figure C.8: T-Plot analysis of N-BEA-50.

C.9 Zeolite Beta-N-BEA-100

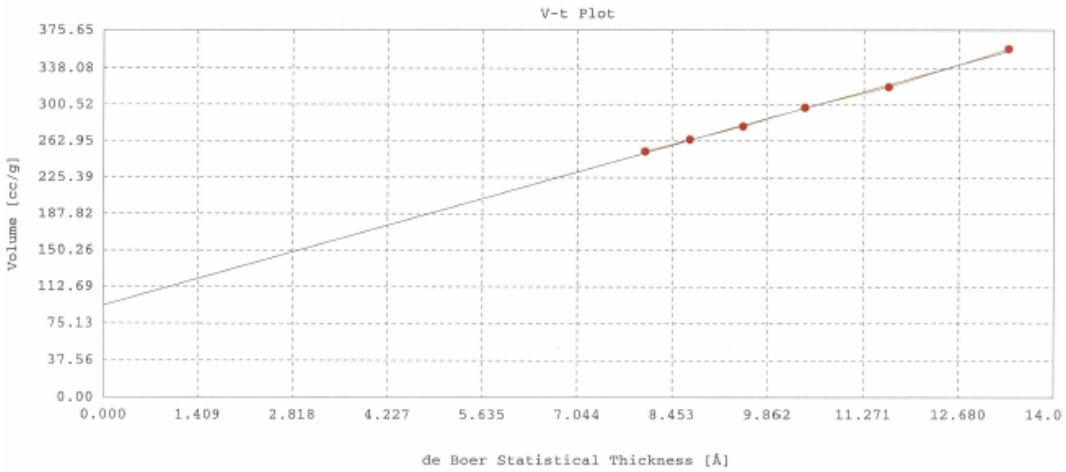

Figure C.9: T-Plot analysis of N-BEA-100.

C.10 Heat Treated Zeolite Beta-BEA-1

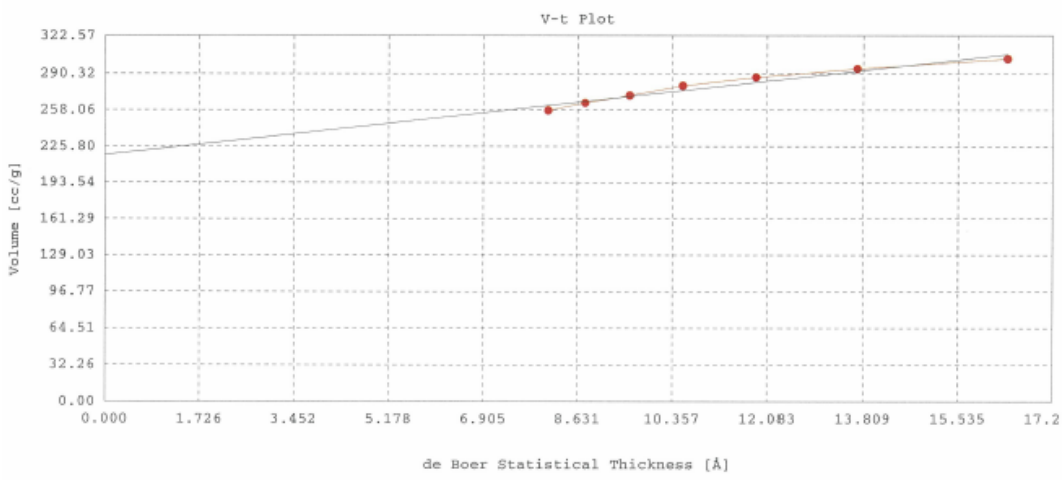

Figure C.10: T-Plot analysis of BEA-1.

C.11 Heat Treated Zeolite Beta-BEA-2

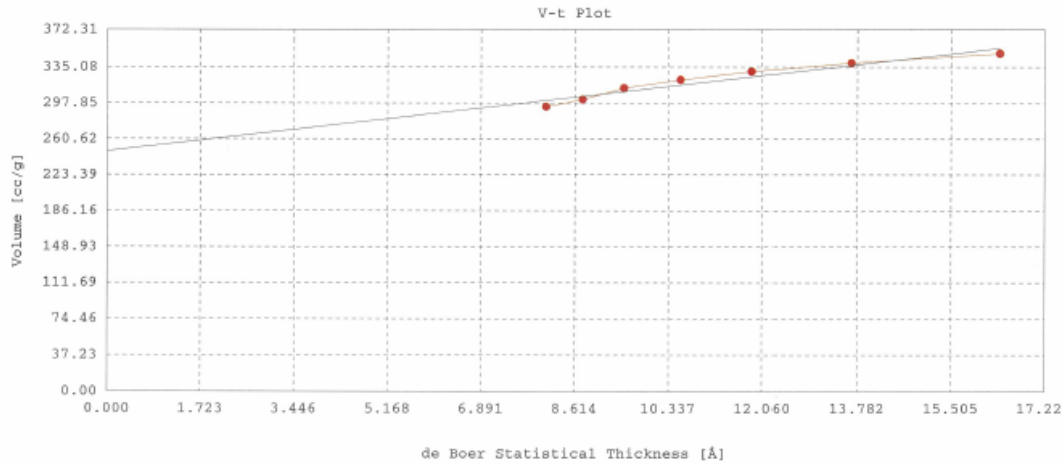

Figure C.11: T-Plot analysis of BEA-2.

C.12 Heat Treated Zeolite Beta-BEA-3

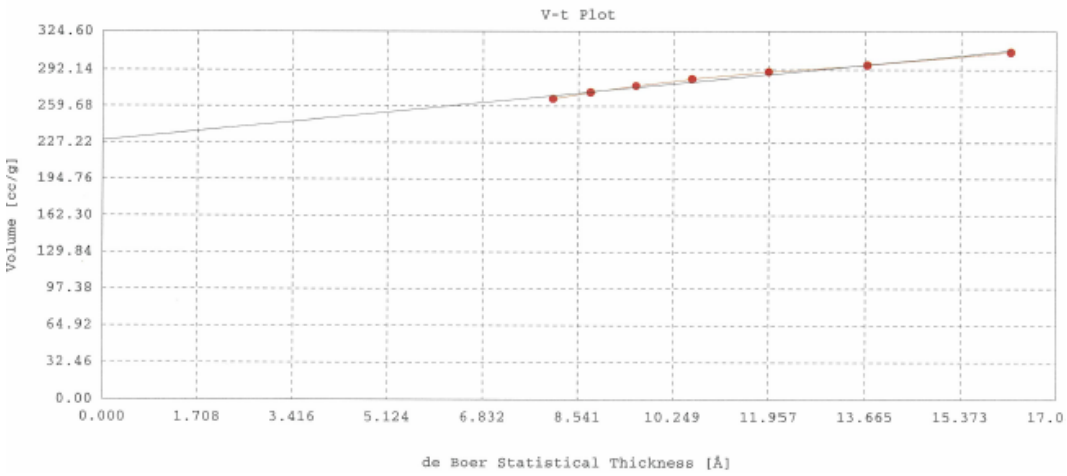

Figure C.12: T-Plot analysis of BEA-3.

C.13 Silicalite

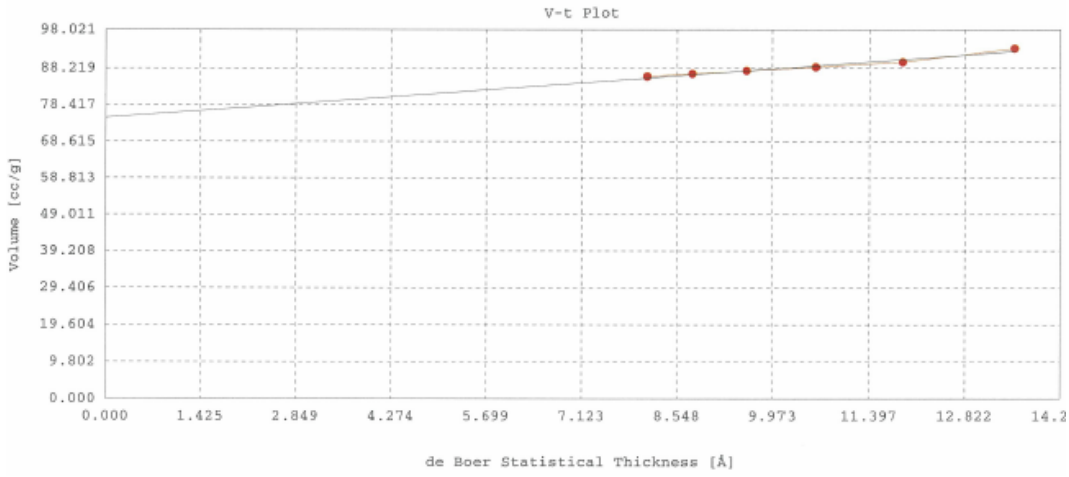

Figure C.13: T-Plot analysis of Silicalite.

C.14 SBA-15

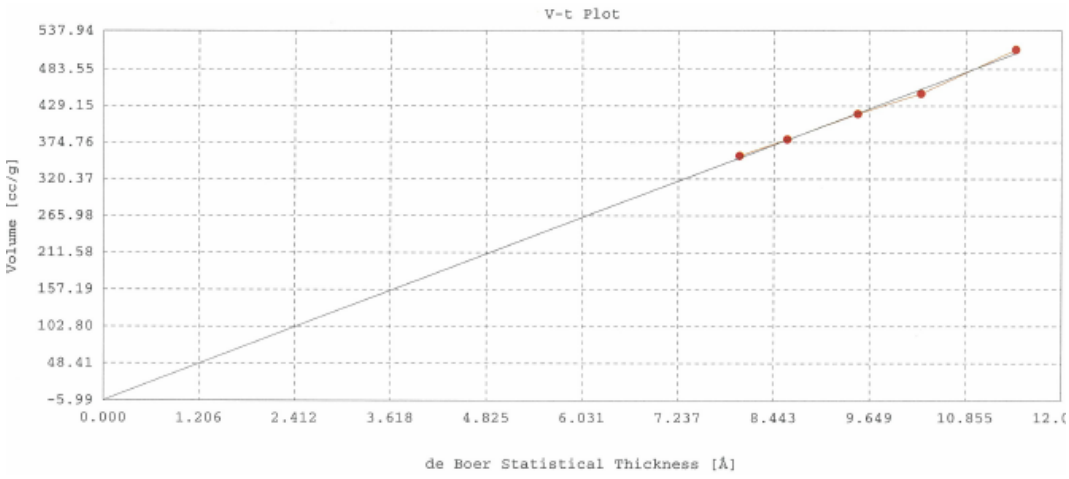

Figure C.14: T-Plot analysis of SBA-15.

APPENDIX D

UV-VIS ABSORPTION SPECTRA OF PROTEINS

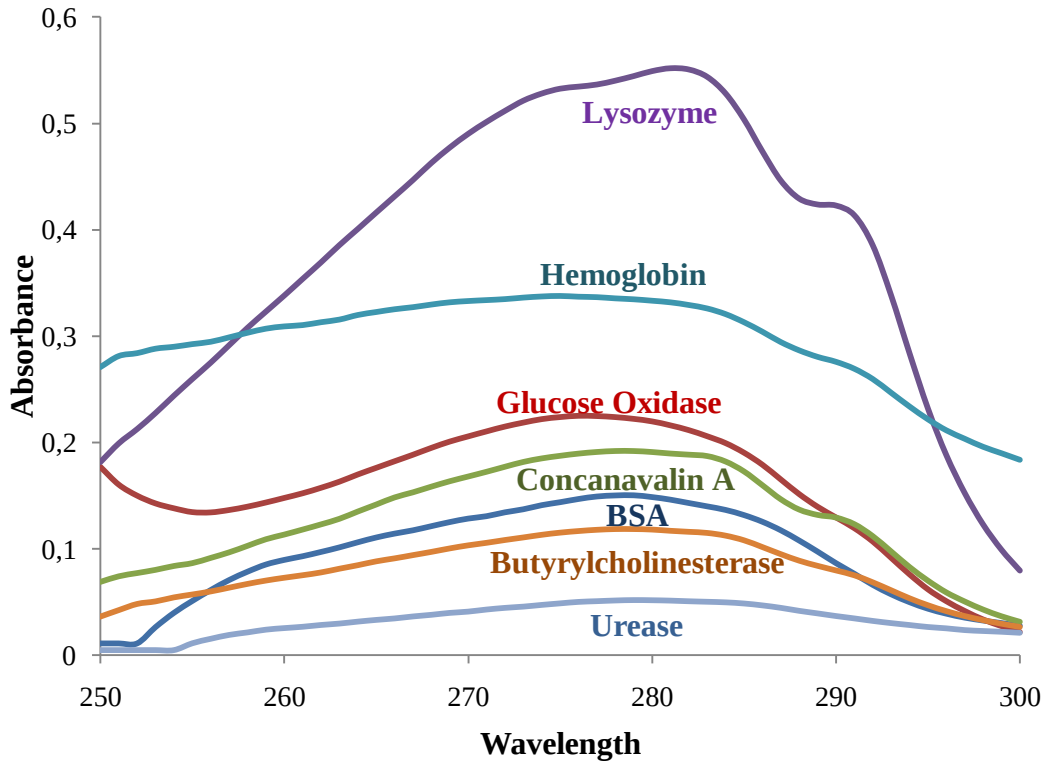

Figure D.1: UV-VIS adsorption spectra of non-adsorbed lysozyme, hemoglobin, glucose oxidase, concanavalin A, BSA, butyrylcholiesterase, and urease.

APPENDIX E

MASS BALANCE CALCULATION OF ADSORBED PROTEINS

The amount of protein in the liquid and zeolite phases was calculated by using the mass balance. The amount of adsorption at time *t*, q_t was obtained as follows:

$$\boldsymbol{q_t} = \frac{v(C_0 - C_t)}{w}$$

where C_o and C_t (mg protein/mL solution) are the liquid phase concentrations of protein initially and at time *t*, respectively. q_t (mg protein/mg zeolite) is the zeolite phase concentration of protein at time *t*, *v* the volume of aqueous phase (ml) and *w* is the weight of zeolite (mg).